# Chiral Peropyrene: Synthesis, Structure, and Properties

Wenlong Yang,[†] Giovanna Longhi,[‡] Sergio Abbate,[‡] Andrea Lucotti,[§] Matteo Tommasini,[§] Claudio Villani,[#] Vincent J. Catalano,[†] Aleksandr O. Lykhin,[†] Sergey A. Varganov,[†] and Wesley A. Chalifoux*[†]


[†]Department of Chemistry, University of Nevada—Reno, Reno, NV, 89557, USA

[‡]Dipartimento di Medicina Molecolare e Traslazionale, Università di Brescia, Viale Europa 11, 25123 Brescia, Italy

[§]Politecnico di Milano, Dipartimento di Chimica, Materiali e Ingegneria Chimica "G. Natta," Piazza Leonardo da Vinci 32, 20133 Milano, Italy

[#]Dipartimento di Chimica e Tecnologie del Farmaco, Universitá di Roma "La Sapienza", 00185 Roma, Italy


*Email: wchalifoux@unr.edu

## Table of contents

# 1. General experimental section

All reactions dealing with air- or moisture-sensitive compounds were carried out in a dry reaction vessel under nitrogen. Anhydrous tetrahydrofuran (THF) and dichloromethane (DCM) were obtained by passing the solvent (HPLC grade) through an activated alumina column on a PureSolv MD 5 solvent drying system. $^1$H and $^{13}$C NMR spectra were recorded on Varian 400 MHz or Varian 500 MHz NMR Systems Spectrometers. Spectra were recorded in deuterated chloroform (CDCl$_3$), dimethyl sulfoxide (*d*-DMSO), and 1,1,2,2-tetrachloroethane (C$_2$D$_2$Cl$_4$). Tetramethylsilane (TMS, set to 0 ppm) was used as an internal standard for chemical shifts or referenced to the residual protio-solvent peaks (CDCl$_3$: 7.26 ppm for $^1$H and 77.16 ppm for $^{13}$C; *d*-DMSO: 2.50 ppm for $^1$H and 39.52 ppm for $^{13}$C; C$_2$D$_2$Cl$_4$: 6.00 ppm for $^1$H and 73.78 ppm for $^{13}$C). Chemical shifts are reported in part per million (ppm) from low to high frequency and referenced to the residual solvent resonance. Coupling constants (J) are reported in Hz. The multiplicity of $^1$H signals are indicated as: s = singlet, d = doublet, t = triplet, m = multiplet, br = broad. For simplicity, the coupling constants of the aryl protons for *para*-substituted aryl groups have been reported as pseudo first-order (i.e., doublets), even though they are second-order (AA'XX') spin systems. High resolution ESI mass spectrometry was recorded using an Agilent 6230 TOF MS and TFA was added to samples to promote ionization. MALDI-TOF mass spectra were recorded on a Bruker microflex MALDI-TOF spectrometer. TLC information was recorded on Silica gel 60 F254 glass plates. Purification of reaction products was carried out by flash chromatography using Silica Gel 60 (230-400 mesh).

A suitable crystal was mounted on a glass fiber and placed in the low-temperature nitrogen stream. Data were collected on a Bruker SMART CCD area detector diffractometer equipped with a low-temperature device, using graphite-monochromated Mo Kα radiation ($\lambda$ = 0.71073 Å) and a full sphere of data was collected. Cell parameters were retrieved using SMART[1] software and refined using SAINTPlus[2]on all observed reflections. Data reduction and correction for Lp and decay were performed using the SAINTPlus[2] software. Multi-scan absorption

corrections were applied using SADABS,[3] unless otherwise indicated. The structures were solved by direct methods and refined by least square methods on $F^2$ using the SHELXTL[4] program package. All non-hydrogen atoms were refined anisotropically. The majority of the hydrogen atoms were added geometrically and their parameters constrained to the parent site.

**HPLC Separation**. The HPLC unit was composed of a Jasco (Tokyo, Japan) PU980 pump, a Rheodyne (Cotati, CA) 7125 20 µL injector, and Jasco UV 975 and UV/CD 995 detectors connected in series. HPLC analytical runs were performed at flow rates of 1.0 mL/min and monitored by simultaneous UV and CD detections. Column temperature was maintained at $25 \pm 0.1$ °C using a home-made cooling/heating device. Samples were dissolved in $CH_2Cl_2$ and diluted with the eluent. The enantiomers of peropyrene **8b** have retention times of 3.2 min (1st eluted) and 5.2 min (2nd eluted). Semi-preparative liquid chromatography was performed on a Waters chromatograph equipped with a Rheodyne model 7012 500 µL loop injector, and a spectrophotometer UV SpectraMonitor 4100 detector. HPLC semipreparative runs were performed at a flow rate of 3.0 mL/min and monitored by UV detection. Columns ($250 \times 4.6$ mm ID and 250 x 10 mm ID) packed with 5 µm Chiralpak-IA chiral stationary phase were obtained from Chiral Technologies Europe. Racemization of peropyrene **8b**. About 1 mg of (*M,M*)-(–)-**8b** was dissolved in 100 µL of decalin and added via syringe to a vessel containing 2 ml of decalin thermostatted at T = $100 \pm 0.2$ °C; variation of e.e. with time was monitored by sampling 20 µl of the mixture, quenching with 200 µl of eluent (hexane/2-propanol 98/2), and HPLC analysis on the analytical column.

| t (min) | Area 1st | Area 2nd | e.e. | ln e.e. |
|---|---|---|---|---|
| 0 | 0,92 | 99,08 | 98,16 | 4,59 |
| 30 | 4,39 | 95,61 | 91,22 | 4,51 |
| 60 | 9,03 | 90,97 | 81,94 | 4,41 |
| 120 | 14,28 | 85,72 | 71,44 | 4,27 |
| 240 | 23,68 | 76,32 | 52,64 | 3,96 |
| 360 | 31,68 | 68,73 | 36,90 | 3,61 |
| 480 | 36,52 | 63,48 | 26,96 | 3,29 |
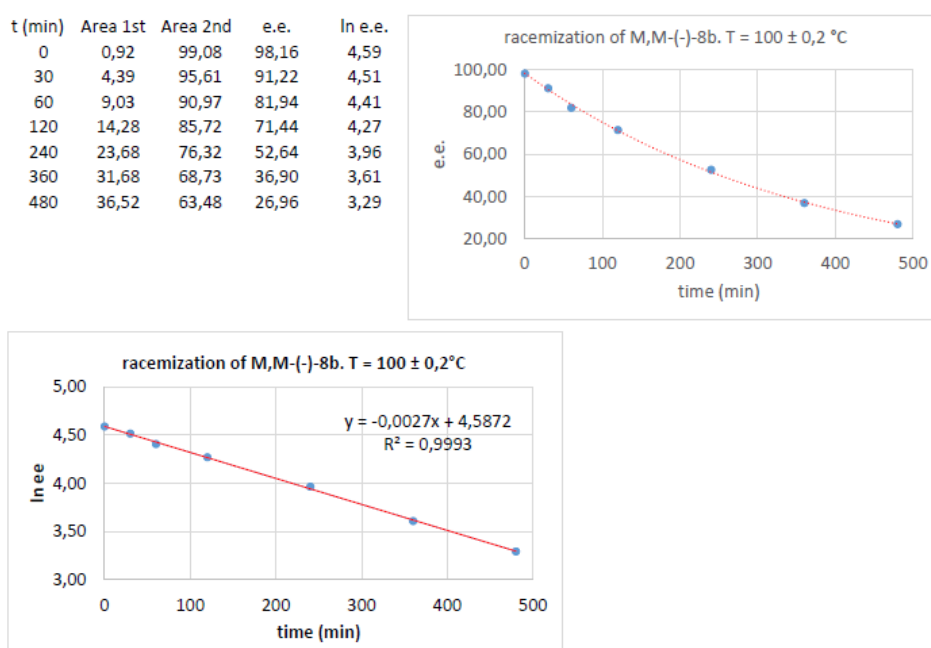
**Figure S1.** Racemization study in decalin at 100 °C.

**Chiroptical Spectroscopies**. *Polarimetric Mesurements* was performed on a Jasco P 1030 polarimeter, with temperature control and Na and Hg sources and filters for studying ORD. A 10 mm cylindrical cuvette was used on $CH_2Cl_2$ solutions, c = $8.69 \times 10^{-3}$ g/L. *UV-CD spectra* were run on Jasco 815SE CD spectrometer on $1.1 \times 10^{-4}$ M/$CH_2Cl_2$ solutions in 2 mm quartz cuvette. *Fluorescence and CPL spectra* were recorded on a home-built apparatus using a Jasco FP8200 polarimeter as a source with radiation brought to the sample through a water-filled optical fiber. Measurements were made with a 90° geometry on $10^{-5}$ M/$CH_2Cl_2$ solutions contained in a 2 mm x 10 mm fluorescence cuvette. 5 scans were necessary in order to increase signal-to-noise.

**Raman Spectroscopy**. The FT-Raman spectrum of **8b** was recorded on powder samples as received from the chemical synthesis. FT-Raman Nicolet NXR9650 equipment was used, with Nd-$YVO_4$ laser excitation at 1064 nm, a Peltier cooled InGaAs detector, and a spectral resolution of 4 $cm^{-1}$. Unpolarized Raman scattering was recorded in the backscattering geometry.

**Computational Methods**. Density Functional Theory calculations were carried out with the Gaussian09[5] quantum chemistry code at the B3LYP/6-31G(d,p) level to obtain the equilibrium structure of in the ground state, the normal modes of vibration, the simulated Raman spectrum in off-resonance conditions. Custom codes developed

in-house were used to post-process the data obtained from Gaussian09 calculations to obtain simulated spectra and the representation of the normal modes.

For the absorption and emission spectra TD-DFT calculations have been performed at the CAM-B3LYP/6-31G(d,p) level to obtain the results presented in Figure 4. A simplified model of **8b**, *i.e.,* **8a** has been considered, where the alkoxy groups of **8b** are simplified by methoxy groups. Gaussian bandwidths of 0.22 eV have been adopted. Calculated spectra have been red-shifted by 50 nm.

Calculations of the vibronic profile of the absorption/emission related with the $S_1$ excited state were carried out as described previously.[6-8] Briefly one evaluates the Huang-Rhys factors from the displacement $\Delta x$ of the equilibrium geometry from the ground to the excited state of interest (in our case computed with TD-CAM-B3LYP/6-31G(d,p) by Gaussian09 code). In the displaced harmonic oscillator approximation, a simple analytical expression provides the needed Franck-Condon (FC) factors as a function of the Huang-Rhys (HR) factors, which are evaluated from the dot product of the geometry displacement $\Delta x$ and the displacement vectors of the normal modes of the ground state.[6] The vibronic contributions to the total absorption/emission lineshape are finally determined (by a custom in-house developed program) by adding Lorenzian functions whose intensities are given by the Franck-Condon factors. Several half widths were considered in the range $100 - 500$ cm$^{-1}$. The choice of $300$ cm$^{-1}$ provides the best comparison with experimental data. In simulating the absorption and emission profiles we have adopted the observed $E_{00}$ transition at 2.38 eV (521 nm) to ease the comparison with experimental data. The selected 6 modes listed in Table 1 (HR factors > 0.1) were considered in the calculation of the vibronic absorption/emission line-shapes; FC of the form $< \boldsymbol{0} \,|\, \boldsymbol{n} >$ were evaluated for occupation numbers $n_k$ up to 20 for each *k-th* mode, leading to the summation of $6^{20}$ contributions (*i.e.*, approximately $3.6 \times 10^{15}$). TD-DFT calculations of the $S_1$ state and related HR factors were carried out on **8a** (a simplified model of **8b**)

## 2. Synthesis and characterization



**1a**　　　　　　**1b**　　　　　　**1d**
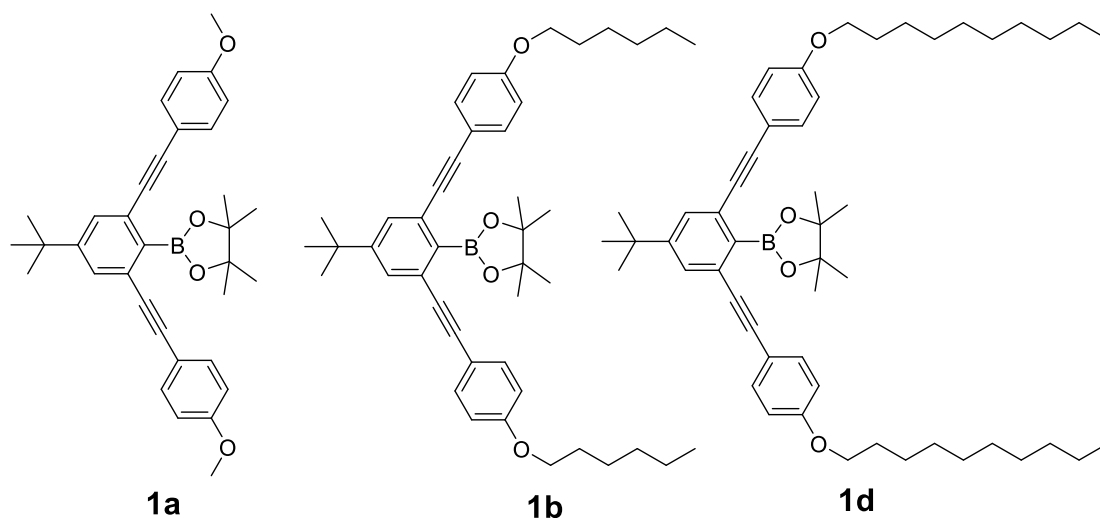
Compounds **1a**, **1b** and **1d** were synthesized according to previous report.[9]

### 2.1 Synthesis of 2,6-diynylphenyl borate 1c
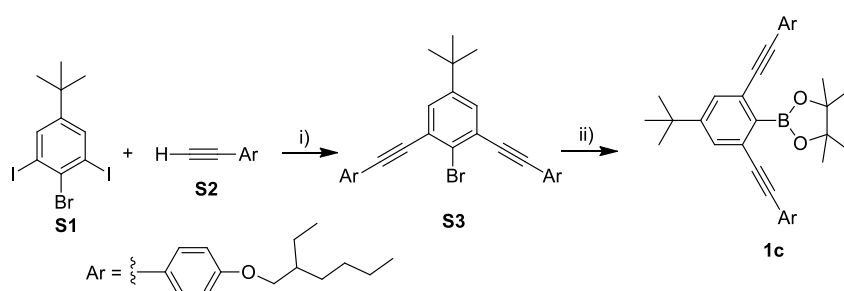


**Scheme S1:** Reagents and conditions: i) Pd(PPh₃)₂Cl₂, CuI, THF/Et₃N, RT, 14 h; ii) *n*-butyllithium (*n*-BuLi), THF, -78 °C, 1 h; isopropoxyboronic acid pinacol ester, r.t..

Synthesis of Compound **S3**:

To the solution of 2-bromo-5-(*tert*-butyl)-1,3-diiodobenzene **S1** (4.65 g, 10.0 mmol, 1.00 equiv.) and the terminal alkyne S2 (5.75 g, 25.0 mmol, 2.5 equiv.) in Et₃N (40 mL) and THF (80 mL), were added Pd(PPh₃)₂Cl₂ (70.0 mg, 0.997 mmol) and CuI (38.0 mg, 0.200 mmol). The resulting mixture was stirred under a N₂ atmosphere at room temperature for 14 h. The ammonium salt was then removed by filtration. The solvent was removed under reduced pressure and the residue was purified by column

chromatography (SiO$_2$, hexane/DCM = 8:1) to afford the product **S3** (5.83 g, 87 %). R$_f$ = 0.3 (hexane/DCM 6:1); $^1$H NMR (400 MHz, CDCl$_3$) δ 7.55 (d, $J$ = 8.9 Hz, 4H), 7.51 (s, 2H), 6.91 (d, $J$ = 8.9 Hz, 4H), 3.88 (d, $J$ = 5.8, 4H), 1.75 (dt, $J$ = 12.2, 6.1 Hz, 2H), 1.53 – 1.32 (m, 25H), 0.94 ppm (m, 12H); $^{13}$C NMR (125 MHz, CDCl$_3$) δ 159.9, 150.1, 133.3, 129.7, 126.2, 125.1, 114.8, 114.7, 93.8, 87.5, 70.7, 39.5, 34.7, 31.2, 30.6, 29.2, 24.0, 23.2, 14.2, 11.3 ppm; HRMS (ESI, positive) *m/z* calcd for C$_{42}$H$_{53}$BrO$_2$ [M + Na]$^+$ 691.3127, found 691.3114.

Synthesis of Compound **1c**:

To a solution of aryl bromide **S3** (6.70 g, 10.0 mmol, 1.0 equiv.) in THF (50 mL) at -78 °C was added a solution of *n*-butyllithium in hexanes (5 mL, 2.5 M, 1.25 equiv.). After stirring for 1 h at -78 °C, isopropoxyboronic acid pinacol ester (2.79 g, 15.0 mmol, 1.5 equiv.) was added, the reaction removed from the cooling bath and allowed to warm. Upon reaching room temperature the reaction was quenched by the addition of H$_2$O, and then extracted with DCM. The extract was washed with water, dried with Na$_2$SO$_4$, filtered and concentrated in vacuo. The residue was purified by flash column chromatography (SiO$_2$, hexane/DCM = 2:1) to afford product **1c** (4.37 g, 61 %). R$_f$ = 0.3 (hexane/DCM 1:1); $^1$H NMR (400 MHz, CDCl$_3$) δ 7.53 (s, 2H), 7.50 (d, J = 8.9 Hz, 4H), 6.90 (d, J = 8.9 Hz, 4H), 3.87 (d, J = 5.9 Hz, 4H), 1.75 (dt, J = 12.1, 6.1 Hz, 2H), 1.57 – 1.28 (m, 37H), 0.99 – 0.91 ppm (m, 12H); $^{13}$C NMR (125 MHz, CDCl$_3$) δ 159.4, 152.0, 132.9, 128.5, 126.9, 115.4, 114.5, 90.0, 88.7, 84.0, 70.5, 39.4, 34.6, 31.6, 31.0, 30.6, 29.1, 25.0, 23.9, 23.1, 22.7, 14.1, 11.2 ppm; HRMS (ESI, positive) *m/z* calcd for C$_{48}$H$_{66}$BO$_4$ [M + H]$^+$ 717.5054, found 717.5053.

## 2.3 Synthesis of *para*-terphenyl derivatives 2
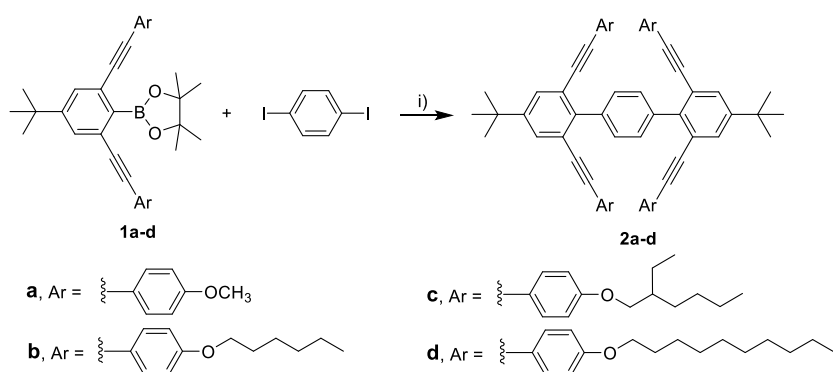
**Scheme S2:** Conditions: i) $Pd(PPh_3)_4$, $Ag_2CO_3$, THF, 80 °C, 24 h.

Synthesis of compound **2**:

1,4-diiodobenzene (330 mg, 1.00 mmol, 1.0 equiv.), 2,6-diynylphenyl borate **1** (2.20 mmol, 2.2 equiv.) and $Ag_2CO_3$ (1.10 g, 4.00 mmol, 4 equiv.) were dissolved in anhydrous THF (60 mL). $Pd(PPh_3)_4$ (116 mg, 0.10 mmol, 0.1 equiv.) was added to the solution before degassing the mixture via bubbling nitrogen for 30 min. The resulting mixture was stirred under a $N_2$ atmosphere at 80 °C for 24 h. After the reaction was complete, the mixture was diluted with DCM, washed with $H_2O$ and dried over $Na_2SO_4$. The solvent was removed under reduced pressure and the residue was purified by column chromatography to give compound **2**.

**2a**: Purification by flash column chromatography (silica gel, hexane:DCM = 1:1, v/v) yielded pure **2a** as an orange solid (362 mg, 42 %). $R_f$ = 0.3 (hexane/DCM 2:3); FTIR (neat) 2955, 2835, 2205, 1604, 1567, 1507, 1463, 1440 $cm^{-1}$; $^1H$ NMR (500 MHz, CDCl$_3$) δ 7.71 (s, 4H), 7.65 (s, 4H), 7.04 (d, $J$ = 8.8 Hz, 8H), 6.53 (d, $J$ = 8.8 Hz, 8H), 3.64 (s, 12H), 1.45 ppm (s, 18H). $^{13}C$ NMR (125 MHz, CDCl$_3$) δ 159.3, 150.2, 143.7, 138.8, 133.0, 129.6, 128.6, 123.5, 115.3, 113.8, 92.9, 88.3, 55.2, 34.8, 31.4 ppm; HRMS (ESI, positive) $m/z$ calcd for $C_{62}H_{54}O_4$ [M + Na]$^+$ 885.3920, found 885.3904.

**2b**: Purification by flash column chromatography (silica gel, hexane:DCM = 3:1, v/v) yielded pure **2b** as a white solid (446 mg, 39 %). $R_f$ = 0.3 (hexane/DCM 2:1); FTIR (neat) 2929, 2858, 2206, 1605, 1586, 1566, 1507, 1467 $cm^{-1}$; $^1H$ NMR (400 MHz, CDCl$_3$) δ 7.78 (s, 4H), 7.71 (s, 4H), 7.10 (d, $J$ = 8.7 Hz, 8H), 6.58 (d, $J$ = 8.8 Hz, 8H),

3.80 (t, $J$ = 6.5 Hz, 8H), 1.76 – 1.68 (m, 8H), 1.51 – 1.34 (m, 42H), 0.95 ppm (t, $J$ = 6.8 Hz, 12H); $^{13}$C NMR (100 MHz, CDCl$_3$) δ 158.9, 150.1, 143.6, 138.8, 132.9, 129.6, 128.5, 123.6, 115.0, 114.3, 93.1, 88.2, 67.9, 34.7, 31.7, 31.3, 29.2, 25.8, 22.7, 14.2 ppm; HRMS (ESI, positive) $m/z$ calcd for C$_{82}$H$_{94}$O$_4$ [M + Na]$^+$ 1165.7044, found 1165.7044.

**2c**: Purification by flash column chromatography (silica gel, hexane:DCM = 4:1, v/v) yielded pure **2c** as a yellow oil (590 mg, 47 %). R$_f$ = 0.5 (hexane/DCM 2:1); FTIR (neat) 2956, 2925, 2859, 2206, 1604, 1586, 1565, 1538, 1507, 1463 cm$^{-1}$; $^1$H NMR (500 MHz, CDCl$_3$) δ 7.72 (s, 4H), 7.66 (s, 4H), 7.05 (d, $J$ = 8.8 Hz, 8H), 6.54 (d, $J$ = 8.8 Hz, 8H), 3.66 (m, 8H), 1.68 – 1.60 (m, 4H), 1.46 (s, 18H), 1.42 – 1.27 (m, 32H), 0.94 – 0.87 ppm (m, 24H); $^{13}$C NMR (125 MHz, CDCl$_3$) δ 159.2, 150.1, 143.7, 138.8, 132.9, 129.6, 128.5, 123.6, 115.0, 114.4, 93.1, 88.2, 70.5, 39.4, 34.7, 31.7, 31.4, 30.6, 29.2, 24.0, 23.2, 22.8, 14.2, 11.2 ppm; HRMS (ESI, positive) $m/z$ calcd for C$_{90}$H$_{110}$O$_4$ [M + H]$^+$ 1255.8482, found 1255.8454.

**2d**: Purification by flash column chromatography (silica gel, hexane:DCM = 3:1, v/v) yielded pure **2d** as a brown oil (602 mg, 44 %). R$_f$ = 0.25 (hexane/DCM 3:1); FTIR (neat) 2922, 2852, 2206, 1604, 1586, 1565, 1507, 1467 cm$^{-1}$; $^1$H NMR (500 MHz, CDCl$_3$) δ 7.76 (s, 4H), 7.70 (s, 4H), 7.09 (d, $J$ = 8.7 Hz, 8H), 6.56 (d, $J$ = 8.8 Hz, 8H), 3.80 (t, $J$ = 6.6 Hz, 8H), 1.74 – 1.69 (m, 8H), 1.50 – 1.31 (m, 74H), 0.94 ppm (t, $J$ = 6.9 Hz, 12H); $^{13}$C NMR (125 MHz, CDCl$_3$) δ 159.0, 150.0, 143.6, 138.8, 132.9, 129.6, 128.5, 123.6, 115.0, 114.3, 93.1, 88.2, 67.9, 34.7, 32.0, 31.4, 29.7, 29.7, 29.5, 29.5, 29.3, 26.2, 22.8, 14.3 ppm; HRMS (ESI, positive) $m/z$ calcd for C$_{98}$H$_{126}$O$_4$ [M +Na]$^+$ 1389.9548, found 1389.9539.

**2.4 Synthesis of bis-cyclization products 4**
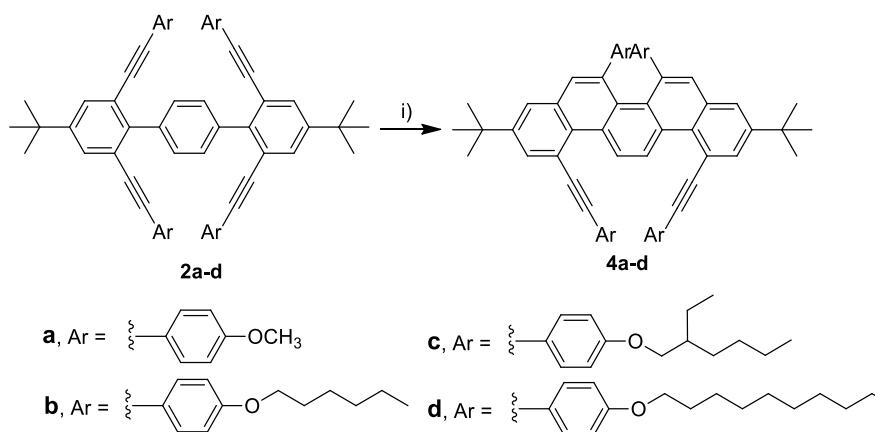
**Scheme S3:** Conditions: i) Trifluoroacetic acid (TFA), DCM, 0 °C, 1h.

Synthesis of bis-cyclization product **4**:

In a flame dried flask under a nitrogen atmosphere, **2** (0.100 mmol) was dissolved in anhydrous DCM (50 mL), and cooled to 0 °C. TFA (570 mg, 5.00 mmol) was added by syringe to the solution. The reaction mixture was stirred for 1 h, and then quenched with saturated $NaHCO_3$ aqueous solution (10 mL). The mixture was washed with $H_2O$ (2 x 20 mL) and dried over $Na_2SO_4$. The solvent was then removed under reduced pressure and the residue was purified by column chromatography to give the bis-cyclization product **4**.

**4a:** Purification by flash column chromatography (silica gel, hexane:DCM = 2:3, v/v) yielded pure **4a** as a light yellow solid (83 mg, 97 %). $R_f$ = 0.2 (hexane/DCM 2:3); FTIR (neat) 2952, 2834, 2194, 1604, 1568, 1508, 1460, 1438 cm$^{-1}$; $^1$H NMR (500 MHz, CDCl$_3$) δ 10.40 (s, 2H), 8.07 (d, $J$ = 2.2 Hz, 2H), 7.85 (d, $J$ = 2.1 Hz, 2H), 7.67 (d, $J$ = 8.9 Hz, 4H), 7.39 (s, 2H), 6.85 (d, $J$ = 8.9 Hz, 4H), 6.43 – 6.75 (br, 8H), 3.83 (s, 6H), 3.82 (s, 6H), 1.53 ppm (s, 18H); $^{13}$C NMR (125 MHz, CDCl$_3$) δ 159.8, 158.4, 148.6, 140.1, 136.3, 133.4, 132.9, 132.5, 131.4, 129.4 (br), 128.6, 128.5, 128.3 (br), 126.5, 125.3, 123.5, 119.4, 116.1, 114.6 (br), 114.3, 112.5 (br), 94.4, 91.7, 55.5, 55.4, 34.8, 31.7, 31.4, 22.8, 14.3 ppm; HRMS (ESI, positive) $m/z$ calcd for C$_{62}$H$_{54}$O$_4$ [M + Na]$^+$ 885.3920, found 885.3923.

**4b**: Purification by flash column chromatography (silica gel, hexane:DCM = 2:1, v/v)

yielded pure **4b** as an orange solid (107 mg, 94 %). $R_f$ = 0.25 (hexane/DCM 2:1); FTIR (neat) 2952, 2928, 2858, 2197, 1604, 1508, 1466 cm$^{-1}$; $^1$H NMR (400 MHz, CDCl$_3$) δ 10.35 (s, 2H), 8.02 (s, 2H), 7.80 (s, 2H), 7.61 (d, $J$ = 7.4 Hz, 4H), 7.35 (s, 2H), 6.81 (d, $J$ = 8.3 Hz, 4H), 6.39 – 6.65 (br, 8H), 3.97 – 3.86 (m, 8H), 1.83 – 1.74 (m, 8H), 1.50 – 1.33 (m, 42H), 0.92 ppm (d, $J$ = 2.4 Hz, 12H); $^{13}$C NMR (100 MHz, CDCl$_3$) δ 159.4, 157.9, 148.5, 140.2, 136.2, 133.4, 132.9, 132.5, 131.4, 128.60, 128.56, 126.5, 125.2, 123.5, 119.4, 115.8, 114.9, 94.5, 91.6, 68.3, 68.2, 34.8, 31.83, 31.77, 31.4, 29.5, 29.4, 25.91, 25.89, 22.80, 22.77, 14.23, 14.20 ppm; HRMS (ESI, positive) $m/z$ calcd for C$_{82}$H$_{94}$O$_4$ [M + Na]$^+$ 1165.7044, found 1165.7048.

**4c**: Purification by flash column chromatography (silica gel, hexane:DCM = 4:1, v/v) yielded pure **4c** as a yellow oil (121 mg, 96 %). $R_f$ = 0.2 (hexane/DCM 4:1); FTIR (neat) 2956, 2925, 2858, 2196, 1604, 1508, 1462 cm$^{-1}$; $^1$H NMR (500 MHz, CDCl$_3$) δ 10.39 (s, 2H), 8.08 (d, $J$ = 2.1 Hz, 2H), 7.87 (d, $J$ = 2.1 Hz, 2H), 7.68 (d, $J$ = 8.8 Hz, 4H), 7.41 (s, 2H), 6.90 (d, $J$ = 8.8 Hz, 4H), 6.53 – 6.72 (br, 8H), 3.92 – 3.85 (m, 8H), 1.80 (m, 4H), 1.56 – 1.33 (m, 50H), 1.06 – 0.96 ppm (m, 24H); $^{13}$C NMR (125 MHz, CDCl$_3$) δ 159.7, 158.2, 158.2, 148.5, 140.3, 136.1, 133.4, 132.9, 132.4, 131.4, 129.3 (br), 128.7, 128.6, 128.3 (br), 126.5, 125.2, 123.5, 119.5, 115.7, 115.2 (br), 114.9, 113.4 (br), 94.5, 91.6, 70.9, 70.9, 70.8, 70.8, 39.6, 39.5, 34.8, 31.4, 30.7, 30.7, 30.6, 29.3, 29.3, 29.2, 24.1, 24.0, 24.0, 23.3, 23.3, 23.2, 14.3, 14.3, 11.3, 11.3, 11.3, 11.3 ppm; HRMS (ESI, positive) $m/z$ calcd for C$_{90}$H$_{110}$O$_4$ [M + Na]$^+$ 1277.8296, found 1277.8295.

**4d**: Purification by flash column chromatography (silica gel, hexane:DCM = 3:1, v/v) yielded pure **4d** as yellow oil (130 mg, 95 %). $R_f$ = 0.2 (hexane/DCM 3:1); FTIR (neat) 2922, 2852, 2197, 1775, 1604, 1508, 1467 cm$^{-1}$; $^1$H NMR (400 MHz, CDCl$_3$) δ 10.36 (s, 2H), 8.03 (d, $J$ = 1.9 Hz, 2H), 7.81 (d, $J$ = 1.8 Hz, 2H), 7.63 (d, $J$ = 8.6 Hz, 4H), 7.36 (s, 2H), 6.83 (d, $J$ = 8.7 Hz, 4H), 6.48 - 6.57 (br, 8H), 4.03 – 3.87 (m, 8H), 1.81 (d, $J$ = 6.0 Hz, 8H), 1.55 – 1.21 (m, 74H), 0.90 ppm (m, 12H); $^{13}$C NMR (125 MHz, CDCl$_3$) δ 159.3, 157.8, 148.4, 140.1, 136.0, 133.2, 132.8, 132.3, 131.2, 129.3 (br), 128.5, 128.4, 128.2 (br), 126.3, 125.1, 123.3, 119.3, 115.7, 115.1 (br), 114.7, 113.5 (br), 94.3, 91.5,

68.15, 68.09, 34.6, 31.9, 31.3, 29.64, 29.61, 29.50, 29.48, 29.38, 29.36, 29.3, 26.10, 26.09, 22.7, 14.1ppm; HRMS (ESI, positive) $m/z$ calcd for $C_{98}H_{126}O_4$ [M + Na]$^+$ 1389.9548, found 1389.9554.

## 2.5 Synthesis of chiral peropyrenes 8
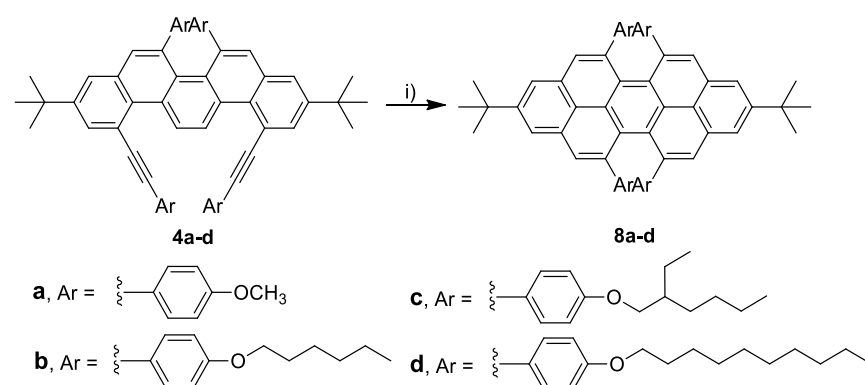


**Scheme S4:** Conditions: i) triflic acid, DCM, -40 °C, 30 min, then lowly warmed to -10 °C.

Synthesis of chiral peropyrenes **8**:

To a solution of triflic acid (150 mg, 1.00 mmol, 20 equiv.) in 30 mL of anhydrous $CH_2Cl_2$ at -40 °C was added dropwise anhydrous $CH_2Cl_2$ (20 mL) solution of **4** (0.05 mmol, 1 equiv.) by syringe. After stirring for 30 min -40 °C, the reaction was warmed slowly to -10 °C over 30 minutes. The solution was quenched with saturated NaHCO$_3$ solution (5 mL), and then washed with H$_2$O (2 x 20 mL). The solvent was dried (Na$_2$SO$_4$) and removed under reduced pressure. The residue was purified by column chromatography give chiral peropyrenes **8**.

**8a**: Purification by flash column chromatography (SiO$_2$, hexane/DCM = 1:1, v/v) yielded pure **8a** as an orange solid (12 mg, 28 %).{Tri-cyclized side product **7a** was isolated as light yellow solid (2 mg)}
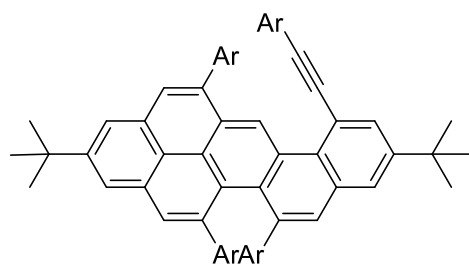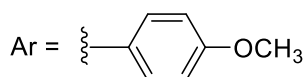
**7a**: $R_f = 0.2$ (hexane/DCM 2:3); FTIR (neat) 2955, 2904, 2835, 2195, 1606, 1510, 1245 cm$^{-1}$; $^1$H NMR (500 MHz, CDCl3) δ 10.71 (s, 1H), 8.17 – 8.14 (m, 2H), 7.97 (d, J = 2.1 Hz, 1H), 7.93 (s, 1H), 7.85 (d, J = 2.1 Hz, 1H), 7.77 (s, 1H), 7.61 (d, J = 8.8 Hz, 2H), 7.35 (s, 1H), 7.18 (d, J = 8.8 Hz, 2H), 6.85 – 6.82 (m, 2H), 6.76 – 6.879 (m, 2H), 6.72 – 6.41 (br, 8H), 3.88 (s, 3H), 3.842 (s, 3H), 3.838 (s, 3H), 3.80 (s, 3H), 1.60 (s, 9H), 1.50 ppm (s, 9H); $^{13}$C NMR (100 MHz, CDCl$_3$) δ 159.6, 159.1, 158.4, 158.3, 149.7, 148.9, 140.3, 139.94, 139.85, 137.1, 136.5, 133.35, 133.30, 133.1, 132.3, 131.5, 131.35, 131.30, 130.0, 129.0 (br), 128.7, 128.24, 128.2 (br), 128.0, 127.8, 127.5, 125.9, 125.81, 125.76, 125.0, 123.0, 122.5, 122.0, 121.4, 119.9, 115.9, 114.7 (br), 113.82, 113.76, 112.6 (br), 93.4, 90.4, 55.58, 55.53, 55.3, 35.4, 34.8, 32.0, 31.5 ppm, {four carbon signals are missing due to broaden and the poor solubility}; MS (MALDI-TOF): calcd for C$_{62}$H$_{54}$O$_4$ [M + H]$^+$ 863.409, found 863.203.

**8a**: $R_f = 0.1$ (hexane/DCM 2:3); FTIR (neat) 2948, 2833, 1607, 1568, 1506, 1460 cm$^{-1}$; $^1$H NMR (400 MHz, CDCl3) δ 8.23 (s, 4H), 7.79 (s, 4H), 6.51– 6.91 (br, 16H), 3.85 (s, 12H), 1.62 ppm (s, 18H); $^{13}$C NMR (125 MHz, CDCl$_3$) δ 158.5, 149.6, 139.8, 136.7, 131.6, 128.2, 126.1, 124.1, 122.9, 120.5, 55.6, 35.4, 32.1 ppm, {four carbon signals are missing due to broaden and the poor solubility}; HRMS (ESI, positive) *m/z* calcd for C$_{62}$H$_{54}$O$_4$ [M + Na]$^+$ 885.3920, found 885.3922.

**8b**: Purification by flash column chromatography (SiO$_2$, hexane/DCM = 2:1, v/v) yielded pure **8b** as an orange solid (23 mg, 40 %). $R_f = 0.2$ (hexane/DCM 2:1); FTIR (neat) 2950, 2927, 2857, 1606, 1580, 1505, 1465 cm$^{-1}$; $^1$H NMR (400 MHz, CDCl$_3$) δ 8.23 (s, 4H), 7.80 (s, 4H), 6.74 – 7.02 (br, 16H), 4.12 – 3.87 (m, 8H), 1.97 – 1.74 (m, 8H), 1.74 – 1.55 (m, 18H), 1.54 – 1.18 (m, 24H), 1.05 – 0.85 ppm (m, 12H); $^{13}$C NMR (100 MHz, CDCl$_3$) δ 158.0, 149.5, 139.9, 136.6, 131.6, 129.0 (br), 128.1, 128.0 (br), 126.1, 124.1, 122.8, 120.4, 115.3 (br), 113.7 (br), 68.3, 35.3, 32.1, 31.9, 29.5, 25.9, 22.8,

14.3 ppm; HRMS (ESI, positive) $m/z$ calcd for $C_{82}H_{94}O_4$ $[M + Na]^+$ 1165.7044, found 1165.7038.

**8c**: Purification by flash column chromatography (SiO$_2$, hexane/DCM = 3:1, v/v) yielded pure **8c** as brown solid (24 mg, 38 %). $R_f$ = 0.25 (hexane/DCM 2:1); FTIR (neat) 2956, 2925, 2858, 1605, 1567, 1505, 1461 cm$^{-1}$; $^1$H NMR (500 MHz, CDCl$_3$) δ 8.23 (s, 4H), 7.79 (s, 4H), 6.46 – 6.94 (br, 16H), 4.00 – 3.77 (m, 8H), 1.80 (m, 4H), 1.74 – 1.17 (m, 50H), 1.17 – 0.77 ppm (m, 24H); $^{13}$C NMR (125 MHz, CDCl$_3$) δ 158.3, 149.5, 140.0, 136.5, 131.6, 128.9 (br), 128.2, 128.0 (br), 126.1, 124.1, 122.8, 120.4, 115.5 (br), 113.7 (br), 71.0, 70.9, 39.6, 39.5, 35.4, 32.1, 30.8, 29.9, 29.3, 24.1, 23.3, 23.3, 14.3, 14.3, 11.3, 11.3 ppm; HRMS (ESI, positive) $m/z$ calcd for $C_{90}H_{110}O_4$ $[M + H]^+$ 1255.8482, found 1255.8457.

**8d**: Purification by flash column chromatography (SiO$_2$, hexane/DCM = 2:1, v/v) yielded pure **8d** as an orange sticky oil (24 mg, 35 %). $R_f$ = 0.2 (hexane/DCM 2:1); FTIR (neat) 2923, 2853, 1607, 1506 cm$^{-1}$; $^1$H NMR (400 MHz, CDCl$_3$) δ 8.22 (s, 4H), 7.79 (s, 4H), 6.57 – 6.94 (br, 16H), 3.97 – 4.02 (m, 8H), 2.01 – 1.71 (m, 8H), 1.70 – 0.92 (m, 74H), 0.94 – 0.84 ppm (m, 12H); $^{13}$C NMR (100 MHz, CDCl$_3$) δ 158.0, 149.5, 139.9, 136.6, 131.6, 128.9 (br), 128.1, 127.9 (br), 126.1, 124.1, 122.8, 120.4, 115.3 (br), 113.8 (br), 68.3, 35.3, 32.1, 32.1, 29.9, 29.8, 29.8, 29.7, 29.6, 29.5, 26.3, 22.9, 14.3 ppm; HRMS (ESI, positive) $m/z$ calcd for $C_{98}H_{126}O_4$ $[M + Na]^+$ 1389.9548, found 1389.9547.

# 3. Computational, CD, Raman, and quantum yield study

## 3.1 Theoretical study of the interconversion.

The DFT computations on the peropyrene model with methoxyphenyl substituents were performed. In the model, all equatorial *t*-butyl residues were replaced by hydrogen. All electronic structure calculations were carried out using the GAMESS suite of programs[10,11]. The calculations were performed at the spin-restricted B3LYP/def2-SV(P)//B3LYP/def2-TZVP level of theory[12–14] using the Polarizable Continuum Model (PCM) to simulate the $CH_2Cl_2$ solvent.[15] Dispersion corrections were calculated using the Grimme's D3 scheme.[16]
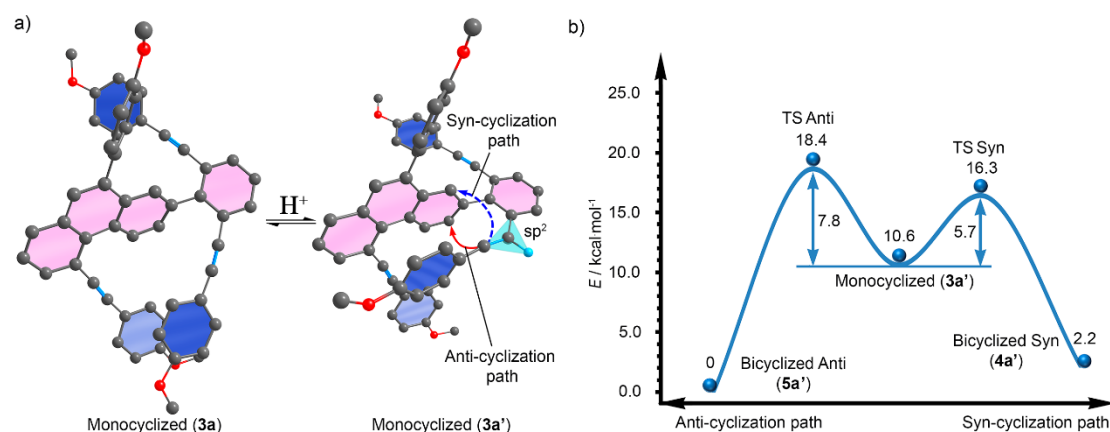


**Figure S2**. Bicyclized derivative formation. a) Protonation of monocyclized precursor **3a**. For clarity, only the hydrogen atom involved in protonation of triple C–C bond is shown. The red solid arrow indicates the *anti*-cyclization path, while the blue dashed line shows the *syn*-cyclization path. b) Reaction paths for bicyclized product formation. Protonated structures are denoted by prime.

**Table S1**. Relative internal and free energies for the bicyclized derivative formation.

| Reaction path | Structure | No Solvent | | PCM-$CH_2Cl_2$ | | | |
| | | Internal Energy, kcal/mol | | Internal Energy, kcal/mol | | Free Energy, kcal/mol | |
| | | Def2-SV(P) | Def2-TZVP | Def2-SV(P) | **Def2-TZVP** | Def2-SV(P) | Def2-TZVP |
| *Syn* | **3a′** | 11.4 | 9.7 | 12.4 | **10.6** | 9.0 | 7.4 |
| | TS (**3a′-4a**) | 17.2 | 16.2 | 17.3 | **16.3** | 16.6 | 15.6 |
| | **4a′** | 2.2 | 2.3 | 2.1 | **2.2** | 2.3 | 2.3 |
| *Syn*-barrier | | 5.8 | 6.5 | 4.9 | **5.7** | 7.6 | 8.2 |
| *Anti* | **3a′** | 11.4 | 9.7 | 12.4 | **10.6** | 9.0 | 7.4 |

| | | | | | | |
|---|---|---|---|---|---|---|
| TS (**3a′-5a**) | 19.6 | 18.3 | 19.7 | **18.4** | 19.0 | 17.9 |
| **5a′** | 0.0 | 0.0 | 0.0 | **0.0** | 0.0 | 0.0 |
| *Anti*-barrier | 8.2 | 8.6 | 7.3 | **7.8** | 10.0 | 10.5 |
| *Syn* vs. *anti* barrier | 2.4 | 2.1 | 2.4 | **2.1** | 2.4 | 2.3 |

**Table S2**. Relative internal and free energies for the tetracyclized derivative formation.

| | No Solvent | | PCM-$CH_2Cl_2$ | | | |
|---|---|---|---|---|---|---|
| | Internal Energy, kcal/mol | | Internal Energy, kcal/mol | | Free Energy, kcal/mol | |
| Structure | Def2-SV(P) | Def2-TZVP | Def2-SV(P) | **Def2-TZVP** | Def2-SV(P) | Def2-TZVP |
| Chiral (*M,M*)-**8a** | 0.0 | 0.0 | 0.0 | **0.0** | 0.0 | 0.0 |
| TS$_1$ (*M,M*)-**8a** – *meso*-**8a** | 28.2 | 29.3 | 28.1 | **29.2** | 29.0 | 30.2 |
| Achiral *meso*-**8a** | 9.8 | 9.9 | 9.9 | **10.0** | 9.6 | 9.7 |
| TS$_2$ *meso*-**8a** – (*P,P*)-**8a** | 28.2 | 29.3 | 28.1 | **29.2** | 29.0 | 30.2 |
| Chiral (*P,P*)-**8a** | 0.0 | 0.0 | 0.0 | **0.0** | 0.0 | 0.0 |

**3.2 CD spectra and ORD curve.**
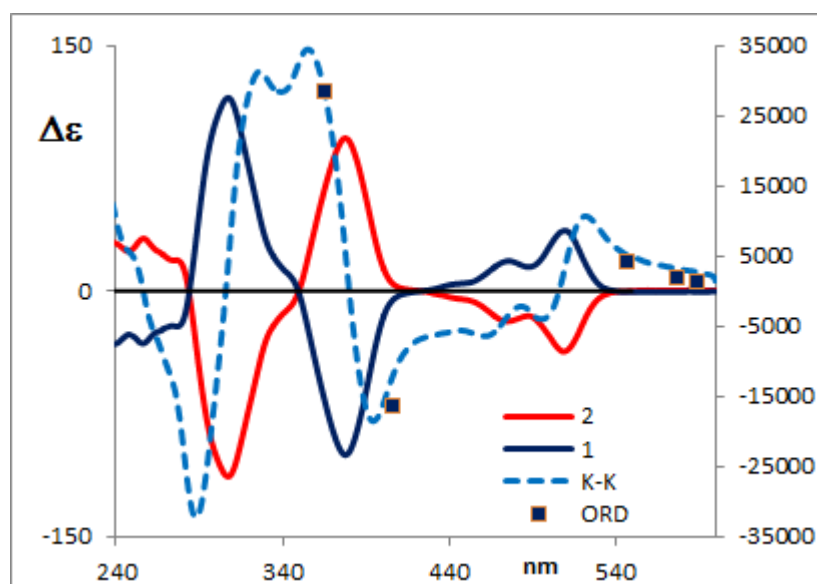


**Figure S3.** CD spectra of **8b** (blue first eluted and red second eluted) and Kramers-Kronig transformation (light blue) of the first eluted CD curve. Experimental ORD data, reported as full squares, nicely fit the K-K plot.

## 3.3 Transition moments and assignment

**Table S3**. Transition energy (eV), wavelength ($\lambda$ nm), dipole strength (D $10^{-40}$ esu$^2$cm$^2$), rotational strength (R $10^{-44}$ esu$^2$cm$^2$), magnitude of the electric and magnetic transition dipoles, |<0|$\mu$|e>|, |<0|m|e>| (atomic units) for some significant features at low energy.
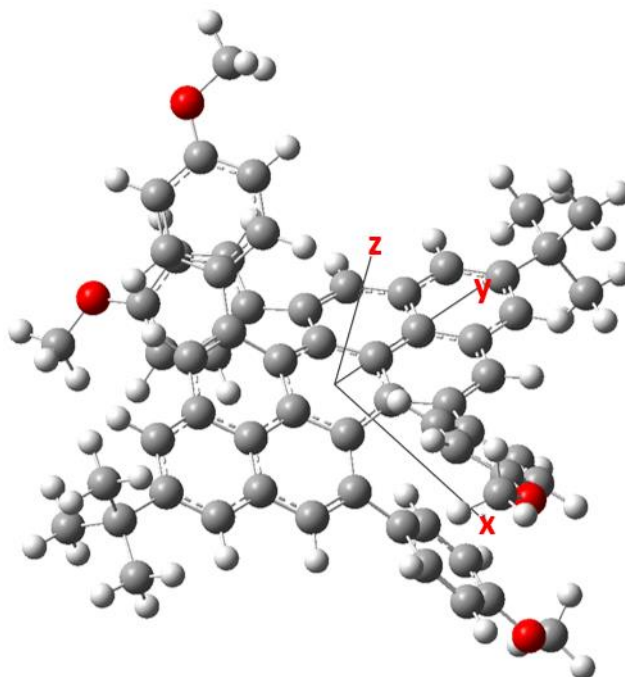


|  | eV | $\lambda$ (nm) | D | R | Transition moment direction | \|$\mu$\| | \|m\| |  |
|---|---|---|---|---|---|---|---|---|
| 1 | 2.80 | 443 | 8.6 | -220.0 | y | 2.94 | 0.32 | 229→230 (0.69) |
| 5 | 3.78 | 328 | 4.3 | 482.1 | x | 2.08 | 0.96 | 228→230(0.44) <br> 229→231 (0.41) <br> 224→230 (0.31) |
| 7 | 4.17 | 297 | 3.4 | 339.0 | x | 1.85 | 0.77 | 224→230(0.54) <br> 229→231 (-.37) |
| 1-exc.state | 2.34 | 530 | 10.7 | -222.6 | y | 3.27 | 0.29 | 229→230 (0.70) |

**3.4 TD-DFT calculation of the ground and first excited state of (M,M)-8a**
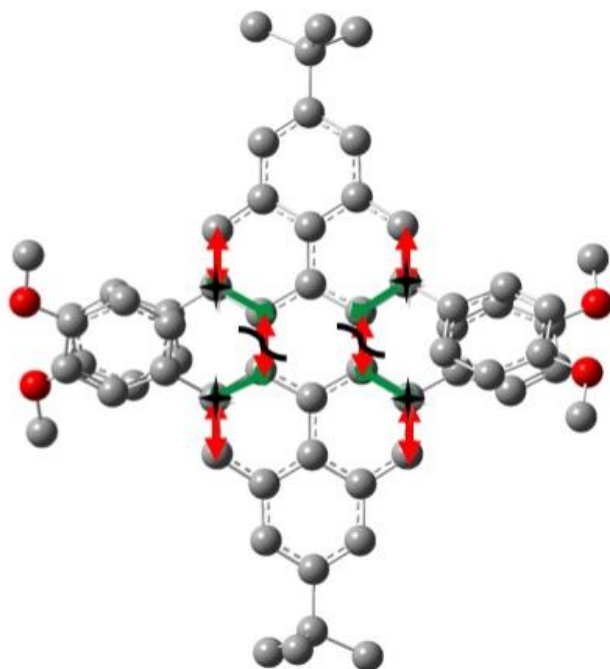


**Figure S4**. The difference of the two geometries (Red = Elongations, Green = Shortenings)

Red CC bonds are stretched in the excited state with respect to the ground state, green ones are shorter in the excited state. The deformation between the two geometries resembles the vibrations found analysing the major Franck Condon factors. The two central marked CC bonds (　　　　) being longer in the excited state, are accompanied by a slightly higher distorsion of the excited state: the dihedral angle defined by the four atoms (　　) changes from 27.6° to 31.1°.

**Table S4**. Other parameters characterizing ground and excited state:

|  |  | eV | nm | D | R(length) | R(velocity) | E-M angle | g |
|---|---|---|---|---|---|---|---|---|
| Ground state | H→L | 2.7987 | 443.0 | 558720 | -223 | -221 | 175 | -0.0016 |
| Excited state | L→H | 2.3414 | 529.5 | 690819 | -226 | -223 | 174 | -0.0013 |

**Table S5**. Characterizing ground and excited state:
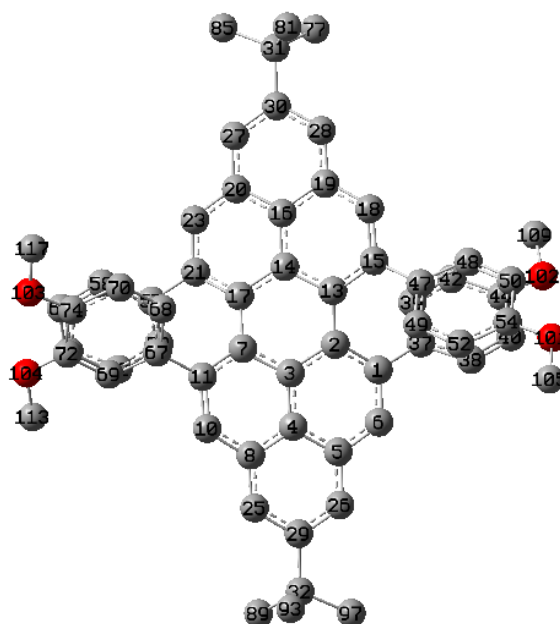


| Definition | Value | Value | |
|---|---|---|---|
| | ground | excited | Δground-excited |
| **R(1,2)** | **1.4572** | **1.4243** | **-0.0329** |
| **R(17,21)** | **1.4572** | **1.4243** | **-0.0329** |
| **R(7,11)** | **1.4584** | **1.4258** | **-0.0326** |
| **R(13,15)** | **1.4584** | **1.4258** | **-0.0326** |
| **R(5,6)** | **1.4283** | **1.4127** | **-0.0156** |
| **R(20,23)** | **1.4283** | **1.4127** | **-0.0156** |
| **R(8,10)** | **1.4295** | **1.4158** | **-0.0137** |
| **R(18,19)** | **1.4295** | **1.4158** | **-0.0137** |
| **R(3,4)** | **1.4293** | **1.4174** | **-0.0119** |
| **R(14,16)** | **1.4293** | **1.4174** | **-0.0119** |
| **R(1,37)** | **1.4878** | **1.484** | **-0.0038** |
| **R(21,57)** | **1.4878** | **1.484** | **-0.0038** |
| **R(11,67)** | **1.4879** | **1.4844** | **-0.0035** |
| **R(15,47)** | **1.4879** | **1.4844** | **-0.0035** |
| R(26,29) | 1.392 | 1.3908 | -0.0012 |
| R(27,30) | 1.392 | 1.3908 | -0.0012 |
| R(39,42) | 1.3918 | 1.3908 | -0.001 |
| R(59,62) | 1.3918 | 1.3908 | -0.001 |
| R(49,52) | 1.3918 | 1.3909 | -0.0009 |
| R(68,70) | 1.3918 | 1.3909 | -0.0009 |
| R(2,3) | 1.426 | 1.4252 | -0.0008 |
| R(14,17) | 1.426 | 1.4252 | -0.0008 |
| R(44,102) | 1.3607 | 1.3599 | -0.0008 |

| | | | |
|---|---|---|---|
| R(64,104) | 1.3607 | 1.3599 | -0.0008 |
| R(54,101) | 1.3607 | 1.3601 | -0.0006 |
| R(74,103) | 1.3607 | 1.3601 | -0.0006 |
| R(31,81) | 1.539 | 1.5389 | -1E-04 |
| R(31,85) | 1.5329 | 1.5328 | -1E-04 |
| R(32,93) | 1.539 | 1.5389 | -1E-04 |
| R(32,97) | 1.5329 | 1.5328 | -1E-04 |
| R(31,77) | 1.5389 | 1.5389 | 0 |
| R(32,89) | 1.5389 | 1.5389 | 0 |
| R(38,40) | 1.381 | 1.381 | 0 |
| R(58,60) | 1.381 | 1.381 | 0 |
| R(40,44) | 1.3962 | 1.3963 | 1E-04 |
| R(48,50) | 1.381 | 1.3811 | 1E-04 |
| R(60,64) | 1.3962 | 1.3963 | 1E-04 |
| R(69,72) | 1.381 | 1.3811 | 1E-04 |
| R(50,54) | 1.3961 | 1.3963 | 0.0002 |
| R(72,74) | 1.3961 | 1.3963 | 0.0002 |
| R(102,109) | 1.41 | 1.4103 | 0.0003 |
| R(104,113) | 1.41 | 1.4103 | 0.0003 |
| R(101,105) | 1.4099 | 1.4103 | 0.0004 |
| R(103,117) | 1.4099 | 1.4103 | 0.0004 |
| R(47,48) | 1.4009 | 1.4014 | 0.0005 |
| R(67,69) | 1.4009 | 1.4014 | 0.0005 |
| R(3,7) | 1.4254 | 1.426 | 0.0006 |
| R(13,14) | 1.4254 | 1.426 | 0.0006 |
| R(37,38) | 1.4009 | 1.4015 | 0.0006 |
| R(57,58) | 1.4009 | 1.4015 | 0.0006 |
| R(29,32) | 1.5338 | 1.5345 | 0.0007 |
| R(30,31) | 1.5338 | 1.5345 | 0.0007 |
| R(52,54) | 1.3924 | 1.3932 | 0.0008 |
| R(70,74) | 1.3924 | 1.3932 | 0.0008 |
| R(42,44) | 1.3924 | 1.3933 | 0.0009 |
| R(62,64) | 1.3924 | 1.3933 | 0.0009 |
| R(37,39) | 1.3931 | 1.3941 | 0.001 |
| R(47,49) | 1.393 | 1.394 | 0.001 |
| R(57,59) | 1.3931 | 1.3941 | 0.001 |
| R(67,68) | 1.393 | 1.394 | 0.001 |
| R(25,29) | 1.3969 | 1.3982 | 0.0013 |
| R(28,30) | 1.3969 | 1.3982 | 0.0013 |
| **R(4,8)** | **1.4133** | **1.4174** | 0.0041 |
| **R(16,19)** | **1.4133** | **1.4174** | 0.0041 |
| **R(4,5)** | **1.4104** | **1.4153** | 0.0049 |
| **R(16,20)** | **1.4104** | **1.4153** | 0.0049 |

| | | | |
|---|---|---|---|
| R(8,25) | 1.3951 | 1.4049 | 0.0098 |
| R(19,28) | 1.3951 | 1.4049 | 0.0098 |
| R(5,26) | 1.4001 | 1.4117 | 0.0116 |
| R(20,27) | 1.4001 | 1.4117 | 0.0116 |
| R(10,11) | 1.3608 | 1.3845 | 0.0237 |
| R(15,18) | 1.3608 | 1.3845 | 0.0237 |
| R(1,6) | 1.3616 | 1.3866 | 0.025 |
| R(21,23) | 1.3616 | 1.3866 | 0.025 |
| R(2,13) | 1.4196 | 1.4636 | 0.044 |
| R(7,17) | 1.4196 | 1.4636 | 0.044 |

## 3.5 Calculated absorption and emission spectra, based on TD-DFT and Huang-Rhys approximation

The calculation of the vibronic structure in absorption/emission of $S_1$ was carried out as described in the main text, using the HR factors listed in Table S7. The top panel of Figure S5 shows the effect of the Lorentzian half width (values given in cm$^{-1}$) in the simulation of the line shapes. The best fit *vs.* the experimental spectra is found for a half width of 300 cm$^{-1}$.
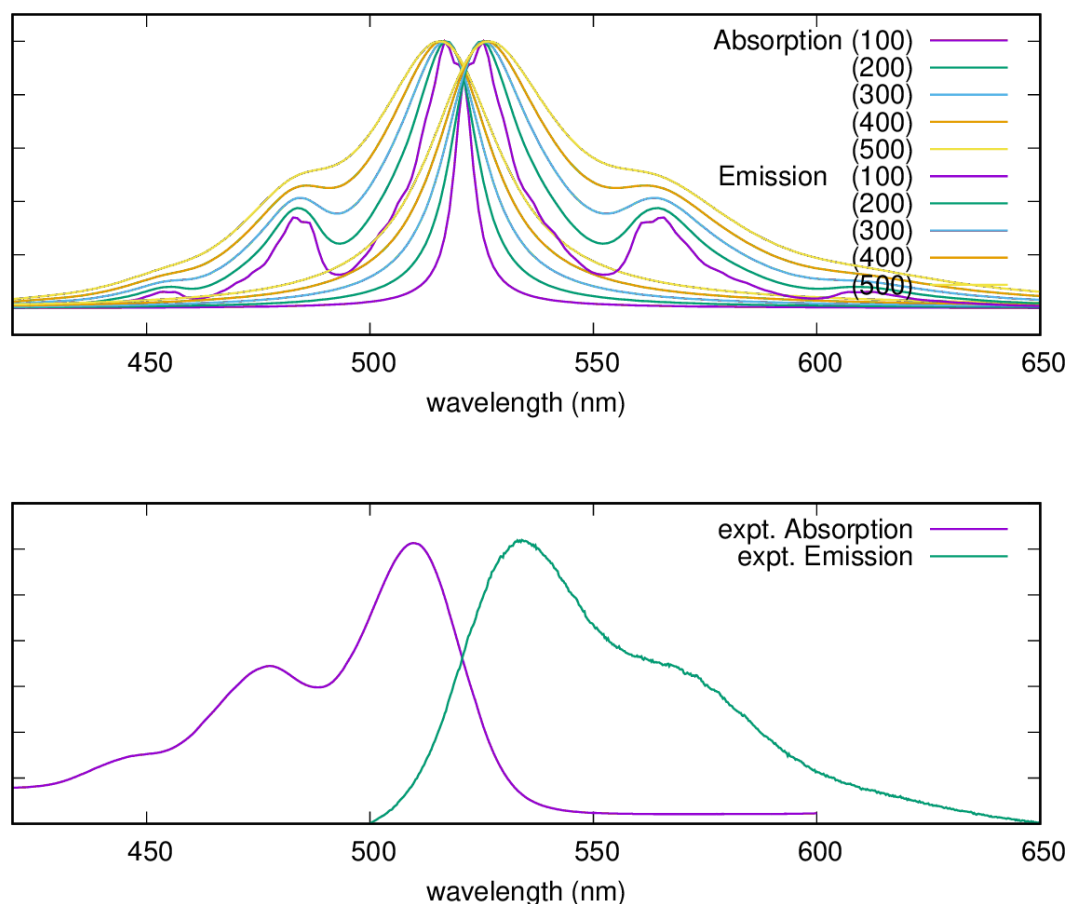
**Figure S5**. (top panel) Simulated absorption/emission line shapes relative to the $S_1$ state of **8a** according to HR factors determined by TD-CAM-B3LYP/6-31G(d,p) calculations. The bottom panel display the corresponding experimental data of **8b** in solution state (see main text for experimental details).

Calculations of the Raman response are commonly carried out with the B3LYP functional, which was shown to reliably account for the vibrational structure of several polycyclic aromatic hydrocarbons (see for instance refs. 24a, 26 of the main text). Hence it is relevant comparing the modes with large HR factors in CAM-B3LYP and B3LYP calculations. This comparison is reported in Table S6 below. The reported

assignment of the modes with large HR factors is based on the inspection of the nuclear displacements (see Figure S5 and the animations enclosed with this Supporting Information). Boldface entries in Table S7 are associated to matching nuclear displacements in CAM-B3LYP and B3LYP calculations. This can be verified by direct inspection of Figure S6. Table S6 reveals that HR factors are generally larger in the CAM-B3LYP case than in B3LYP. This is consistent with the larger Stokes shift determined in the CAM-B3LYP simulated spectrum with respect to the B3LYP case (see Figure S7). In the case of CAM-B3LYP calculations instead of one D mode one finds two closely spaced normal modes. They share with the D mode determined by B3LYP the characteristic nuclear displacements at the center of the molecule and merely differ by the in-phase/out-of-phase coupling with the Kekulé vibration at the four phenyl substituents (see Figure S6). The longitudinal stretching mode determined by B3LYP (with the smallest HR factor) is not included in CAM-B3LYP due to the larger threshold used in the latter.

**Table S6**. Absorption, emission maxima, Stokes shift, and emission efficiencies obtained for the compounds **8b**.

| compound | absorption$_{max}$ (nm) | emission$_{max}$ (nm) | stokes shift (cm$^{-1}$) | emission efficiencies ($\phi$) |
|:---:|:---:|:---:|:---:|:---:|
| **8b** | 512 | 531 | 680 | 22.2 ± 0.3 |

**Table S7**. List of HR factors considered in the calculation of the vibronic line-shape reported in Figures S4 and S6. Functional for ground state vibrational structure and TD calculations: (a) B3LYP; (b) CAM-B3LYP. Just the modes with HR > 0.05 (B3LYP) or HR > 0.1 (CAM-B3LYP) have been selected to keep reasonable the computational cost of the simulation of the vibronic line shape.

| (a) B3LYP (HR > 0.05) | | |
|---|---|---|
| **145.1 cm$^{-1}$** | **0.3467** | **tearing mode** |
| 161.0 cm$^{-1}$ | 0.0574 | longitudinal stretching |
| **186.8 cm$^{-1}$** | **0.2597** | **transversal stretching** |
| **550.7 cm$^{-1}$** | **0.0882** | **t-Bu umbrella** |
| **1329.7 cm$^{-1}$** | **0.1315** | **D line** |
| 1654.3 cm$^{-1}$ | 0.0586 | G$_1$ line, longitudinal |
| (b) CAM-B3LYP (HR > 0.1) | | |
| 108.8 cm$^{-1}$ | 0.1887 | molecular torsion |
| **147.2 cm$^{-1}$** | **0.5581** | **tearing mode** |
| **189.6 cm$^{-1}$** | **0.4194** | **transversal stretching** |
| **559.0 cm$^{-1}$** | **0.1556** | **t-Bu umbrella** |
| **1351.3 cm$^{-1}$** | **0.1801** | **D line (mode 1)** |
| **1360.8 cm$^{-1}$** | **0.1369** | **D line (mode 2)** |

1351 cm$^{-1}$; 0 km/mol; 3775 A$^4$/amu          1361 cm$^{-1}$; 0 km/mol; 2363 A$^4$/amu

**D modes**

CAM-B3LYP/6-31G(d,p)
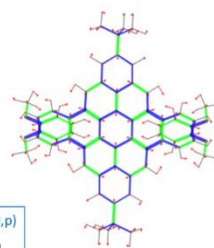
corresponding mode in B3LYP/6-31G(d,p)

1330 cm$^{-1}$; 9 km/mol; 4943 A$^4$/amu
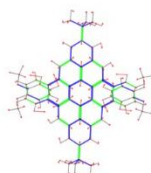
CAM-B3LYP/6-31G(d,p)

147 cm$^{-1}$; 0 km/mol; 22 A$^4$/amu

corresponding mode in B3LYP/6-31G(d,p)

145 cm$^{-1}$; 0 km/mol; 28 A$^4$/amu
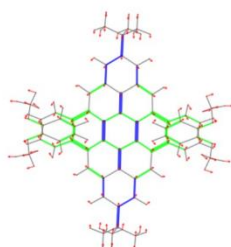
CAM-B3LYP/6-31G(d,p)

190 cm$^{-1}$; 0 km/mol; 4 A$^4$/amu
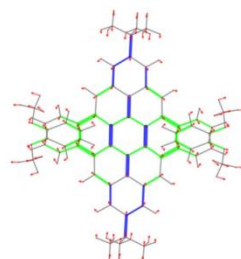
corresponding mode in B3LYP/6-31G(d,p)

187 cm$^{-1}$; 0 km/mol; 6 A$^4$/amu

CAM-B3LYP/6-31G(d,p)

559 cm$^{-1}$; 0 km/mol; 19 A$^4$/amu

corresponding mode in B3LYP/6-31G(d,p)

551 cm$^{-1}$; 0 km/mol; 32 A$^4$/amu
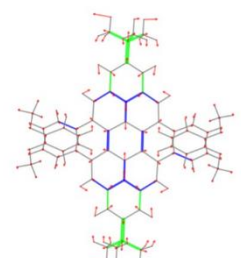
**Figure S6**. Nuclear displacements of the modes which do correspond in CAM-B3LYP and B3LYP calculations of the HR factors (see also Table S7 and the animations enclosed with this Supplementary Information).
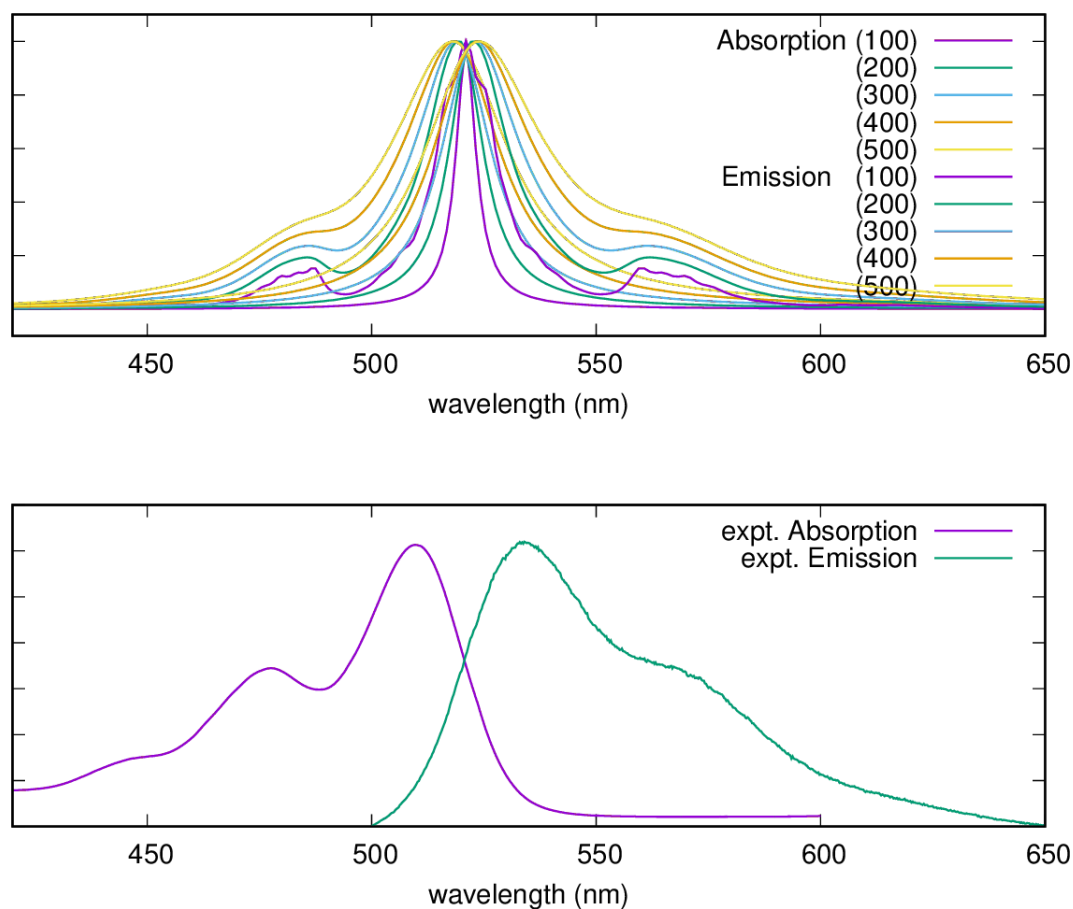
**Figure S7**. (top panel) simulated absorption/emission line shapes relative to the $S_1$ state of **8a** according to HR factors determined by TD-B3LYP/6-31G(d,p) calculations. The bottom panel display the corresponding experimental data of **8b** in solution state (see main text for experimental details).

Finally, the different role of the modes with large HR factors in determining the vibronic line-shape can be evidenced by a series of *ad hoc* calculations. Starting with the case of just the two D modes, one can progressively include the modes with lower wavenumber. As evident in Figure S8, the spacing across the vibronic progression is essentially determined by the D modes. The lower wavenumber modes significantly contribute to the broadening of the vibronic progression and to the increase of the Stokes shift.
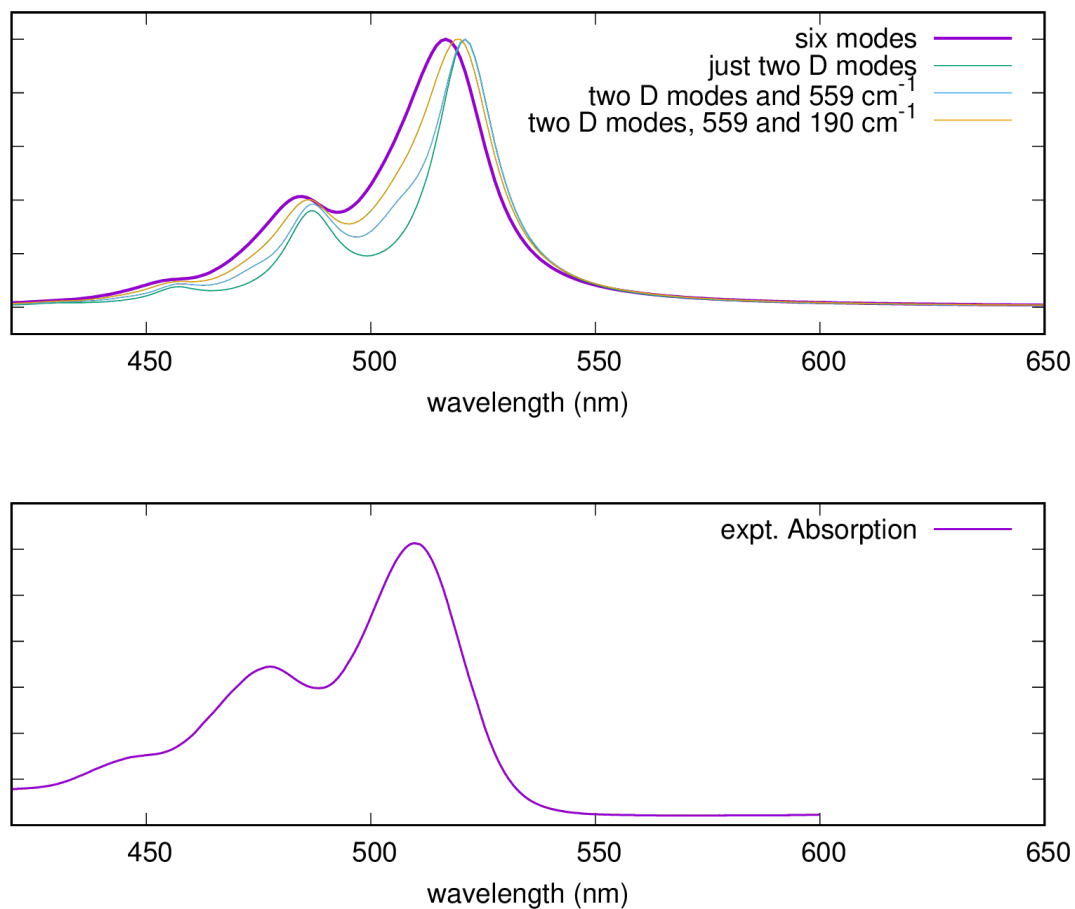
**Figure S8**. (top panel) simulated absorption/emission line shapes relative to the $S_1$ state of **8a** according to HR factors determined by TD-B3LYP/6-31G(d,p) calculations. A different number of modes is included in the calculations by selecting the entries given in Table S7(b) as indicated in the legend. The bottom panel display the corresponding experimental data of **8b** in solution state (see main text for experimental details).

**3.6 Quantum yield**

The quantum yield (QY) was calculated by preparing solutions of the sample at varying concentrations in toluene, and measuring the absorbance at 347 nm and the area under the emission peak at each different concentration. The absorbance was plotted against the area and compared to a standard of known quantum yield (quinine sulphate). This data was used to obtain a value for the quantum yield.

The quantum yield of compounds in toluene was calculated using the following equation:

$$\Phi_x = \frac{Grad_x}{Grad_{std}} \times \frac{n_x^2}{n_{std}^2} \times \Phi_{std}$$

*Grad* is the slope of the plot 'Emission area vs Absorbance', *n* is the refractive index of the solvent and *Φ* is the quantum yield for sample *x* and standard *std*.

Here Quinine Sulphate was used as reference, which has a quantum yield of 55 % when dissolved in 1N $H_2SO_4$. 1N (0.5M) $H_2SO_4$ had a refractive index of 1.346, while the refractive index of toluene is 1.4968.
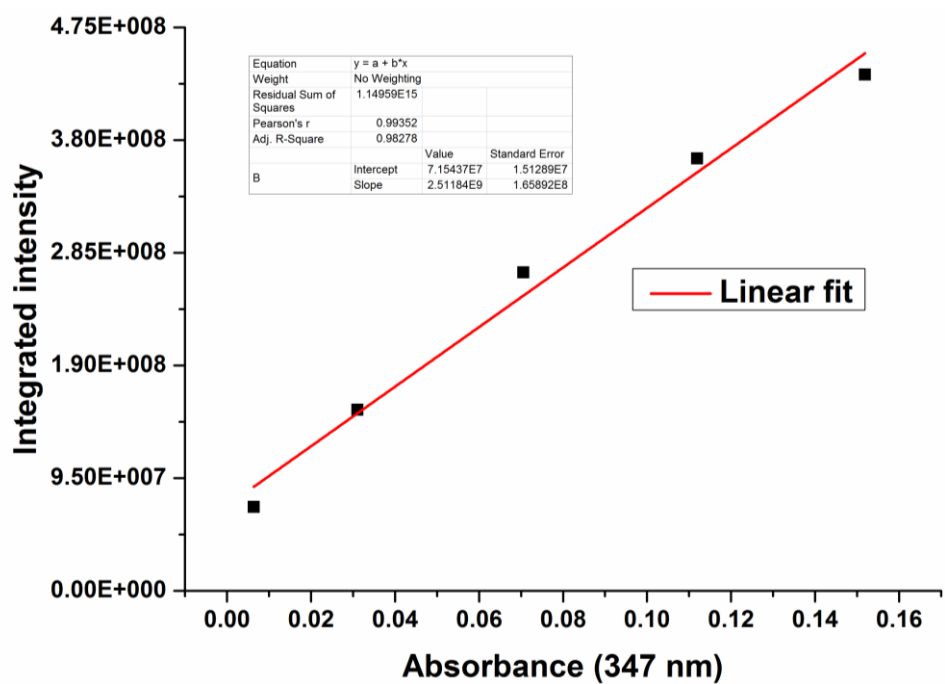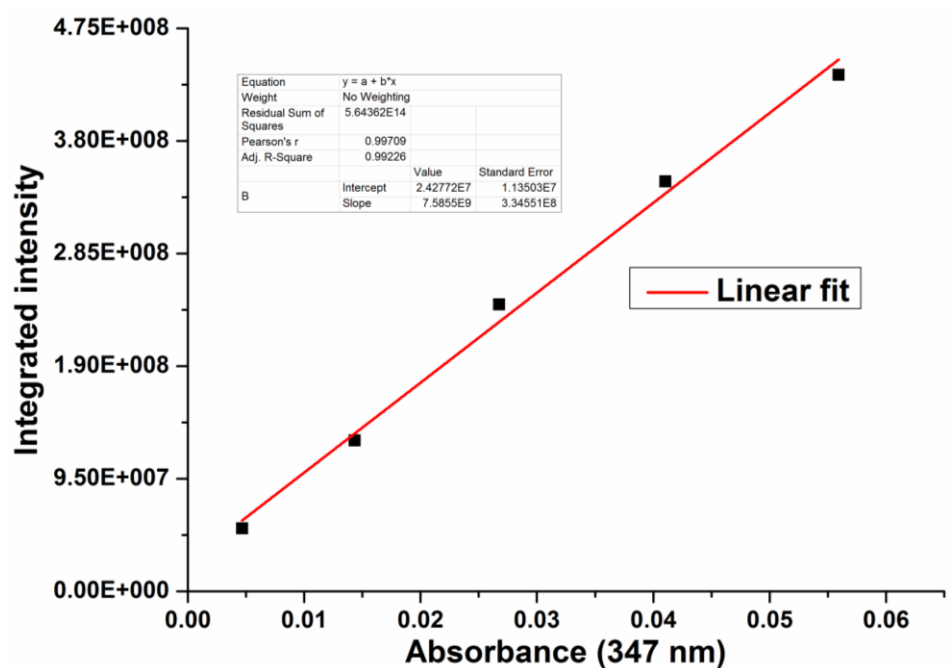
**Figure S9**. Plots of 'Emission area vs. Absorbance' for quinine sulphate (top) and compound **8b**. The concentrations of the solutions were in the range $1 \times 10^{-5} - 1 \times 10^{-6}$ M in toluene. Inserts show linear regression analysis of the fit (red lines).

# 4. X-ray crystallographic analysis

Crystals of **2a**, **4a**, and **8b** were both grown by slow diffusing methanol to the solutions in CDCl$_3$ solution.

Crystallographic data for **2a**: C$_{62}$H$_{54}$O$_4$; *Mr*=863.05; crystal size= 0.409 x 0.268 x 0.245 mm$^3$; triclinic; space group P-1; *a*=13.6105(18), *b*=14.975(2), *c*=15.350(2) Å; α=96.317(2)°, β=109.352(2)°, γ=116.970(2)°; *V*=2501.5(6) Å$^3$; Z=2, ρcalcd=1.146 Mg/m$^3$; μ=0.070 mm$^{-1}$; λ=0.71073 Å; *T*=100(2) K; 2θmax=50.00°; reflections measured 56082, independent 13466 [*R(int)*=0.0648]; *R1*=0.0526, *wR2*=0.1310 (I>2σ(I)); residual electron density=0.894 and -0.246 e.Å$^{-3}$.

Crystallographic data for **4a**: C$_{62}$H$_{54}$O$_4$; *Mr*=863.05; crystal size= 0.540 x 0.420 x 0.040 mm$^3$; Monoclinic; space group P2$_1$/c; *a*=10.8602(12), *b*=49.701(6), *c*=9.5330(11) Å; α=90°, β=114.508(2)°, γ=90°; *V*=4861.9(9) Å$^3$; Z=4, ρcalcd=1.224 Mg/m$^3$; μ=0.075 mm$^{-1}$; λ=0.71073 Å; *T*=100(2) K; 2θmax=50.00°; reflections measured 5284, independent 5284 [*R(int)*=0.0571]; *R1*=0.1696, *wR2*=0.4202 (I>2σ(I)); residual electron density=0.659 and -0.596 e.Å$^{-3}$.

Crystallographic data for **8b**: C$_{82}$H$_{94}$O$_4$; *Mr*=1143.62; crystal size= 0.541 x 0.328 x 0.020 mm$^3$; monoclinic; space group *C*2/c; *a*=35.077(2), *b*=8.5903(6), *c*=24.2885(16) Å; α=90°, β=106.5930(10)°, γ=90°; *V*=7013.8(8) Å$^3$; Z=8, ρcalcd=1.157 Mg/m$^3$; μ=0.154 mm$^{-1}$; λ=0.71073 Å; *T*=100(2) K; 2θmax=50.00°; reflections measured 41307, independent 5173 [*R(int)*=0.0743]; *R1*=0.0707, *wR2*=0.1556 (I>2σ(I)); residual electron density=0.571 and –0.244 e.Å$^{-3}$.

## 4.1 X-ray crystallographic analysis of pyrene 2a

### 4.1.1 Crystal structure of 2a
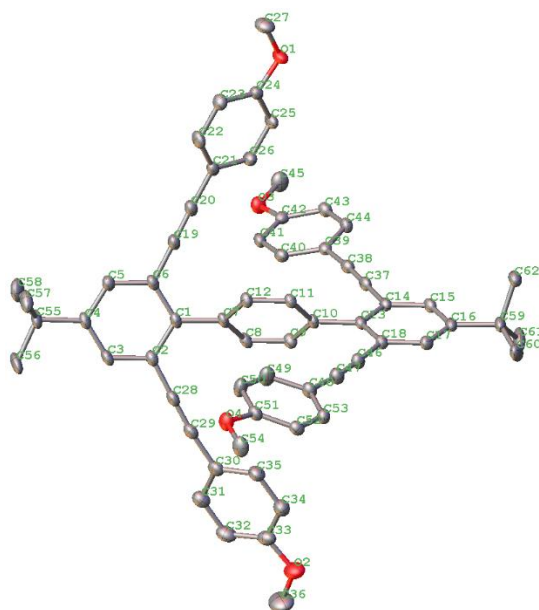


**Figure S10.** Thermal ellipsoids plot of **2a** with ellipsoids at 50% probability. Hydrogen atoms were omitted for clarity.

### 4.1.2 Crystal data and structure refinement for 2a

**Table S8.** Crystal data and structure refinement for **2a**.

| | |
|---|---|
| Empirical formula | C62 H54 O4 |
| Formula weight | 863.05 |
| Temperature | 100(2) K |
| Wavelength | 0.71073 Å |
| Crystal system | Triclinic |
| Space group | P-1 |
| Unit cell dimensions | a = 13.6105(18) Å $\quad$ $\alpha$= 96.317(2)°. |
| | b = 14.975(2) Å $\quad$ $\beta$= 109.352(2)°. |
| | c = 15.350(2) Å $\quad$ $\gamma$ = 116.970(2)°. |
| Volume | 2501.5(6) Å$^3$ |
| Z | 2 |
| Density (calculated) | 1.146 Mg/m$^3$ |
| Absorption coefficient | 0.070 mm$^{-1}$ |
| F(000) | 916 |
| Crystal size | 0.409 x 0.268 x 0.245 mm$^3$ |
| Theta range for data collection | 1.479 to 29.129°. |
| Index ranges | -18<=h<=18, -20<=k<=20, -21<=l<=21 |
| Reflections collected | 56082 |
| Independent reflections | 13466 [R(int) = 0.0648] |

| Completeness to theta = 25.242° | 100.0 % |
|---|---|
| Refinement method | Full-matrix least-squares on $F^2$ |
| Data / restraints / parameters | 13466 / 0 / 605 |
| Goodness-of-fit on $F^2$ | 1.061 |
| Final R indices [I>2sigma(I)] | R1 = 0.0526, wR2 = 0.1310 |
| R indices (all data) | R1 = 0.0951, wR2 = 0.1439 |
| Extinction coefficient | n/a |
| Largest diff. peak and hole | 0.894 and -0.246 e.Å$^{-3}$ |

**Table S9.** Selected bond lengths [Å] for **2a**.

| | | | |
|---|---|---|---|
| C(1)-C(6) | 1.409(2) | C(13)-C(18) | 1.4017(19) |
| C(1)-C(2) | 1.4136(19) | C(13)-C(14) | 1.4084(18) |
| C(1)-C(7) | 1.4913(18) | C(14)-C(15) | 1.4004(19) |
| C(2)-C(3) | 1.4076(19) | C(14)-C(37) | 1.4330(19) |
| C(2)-C(28) | 1.438(2) | C(15)-C(16) | 1.394(2) |
| C(3)-C(4) | 1.383(2) | C(16)-C(17) | 1.386(2) |
| C(4)-C(5) | 1.395(2) | C(16)-C(59) | 1.5343(19) |
| C(4)-C(55) | 1.5349(19) | C(17)-C(18) | 1.4077(19) |
| C(5)-C(6) | 1.3987(19) | C(18)-C(46) | 1.4327(19) |
| C(6)-C(19) | 1.435(2) | C(19)-C(20) | 1.201(2) |
| C(7)-C(8) | 1.394(2) | C(20)-C(21) | 1.435(2) |
| C(7)-C(12) | 1.4010(19) | C(28)-C(29) | 1.196(2) |
| C(8)-C(9) | 1.3905(19) | C(29)-C(30) | 1.442(2) |
| C(9)-C(10) | 1.3953(19) | C(37)-C(38) | 1.200(2) |
| C(10)-C(11) | 1.3916(19) | C(38)-C(39) | 1.432(2) |
| C(10)-C(13) | 1.4925(18) | C(46)-C(47) | 1.199(2) |
| C(11)-C(12) | 1.3850(18) | C(47)-C(48) | 1.435(2) |

**Table S10.** Selected bond angles [°] for **2a**.

| | | | | | |
|---|---|---|---|---|---|
| C(6)-C(1)-C(7) | 121.01(12) | C(12)-C(11)-C(10) | 121.11(12) | C(22)-C(21)-C(20) | 120.57(13) |
| C(2)-C(1)-C(7) | 121.73(13) | C(14)-C(13)-C(10) | 121.44(12) | C(26)-C(21)-C(20) | 121.08(13) |
| C(3)-C(2)-C(28) | 118.83(12) | C(15)-C(14)-C(37) | 120.08(12) | C(29)-C(28)-C(2) | 178.47(16) |
| C(1)-C(2)-C(28) | 120.76(12) | C(11)-C(12)-C(7) | 121.09(13) | C(28)-C(29)-C(30) | 174.08(15) |
| C(3)-C(4)-C(55) | 123.36(13) | C(18)-C(13)-C(10) | 120.51(12) | C(31)-C(30)-C(29) | 121.24(14) |
| C(5)-C(4)-C(55) | 119.35(13) | C(13)-C(14)-C(37) | 119.88(12) | C(38)-C(37)-C(14) | 178.80(14) |
| C(5)-C(6)-C(19) | 117.62(13) | C(17)-C(16)-C(59) | 122.06(13) | C(37)-C(38)-C(39) | 176.08(15) |
| C(1)-C(6)-C(19) | 121.50(12) | C(15)-C(16)-C(59) | 120.65(13) | C(47)-C(46)-C(18) | 177.68(16) |
| C(8)-C(7)-C(1) | 122.19(12) | C(13)-C(18)-C(46) | 120.29(12) | C(46)-C(47)-C(48) | 174.36(17) |
| C(12)-C(7)-C(1) | 119.97(12) | C(17)-C(18)-C(46) | 119.23(13) | C(53)-C(48)-C(47) | 122.14(13) |
| C(11)-C(10)-C(13) | 120.30(12) | C(20)-C(19)-C(6) | 178.72(16) | C(49)-C(48)-C(47) | 119.41(13) |
| C(9)-C(10)-C(13) | 121.77(12) | C(19)-C(20)-C(21) | 176.45(16) | | |

**Table S11.** Selected torsion angles [°] for **2a**.

| | | | |
|---|---|---|---|
| C(7)-C(1)-C(2)-C(3) | 176.57(13) | C(11)-C(10)-C(13)-C(14) | -118.92(15) |
| C(6)-C(1)-C(2)-C(28) | -179.21(13) | C(9)-C(10)-C(13)-C(14) | 62.11(19) |

| | | | |
|---|---:|---|---:|
| C(7)-C(1)-C(2)-C(28) | -1.8(2) | C(10)-C(13)-C(14)-C(15) | 178.50(13) |
| C(28)-C(2)-C(3)-C(4) | 177.91(13) | C(18)-C(13)-C(14)-C(37) | -178.60(12) |
| C(2)-C(3)-C(4)-C(5) | 1.6(2) | C(10)-C(13)-C(14)-C(37) | 0.2(2) |
| C(2)-C(3)-C(4)-C(55) | -177.71(13) | C(37)-C(14)-C(15)-C(16) | 179.24(13) |
| C(55)-C(4)-C(5)-C(6) | 177.93(13) | C(14)-C(15)-C(16)-C(59) | -178.75(13) |
| C(4)-C(5)-C(6)-C(19) | 179.51(14) | C(59)-C(16)-C(17)-C(18) | 177.83(13) |
| C(7)-C(1)-C(6)-C(5) | -176.40(13) | C(10)-C(13)-C(18)-C(17) | -179.38(12) |
| C(2)-C(1)-C(6)-C(19) | -178.37(13) | C(14)-C(13)-C(18)-C(46) | 179.88(13) |
| C(7)-C(1)-C(6)-C(19) | 4.2(2) | C(10)-C(13)-C(18)-C(46) | 1.1(2) |
| C(6)-C(1)-C(7)-C(8) | -132.39(15) | C(16)-C(17)-C(18)-C(13) | 0.8(2) |
| C(2)-C(1)-C(7)-C(8) | 50.28(19) | C(16)-C(17)-C(18)-C(46) | -179.59(14) |
| C(6)-C(1)-C(7)-C(12) | 48.61(19) | C(20)-C(21)-C(22)-C(23) | 177.55(14) |
| C(2)-C(1)-C(7)-C(12) | -128.72(15) | C(20)-C(21)-C(26)-C(25) | -177.64(14) |
| C(1)-C(7)-C(8)-C(9) | -178.13(13) | C(29)-C(30)-C(31)-C(32) | 176.12(14) |
| C(8)-C(9)-C(10)-C(13) | 178.03(13) | C(29)-C(30)-C(35)-C(34) | -176.56(14) |
| C(13)-C(10)-C(11)-C(12) | -178.47(13) | C(38)-C(39)-C(40)-C(41) | -176.42(13) |
| C(10)-C(11)-C(12)-C(7) | 0.6(2) | C(39)-C(40)-C(41)-C(42) | -0.6(2) |
| C(1)-C(7)-C(12)-C(11) | 177.73(13) | C(38)-C(39)-C(44)-C(43) | 176.99(13) |
| C(11)-C(10)-C(13)-C(18) | 59.86(18) | C(47)-C(48)-C(53)-C(52) | 177.14(14) |
| C(9)-C(10)-C(13)-C(18) | -119.11(15) | | |

## 4.2  X-ray crystallographic analysis of pyrene 4a

### 4.2.1  Crystal structure of 4a
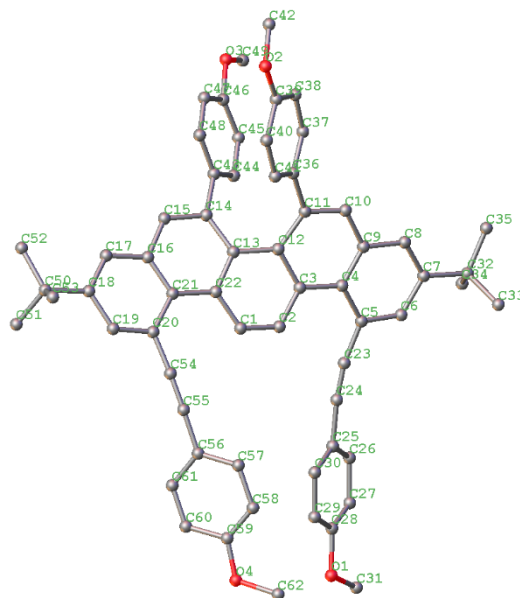


**Figure S11.** Thermal ellipsoids plot of **4a** with ellipsoids at 50% probability. Hydrogen atoms were omitted for clarity.

### 4.2.2  Crystal data and structure refinement for 4a

**Table S12.** Crystal data and structure refinement for **4a**.

| | |
|---|---|
| Empirical formula | C62 H54 O4 |
| Formula weight | 863.05 |
| Temperature | 100(2) K |
| Wavelength | 0.71073 Å |
| Crystal system | Monoclinic |
| Space group | P2$_1$/c |
| Unit cell dimensions | a = 10.8602(12) Å $\quad$ $\alpha$= 90°. |
| | b = 49.701(6) Å $\quad$ $\beta$= 114.508(2)°. |
| | c = 9.5330(11) Å $\quad$ $\gamma$ = 90°. |
| Volume | 4681.9(9) Å$^3$ |
| Z | 4 |
| Density (calculated) | 1.224 Mg/m$^3$ |
| Absorption coefficient | 0.075 mm$^{-1}$ |
| F(000) | 1832 |
| Crystal size | 0.540 x 0.420 x 0.040 mm$^3$ |
| Theta range for data collection | 2.061 to 25.069°. |
| Index ranges | -12<=h<=11, 0<=k<=57, 0<=l<=11 |
| Reflections collected | 5284 |
| Independent reflections | 5284 [R(int) = 0.0571] |
| Completeness to theta = 25.069° | 52.9 % |
| Absorption correction | Semi-empirical from equivalents |
| Max. and min. transmission | 0.8619 and 0.6644 |
| Refinement method | Full-matrix least-squares on F$^2$ |
| Data / restraints / parameters | 5284 / 0 / 266 |
| Goodness-of-fit on F$^2$ | 1.607 |
| Final R indices [I>2sigma(I)] | R1 = 0.1696, wR2 = 0.4202 |
| R indices (all data) | R1 = 0.2106, wR2 = 0.4468 |
| Extinction coefficient | n/a |
| Largest diff. peak and hole | 0.659 and -0.596 e.Å$^{-3}$ |

**Table S13.** Selected bond lengths [Å] for **4a**.

| | | | |
|---|---|---|---|
| C(1)-C(2) | 1.345(15) | C(10)-C(11) | 1.355(14) |
| C(1)-C(22) | 1.400(15) | C(11)-C(12) | 1.447(15) |
| C(2)-C(3) | 1.414(16) | C(12)-C(13) | 1.444(15) |
| C(3)-C(4) | 1.442(15) | C(13)-C(22) | 1.412(15) |
| C(3)-C(12) | 1.454(15) | C(13)-C(14) | 1.440(15) |
| C(4)-C(9) | 1.386(15) | C(14)-C(15) | 1.399(14) |

| | | | |
|---|---|---|---|
| C(4)-C(5) | 1.457(17) | C(15)-C(16) | 1.438(15) |
| C(5)-C(6) | 1.397(15) | C(16)-C(21) | 1.381(15) |
| C(5)-C(23) | 1.435(16) | C(16)-C(17) | 1.414(15) |
| C(6)-C(7) | 1.410(14) | C(17)-C(18) | 1.388(16) |
| C(7)-C(8) | 1.405(15) | C(18)-C(19) | 1.394(15) |
| C(7)-C(32) | 1.529(15) | C(19)-C(20) | 1.381(15) |
| C(8)-C(9) | 1.421(15) | C(20)-C(21) | 1.465(16) |
| C(9)-C(10) | 1.432(15) | C(21)-C(22) | 1.450(15) |

**Table S14.** Selected bond angles [°] for **4a**.

| | | | | | |
|---|---|---|---|---|---|
| C(2)-C(1)-C(22) | 123.0(13) | C(4)-C(9)-C(10) | 120.3(12) | C(21)-C(16)-C(15) | 119.1(12) |
| C(1)-C(2)-C(3) | 122.6(13) | C(8)-C(9)-C(10) | 117.9(11) | C(17)-C(16)-C(15) | 117.3(12) |
| C(2)-C(3)-C(4) | 123.1(12) | C(11)-C(10)-C(9) | 120.7(11) | C(18)-C(17)-C(16) | 120.3(12) |
| C(2)-C(3)-C(12) | 115.8(12) | C(10)-C(11)-C(12) | 122.2(11) | C(17)-C(18)-C(19) | 116.9(13) |
| C(4)-C(3)-C(12) | 120.7(11) | C(13)-C(12)-C(11) | 126.3(10) | C(20)-C(19)-C(18) | 124.3(13) |
| C(9)-C(4)-C(3) | 118.9(12) | C(13)-C(12)-C(3) | 118.2(10) | C(19)-C(20)-C(21) | 118.9(12) |
| C(9)-C(4)-C(5) | 118.1(12) | C(11)-C(12)-C(3) | 115.5(11) | C(16)-C(21)-C(22) | 119.7(11) |
| C(3)-C(4)-C(5) | 122.7(11) | C(22)-C(13)-C(14) | 120.2(11) | C(16)-C(21)-C(20) | 115.7(12) |
| C(6)-C(5)-C(23) | 113.0(11) | C(22)-C(13)-C(12) | 119.6(11) | C(22)-C(21)-C(20) | 124.5(11) |
| C(6)-C(5)-C(4) | 118.2(12) | C(14)-C(13)-C(12) | 120.0(10) | C(1)-C(22)-C(13) | 117.3(12) |
| C(23)-C(5)-C(4) | 128.7(13) | C(15)-C(14)-C(13) | 117.0(11) | C(1)-C(22)-C(21) | 123.2(11) |
| C(5)-C(6)-C(7) | 124.2(12) | C(15)-C(14)-C(43) | 112.4(11) | C(13)-C(22)-C(21) | 119.5(11) |
| C(8)-C(7)-C(6) | 116.4(12) | C(13)-C(14)-C(43) | 130.4(12) | C(24)-C(23)-C(5) | 169.2(15) |
| C(7)-C(8)-C(9) | 121.2(12) | C(14)-C(15)-C(16) | 122.8(12) | C(23)-C(24)-C(25) | 173.7(15) |
| C(4)-C(9)-C(8) | 121.7(12) | C(21)-C(16)-C(17) | 123.6(12) | | |

**Table S15.** Selected torsion angles [°] for **4a**.

| | | | |
|---|---|---|---|
| C(22)-C(1)-C(2)-C(3) | 5(2) | C(3)-C(12)-C(13)-C(14) | -151.0(11) |
| C(1)-C(2)-C(3)-C(4) | 177.6(12) | C(22)-C(13)-C(14)-C(15) | 13.1(17) |
| C(1)-C(2)-C(3)-C(12) | 5.7(19) | C(12)-C(13)-C(14)-C(15) | -173.3(11) |
| C(2)-C(3)-C(4)-C(9) | -165.2(12) | C(13)-C(14)-C(15)-C(16) | -2.6(17) |
| C(12)-C(3)-C(4)-C(9) | 6.3(18) | C(14)-C(15)-C(16)-C(21) | -5.5(18) |
| C(2)-C(3)-C(4)-C(5) | 21.4(19) | C(14)-C(15)-C(16)-C(17) | 174.8(11) |
| C(12)-C(3)-C(4)-C(5) | -167.2(11) | C(21)-C(16)-C(17)-C(18) | 3.3(19) |
| C(9)-C(4)-C(5)-C(6) | 1.8(18) | C(15)-C(16)-C(17)-C(18) | -177.1(11) |
| C(3)-C(4)-C(5)-C(6) | 175.3(11) | C(16)-C(17)-C(18)-C(19) | -4.2(18) |
| C(4)-C(5)-C(6)-C(7) | -0.4(18) | C(17)-C(18)-C(19)-C(20) | 1.2(19) |
| C(5)-C(6)-C(7)-C(8) | 1.7(17) | C(18)-C(19)-C(20)-C(21) | 2.8(19) |
| C(6)-C(7)-C(8)-C(9) | -4.6(17) | C(17)-C(16)-C(21)-C(22) | -177.0(11) |
| C(3)-C(4)-C(9)-C(8) | -178.5(11) | C(15)-C(16)-C(21)-C(22) | 3.3(17) |

| | | | |
|---|---|---|---|
| C(5)-C(4)-C(9)-C(8) | -4.8(18) | C(17)-C(16)-C(21)-C(20) | 0.8(18) |
| C(3)-C(4)-C(9)-C(10) | 5.1(18) | C(15)-C(16)-C(21)-C(20) | -178.9(11) |
| C(5)-C(4)-C(9)-C(10) | 178.9(11) | C(19)-C(20)-C(21)-C(16) | -3.7(17) |
| C(7)-C(8)-C(9)-C(4) | 6.4(19) | C(19)-C(20)-C(21)-C(22) | 174.0(11) |
| C(7)-C(8)-C(9)-C(10) | -177.2(11) | C(2)-C(1)-C(22)-C(13) | -2.0(19) |
| C(4)-C(9)-C(10)-C(11) | -8.5(18) | C(2)-C(1)-C(22)-C(21) | 175.0(12) |
| C(8)-C(9)-C(10)-C(11) | 175.0(11) | C(14)-C(13)-C(22)-C(1) | 161.7(11) |
| C(9)-C(10)-C(11)-C(12) | 0.2(18) | C(12)-C(13)-C(22)-C(1) | -12.0(17) |
| C(10)-C(11)-C(12)-C(13) | -172.3(12) | C(14)-C(13)-C(22)-C(21) | -15.4(17) |
| C(10)-C(11)-C(12)-C(3) | 10.7(17) | C(12)-C(13)-C(22)-C(21) | 170.9(11) |
| C(2)-C(3)-C(12)-C(13) | -19.0(17) | C(16)-C(21)-C(22)-C(1) | -169.9(12) |
| C(4)-C(3)-C(12)-C(13) | 168.9(11) | C(20)-C(21)-C(22)-C(1) | 12.5(19) |
| C(2)-C(3)-C(12)-C(11) | 158.3(11) | C(16)-C(21)-C(22)-C(13) | 7.0(17) |
| C(4)-C(3)-C(12)-C(11) | -13.8(17) | C(20)-C(21)-C(22)-C(13) | -170.6(11) |
| C(11)-C(12)-C(13)-C(22) | -154.3(12) | C(6)-C(5)-C(23)-C(24) | 23(9) |
| C(3)-C(12)-C(13)-C(22) | 22.7(16) | C(4)-C(5)-C(23)-C(24) | -161(8) |
| C(11)-C(12)-C(13)-C(14) | 32.0(18) | | |

## 4.3  X-ray crystallographic analysis of pyrene 8b

### 4.3.1   Crystal structure of 8b
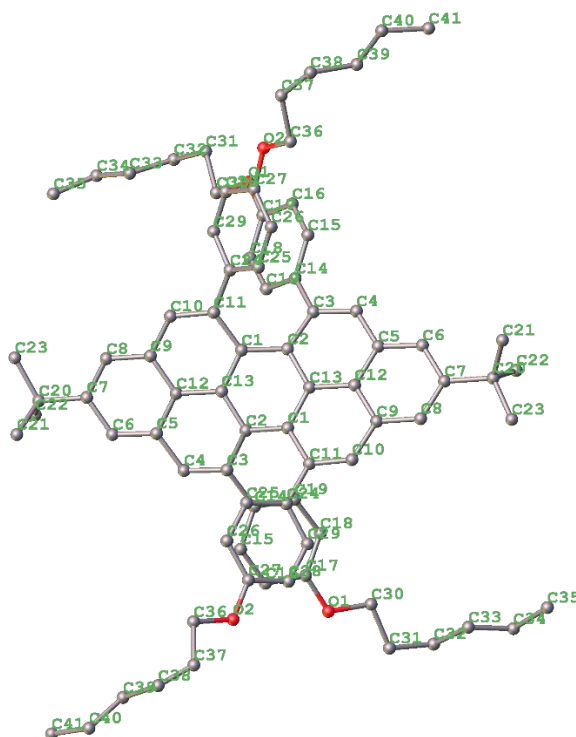


**Figure S12.** Thermal ellipsoids plot of **8b** with ellipsoids at 50% probability. Hydrogen atoms and disordered methyl groups were omitted for clarity.

## 4.3.2 Crystal data and structure refinement for 8b

**Table S16.** Crystal data and structure refinement for **8b**.

| | | |
|---|---|---|
| Empirical formula | $C_{82}H_{94}O_4$ | |
| Formula weight | 1143.62 | |
| Temperature | 100(2) K | |
| Wavelength | 0.71073 Å | |
| Crystal system | Monoclinic | |
| Space group | C2/c | |
| Unit cell dimensions | a = 35.077(2) Å | $\alpha$= 90°. |
| | b = 8.5903(6) Å | $\beta$= 106.5930(10)°. |
| | c = 24.2885(16) Å | $\gamma$ = 90°. |
| Volume | 7013.8(8) Å$^3$ | |
| Z | 8 | |
| Density (calculated) | 1.168 Mg/m$^3$ | |
| Absorption coefficient | 0.156 mm$^{-1}$ | |
| F(000) | 2637 | |
| Crystal size | 0.541 x 0.328 x 0.020 mm$^3$ | |
| Theta range for data collection | 1.750 to 24.997°. | |
| Index ranges | -41<=h<=39, 0<=k<=10, 0<=l<=28 | |
| Reflections collected | 5668 | |
| Independent reflections | 5668 [R(int) = 0.0743] | |
| Completeness to theta = 24.997° | 93.9 % | |
| Absorption correction | Semi-empirical from equivalents | |
| Max. and min. transmission | .745 and .577 | |
| Refinement method | Full-matrix least-squares on F$^2$ | |
| Data / restraints / parameters | 5668 / 52 / 471 | |
| Goodness-of-fit on F$^2$ | 1.051 | |
| Final R indices [I>2sigma(I)] | R1 = 0.0677, wR2 = 0.1417 | |
| R indices (all data) | R1 = 0.0990, wR2 = 0.1525 | |
| Extinction coefficient | n/a | |
| Largest diff. peak and hole | 0.373 and -0.231 e.Å$^{-3}$ | |

**Table S17.** Selected bond lengths [Å] for **8b**.

| | | | |
|---|---|---|---|
| C(1)-C(2) | 1.423(5) | C(6)-C(7) | 1.397(5) |
| C(2)-C(13) | 1.427(5) | C(7)-C(8) | 1.392(5) |
| C(2)-C(3) | 1.465(4) | C(7)-C(20) | 1.531(5) |
| C(3)-C(4) | 1.361(5) | C(8)-C(9) | 1.394(5) |
| C(3)-C(14) | 1.484(5) | C(9)-C(12) | 1.408(5) |
| C(4)-C(5) | 1.434(5) | C(9)-C(10) | 1.432(5) |
| C(5)-C(6) | 1.397(5) | C(10)-C(11) | 1.363(5) |
| C(5)-C(12) | 1.421(4) | C(12)-C(13) | 1.432(4) |

**Table S18.** Selected bond angles [°] for **8b**.

| | | | | | |
|---|---|---|---|---|---|
| C(1)-C(2)-C(13) | 116.9(3) | C(6)-C(7)-C(20) | 119.3(3) | C(15)-C(14)-C(3) | 121.7(3) |

| | | | | | |
|---|---|---|---|---|---|
| C(1)-C(2)-C(3) | 124.7(3) | C(7)-C(8)-C(9) | 122.1(3) | C(16)-C(15)-C(14) | 121.9(3) |
| C(13)-C(2)-C(3) | 118.3(3) | C(8)-C(9)-C(12) | 120.0(3) | C(15)-C(16)-C(17) | 120.2(3) |
| C(4)-C(3)-C(2) | 119.0(3) | C(8)-C(9)-C(10) | 122.1(3) | C(18)-C(17)-C(16) | 119.5(3) |
| C(4)-C(3)-C(14) | 119.0(3) | C(12)-C(9)-C(10) | 117.8(3) | C(17)-C(18)-C(19) | 119.4(3) |
| C(2)-C(3)-C(14) | 121.3(3) | C(11)-C(10)-C(9) | 123.2(3) | C(14)-C(19)-C(18) | 122.1(3) |
| C(3)-C(4)-C(5) | 122.9(3) | C(10)-C(11)-C(24) | 117.6(3) | C(21)-C(20)-C(23) | 108.9(3) |
| C(6)-C(5)-C(12) | 119.3(3) | C(9)-C(12)-C(5) | 118.7(3) | C(21)-C(20)-C(7) | 109.9(3) |
| C(6)-C(5)-C(4) | 122.4(3) | C(9)-C(12)-C(13) | 120.9(3) | C(23)-C(20)-C(7) | 112.6(3) |
| C(12)-C(5)-C(4) | 118.0(3) | C(5)-C(12)-C(13) | 120.4(3) | C(22A)-C(20)-C(7) | 114(3) |
| C(7)-C(6)-C(5) | 122.3(3) | C(2)-C(13)-C(12) | 119.2(3) | C(21)-C(20)-C(22) | 109.2(4) |
| C(8)-C(7)-C(6) | 117.6(3) | C(19)-C(14)-C(15) | 116.8(3) | C(23)-C(20)-C(22) | 107.5(3) |
| C(8)-C(7)-C(20) | 123.1(3) | C(19)-C(14)-C(3) | 121.4(3) | C(7)-C(20)-C(22) | 108.7(3) |

**Table S19.** Selected torsion angles [°] for **8b**.

| | | | |
|---|---|---|---|
| C(13)#1-C(1)-C(2)-C(13) | -27.6(4) | C(4)-C(5)-C(12)-C(9) | 173.9(3) |
| C(11)#1-C(1)-C(2)-C(13) | 152.7(3) | C(6)-C(5)-C(12)-C(13) | -178.6(3) |
| C(13)#1-C(1)-C(2)-C(3) | 150.7(3) | C(4)-C(5)-C(12)-C(13) | -5.0(5) |
| C(11)#1-C(1)-C(2)-C(3) | -29.0(5) | C(1)-C(2)-C(13)-C(1)#1 | 15.4(4) |
| C(1)-C(2)-C(3)-C(4) | 167.0(3) | C(3)-C(2)-C(13)-C(1)#1 | -163.0(3) |
| C(13)-C(2)-C(3)-C(4) | -14.8(5) | C(1)-C(2)-C(13)-C(12) | -165.1(3) |
| C(1)-C(2)-C(3)-C(14) | -22.4(5) | C(3)-C(2)-C(13)-C(12) | 16.5(4) |
| C(13)-C(2)-C(3)-C(14) | 155.9(3) | C(9)-C(12)-C(13)-C(2) | 174.4(3) |
| C(2)-C(3)-C(4)-C(5) | 3.0(5) | C(5)-C(12)-C(13)-C(2) | -6.7(5) |
| C(14)-C(3)-C(4)-C(5) | -167.9(3) | C(9)-C(12)-C(13)-C(1)#1 | -6.1(5) |
| C(3)-C(4)-C(5)-C(6) | -179.7(3) | C(5)-C(12)-C(13)-C(1)#1 | 172.8(3) |
| C(3)-C(4)-C(5)-C(12) | 6.9(5) | C(4)-C(3)-C(14)-C(19) | 135.1(3) |
| C(12)-C(5)-C(6)-C(7) | -0.3(5) | C(2)-C(3)-C(14)-C(19) | -35.6(5) |
| C(4)-C(5)-C(6)-C(7) | -173.7(3) | C(4)-C(3)-C(14)-C(15) | -41.8(5) |
| C(5)-C(6)-C(7)-C(8) | -0.6(5) | C(2)-C(3)-C(14)-C(15) | 147.5(3) |
| C(5)-C(6)-C(7)-C(20) | 178.5(3) | C(19)-C(14)-C(15)-C(16) | 0.7(5) |
| C(6)-C(7)-C(8)-C(9) | 1.7(5) | C(3)-C(14)-C(15)-C(16) | 177.7(3) |
| C(20)-C(7)-C(8)-C(9) | -177.4(3) | C(14)-C(15)-C(16)-C(17) | 0.5(5) |
| C(7)-C(8)-C(9)-C(12) | -1.8(5) | C(15)-C(16)-C(17)-C(18) | -1.6(5) |
| C(7)-C(8)-C(9)-C(10) | -178.6(3) | C(16)-C(17)-C(18)-C(19) | 1.4(5) |
| C(8)-C(9)-C(10)-C(11) | -177.0(3) | C(15)-C(14)-C(19)-C(18) | -0.8(5) |
| C(12)-C(9)-C(10)-C(11) | 6.1(5) | C(3)-C(14)-C(19)-C(18) | -177.9(3) |
| C(9)-C(10)-C(11)-C(1)#1 | 0.9(5) | C(17)-C(18)-C(19)-C(14) | -0.2(5) |
| C(9)-C(10)-C(11)-C(24) | -174.4(3) | C(8)-C(7)-C(20)-C(21) | -124.8(4) |
| C(8)-C(9)-C(12)-C(5) | 0.8(5) | C(6)-C(7)-C(20)-C(21) | 56.1(5) |
| C(10)-C(9)-C(12)-C(5) | 177.7(3) | C(8)-C(7)-C(20)-C(23) | -3.3(5) |
| C(8)-C(9)-C(12)-C(13) | 179.7(3) | C(6)-C(7)-C(20)-C(23) | 177.6(3) |
| C(10)-C(9)-C(12)-C(13) | -3.4(5) | C(8)-C(7)-C(20)-C(22) | 115.7(4) |
| C(6)-C(5)-C(12)-C(9) | 0.3(5) | C(6)-C(7)-C(20)-C(22) | -63.4(4) |

## 5. Variable temperature NMR of chiral peropyrene 8b



**4**     **8**
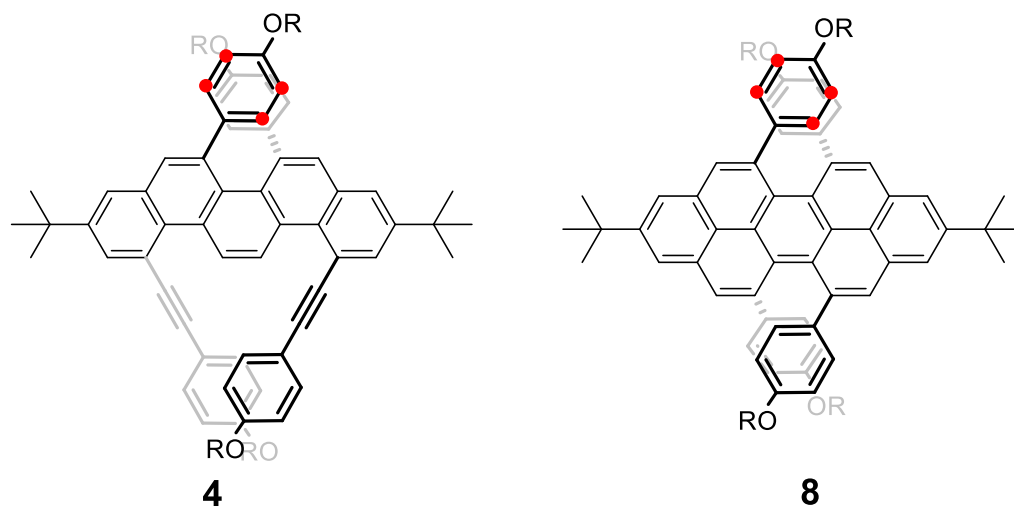
**Note**: All the ^{1}H and ^{13}C NMR spectra of compounds **4** and **8** were recorded at room temperature. We not only observed the broaden peaks in the ^{1}H NMR spectra of compounds **4** and **8**, the four strongly broadened and less intensive signals were also found in their ^{13}C NMR spectra. In order to assign these broaden signals, we obtained the ^{1}H and ^{13}C NMR spectrum of compound **8b** in CDCl$_3$ at 50 °C. After increasing temperature, the whole broaden peaks changed to two relative sharp peaks in the ^{1}H NMR spectrum (Figure S13), and the four signals turned into two relative sharp signals in the ^{13}C NMR spectrum (Figure S14). Therefore, those four signals in the ^{13}C NMR spectrum were assigned to the carbon on the phenyl rings that were restricted free-rotating (highlighted by red spot, see the above scheme), which were further proved by the HSQC study of compound **8b** (Figure 2b). Compound **8b** was also studied by variable temperature ^{1}H NMR spectroscopy in *d*-DMSO between 25−100 °C (Figure S15). The broad peaks resulting from the aryl substituents gradually sharpen as a function of increasing temperature, and the signals recover to broad peaks when the sample is cooled to 25 °C.
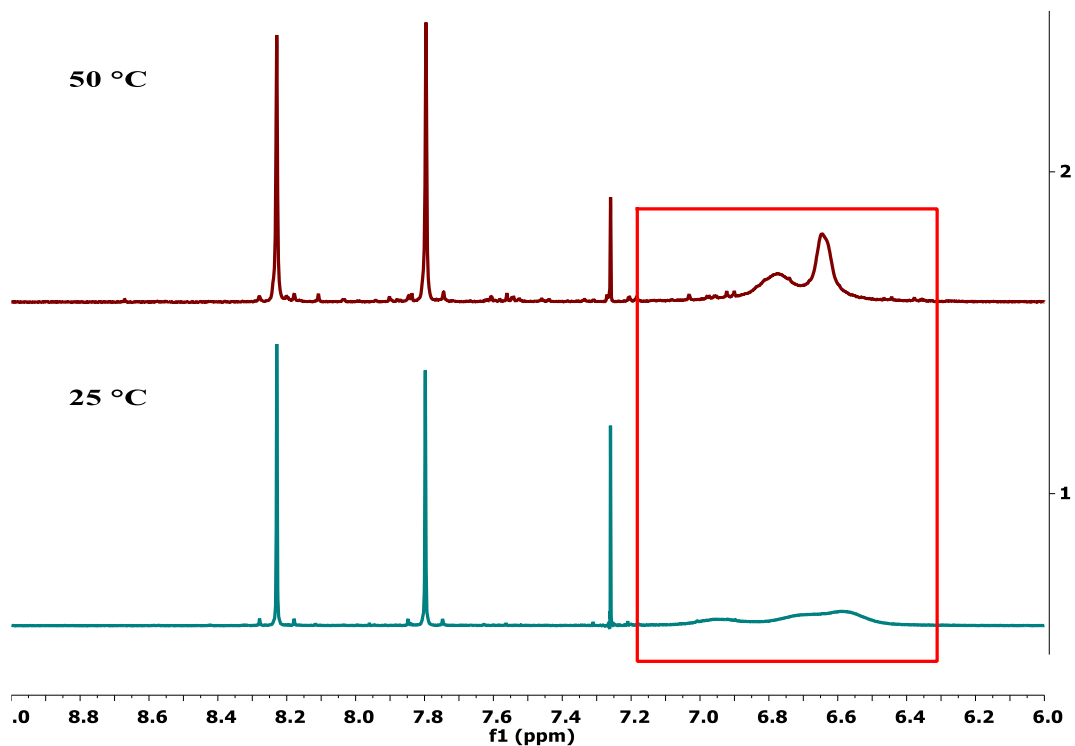
**Figure S13.** Comparison of the aromatic area of $^1$H NMR spectrum for **8b** in CDCl$_3$ at 25 and 50 ℃.
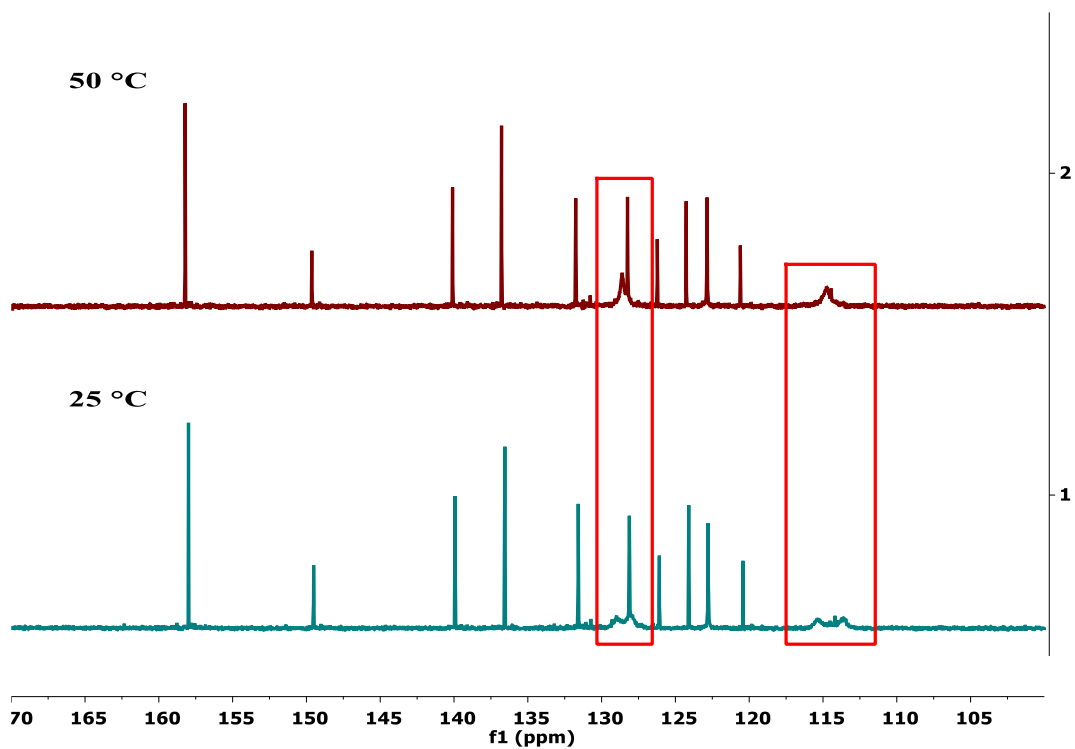


**Figure S14.** Comparison of the aromatic area of $^{13}$C NMR spectrum for **8b** in CDCl$_3$ at 25 and 50 ℃.
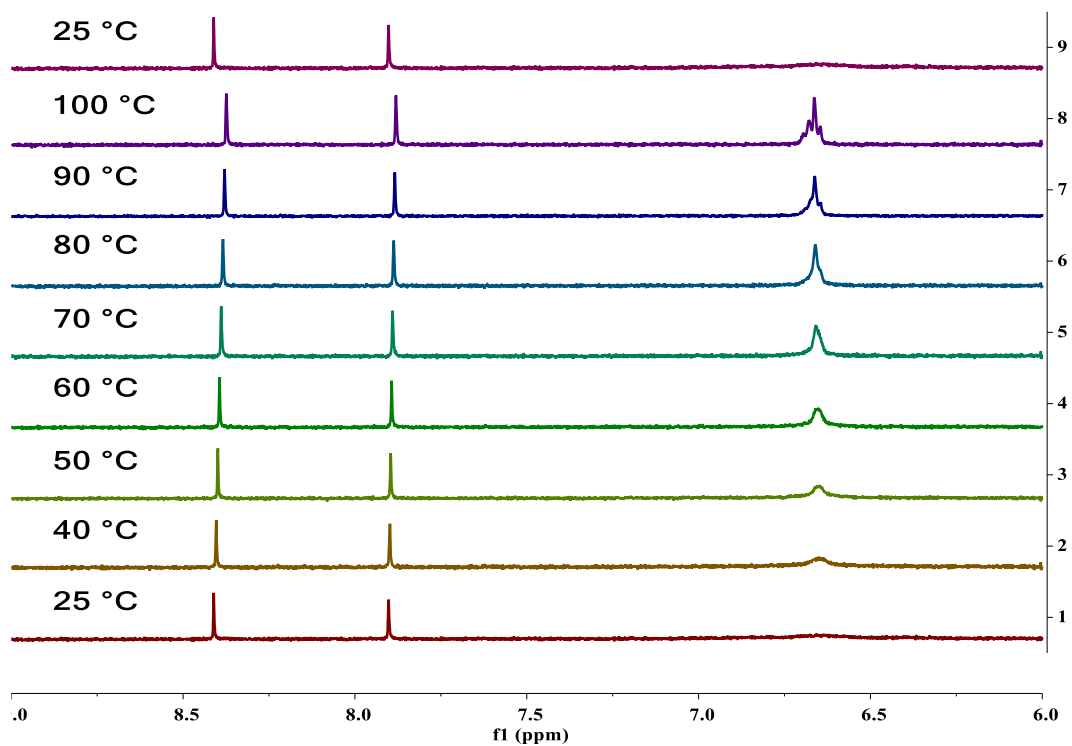
**Figure S15.** Aromatic area of variable temperature $^1$H NMR spectrum for **8b** in *d*-DMSO and the return of the original spectrum when cooled.

## 6. $^1$H and $^{13}$C NMR spectra for new compounds
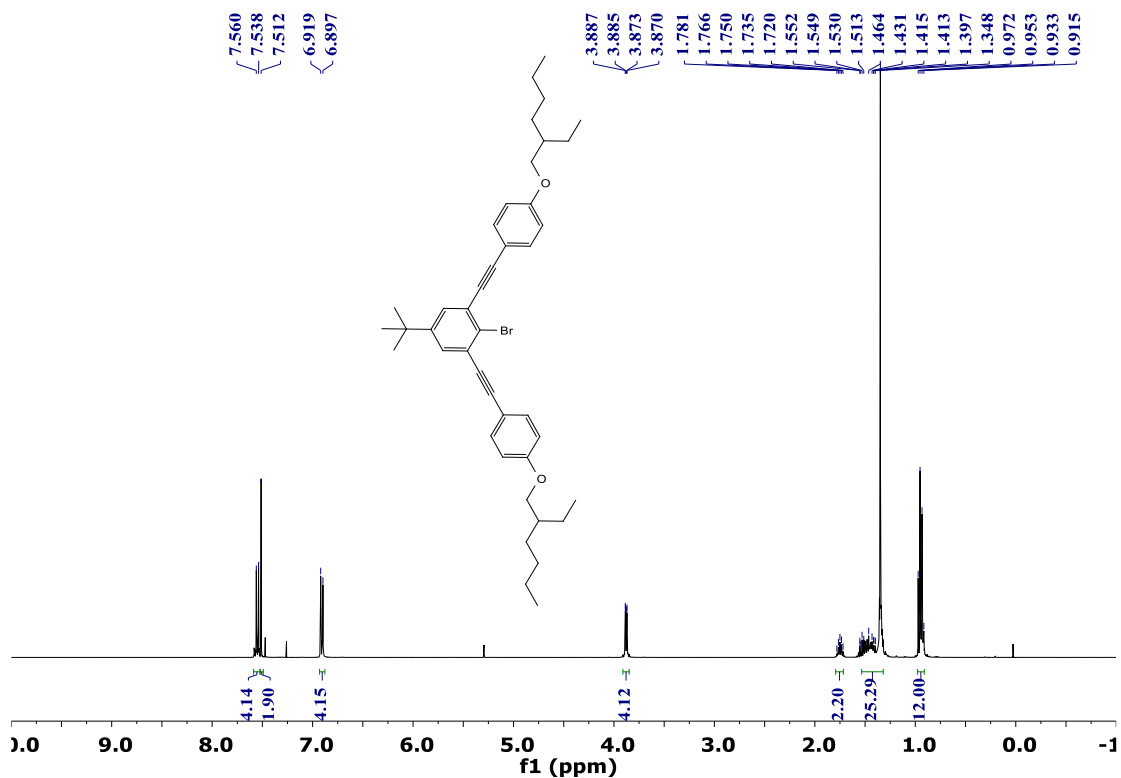


**Figure S16.** $^1$H NMR spectrum for compound **S3** in CDCl$_3$ at 298 K.
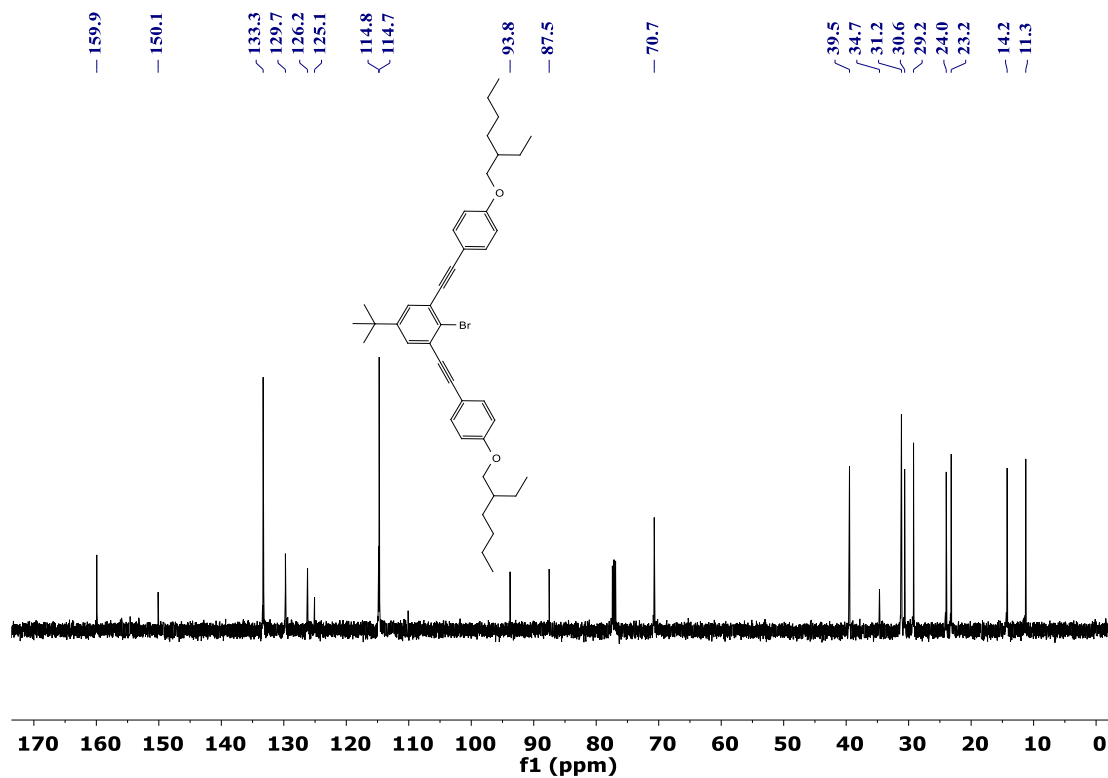


**Figure S17.** $^{13}$C NMR spectrum for compound **S3** in CDCl$_3$ at 298 K.
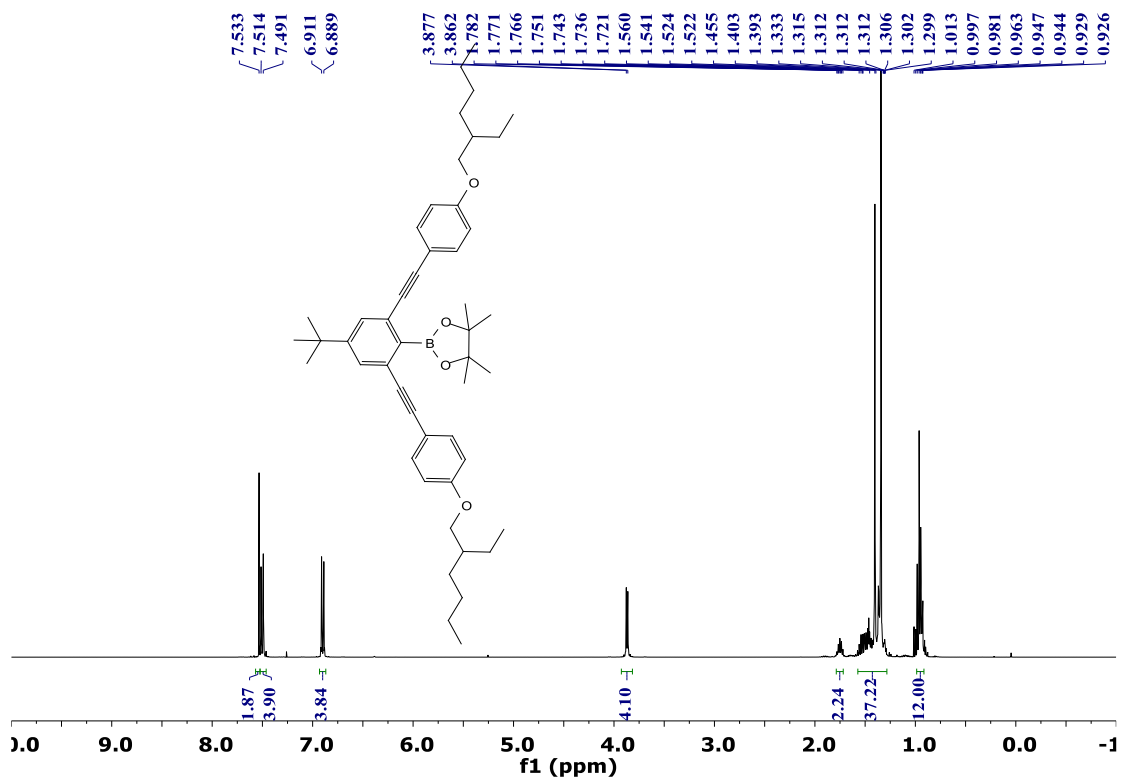
**Figure S18.** $^1$H NMR spectrum for compound **1c** in CDCl$_3$ at 298 K.
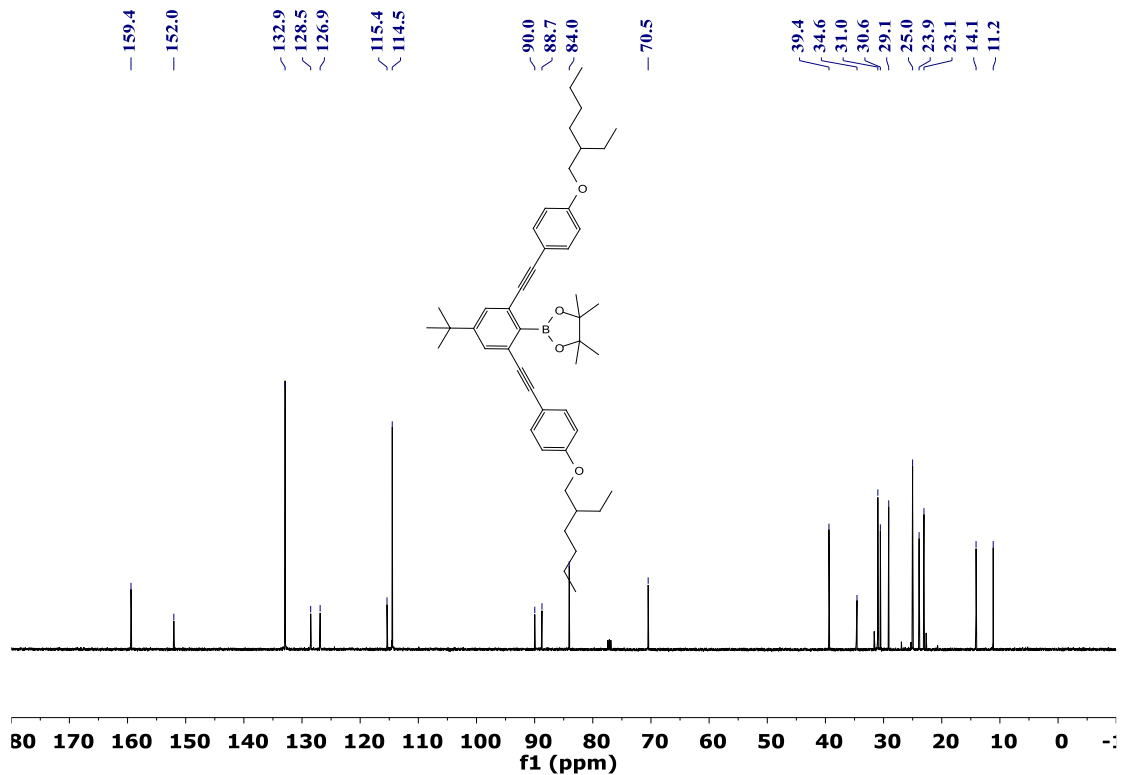


**Figure S19.** $^{13}$C NMR spectrum for compound **1c** in CDCl$_3$ at 298 K.
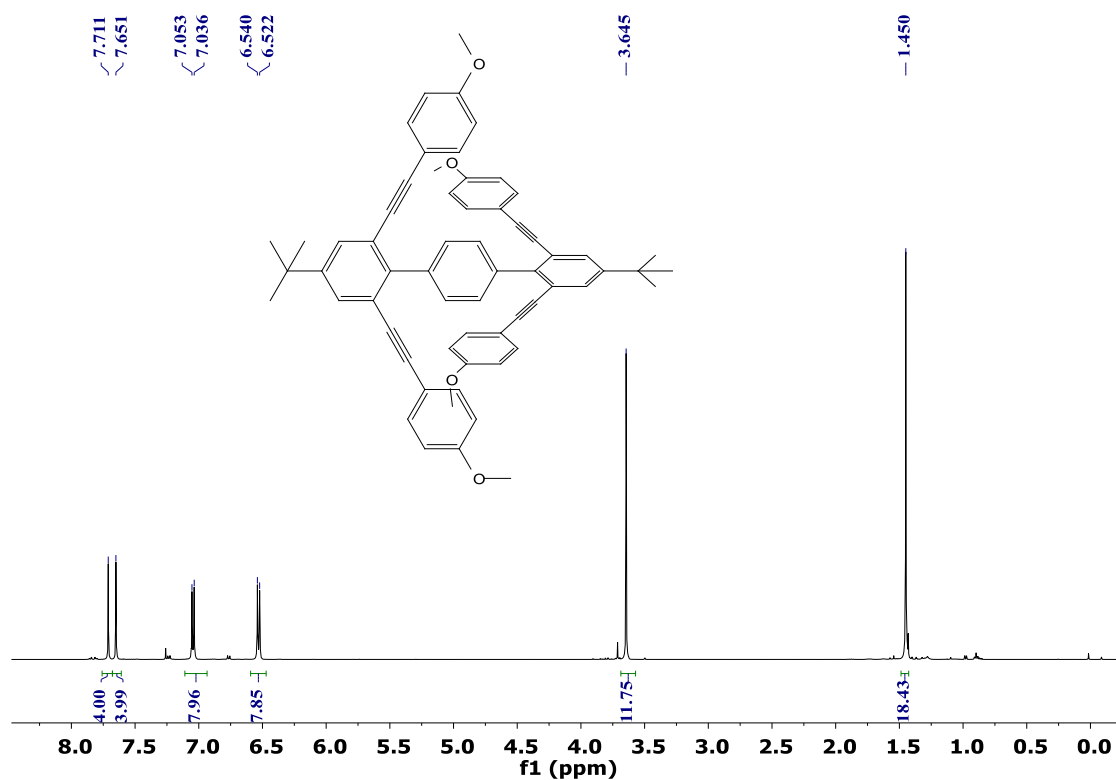
**Figure S20.** $^1$H NMR spectrum for compound **2a** in CDCl$_3$ at 298 K.
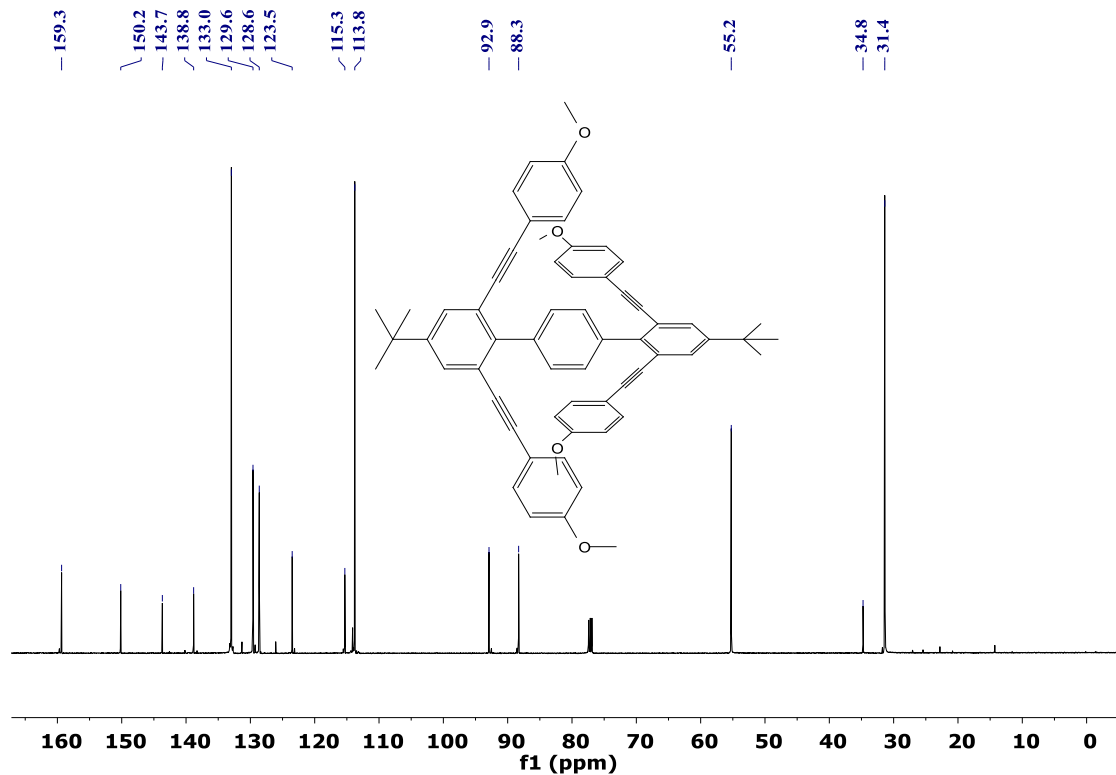


**Figure S21.** $^{13}$C NMR spectrum for compound **2a** in CDCl$_3$ at 298 K.
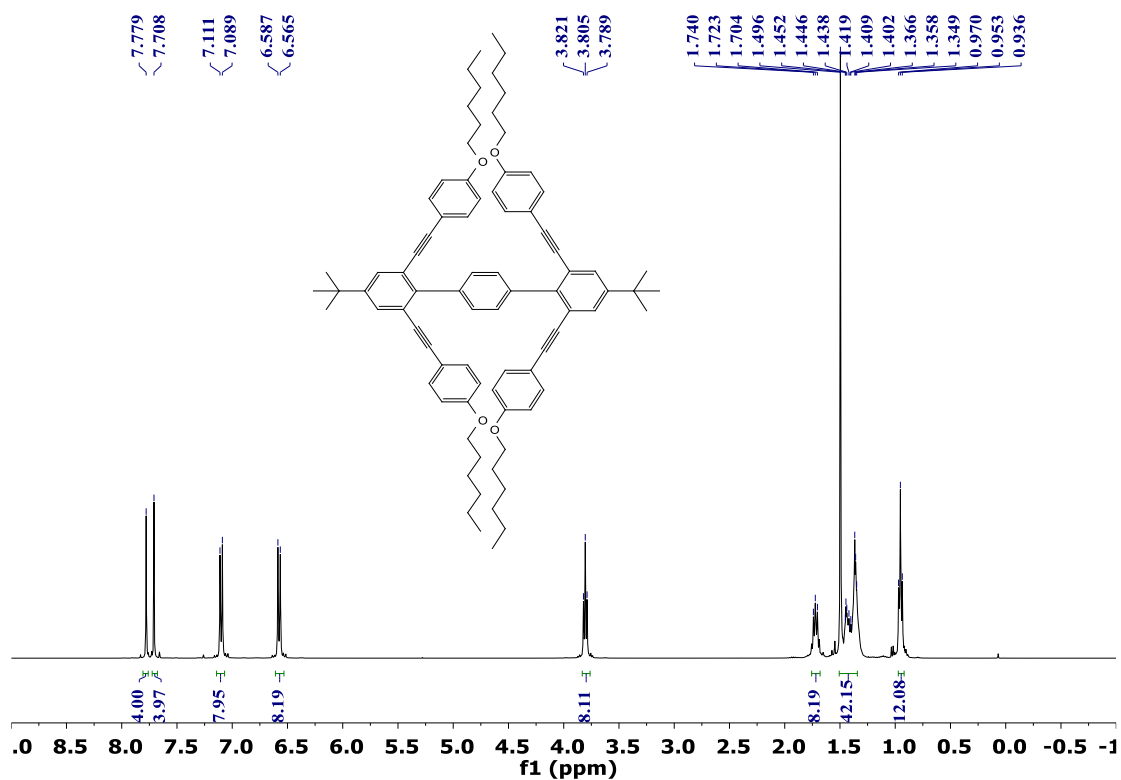
**Figure S22.** $^1$H NMR spectrum for compound **2b** in CDCl$_3$ at 298 K.
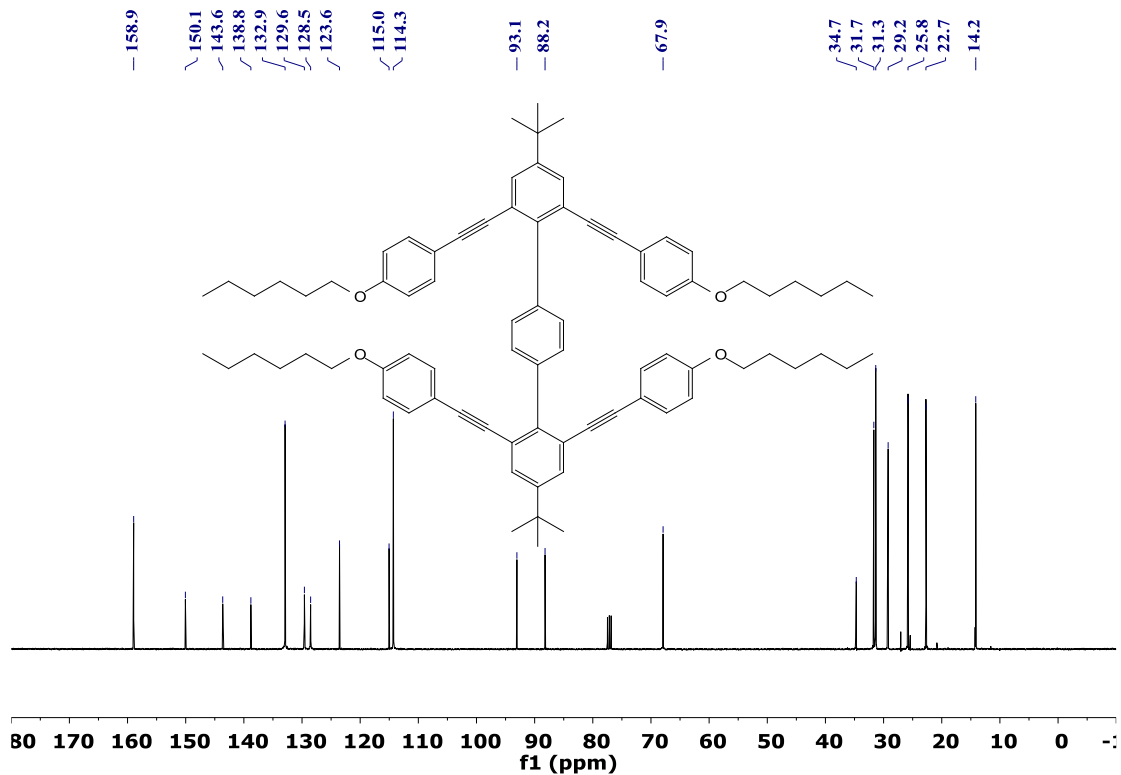


**Figure S23.** $^{13}$C NMR spectrum for compound **2b** in CDCl$_3$ at 298 K.
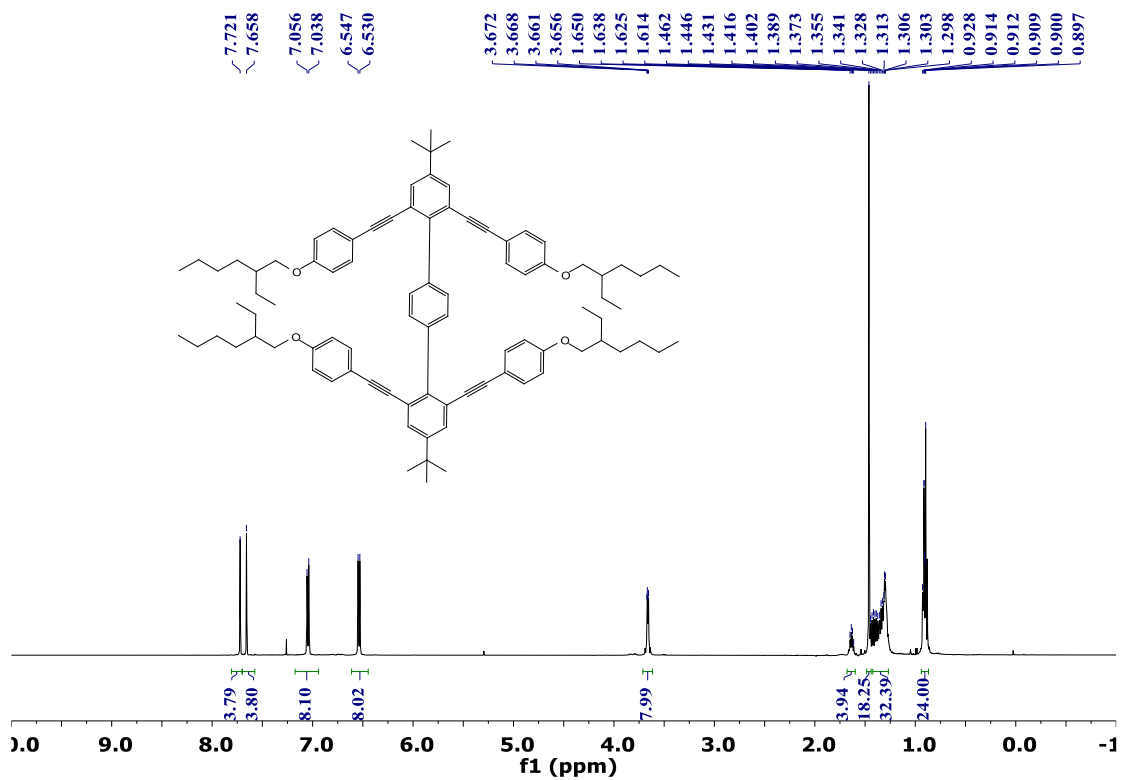
**Figure S24.** $^1$H NMR spectrum for compound **2c** in CDCl$_3$ at 298 K.
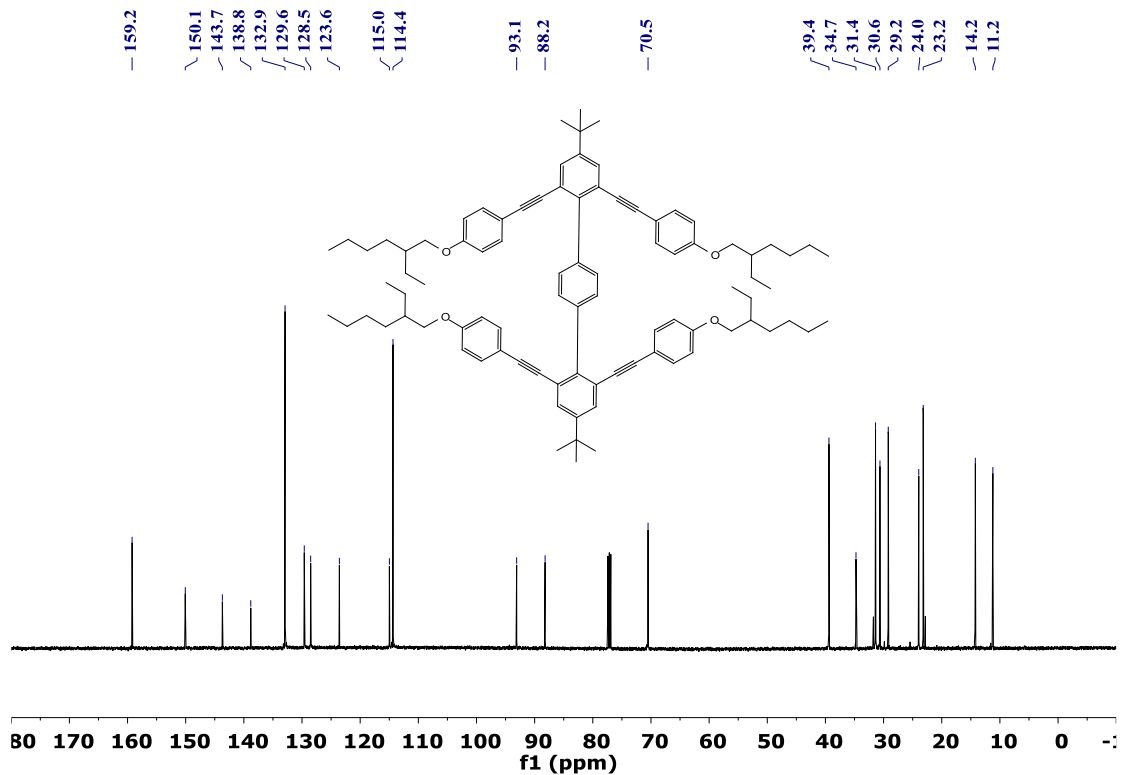


**Figure S25.** $^{13}$C NMR spectrum for compound **2c** in CDCl$_3$ at 298 K.
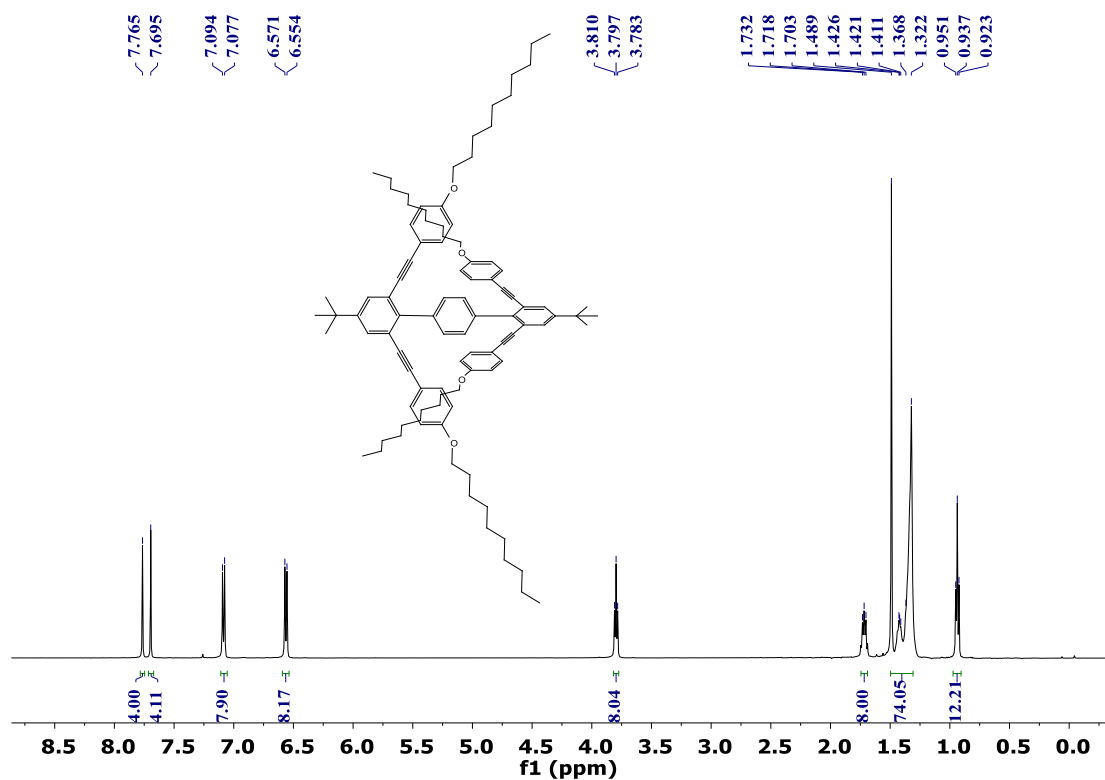
**Figure S26.** ^{1}H NMR spectrum for compound **2d** in CDCl$_3$ at 298 K.
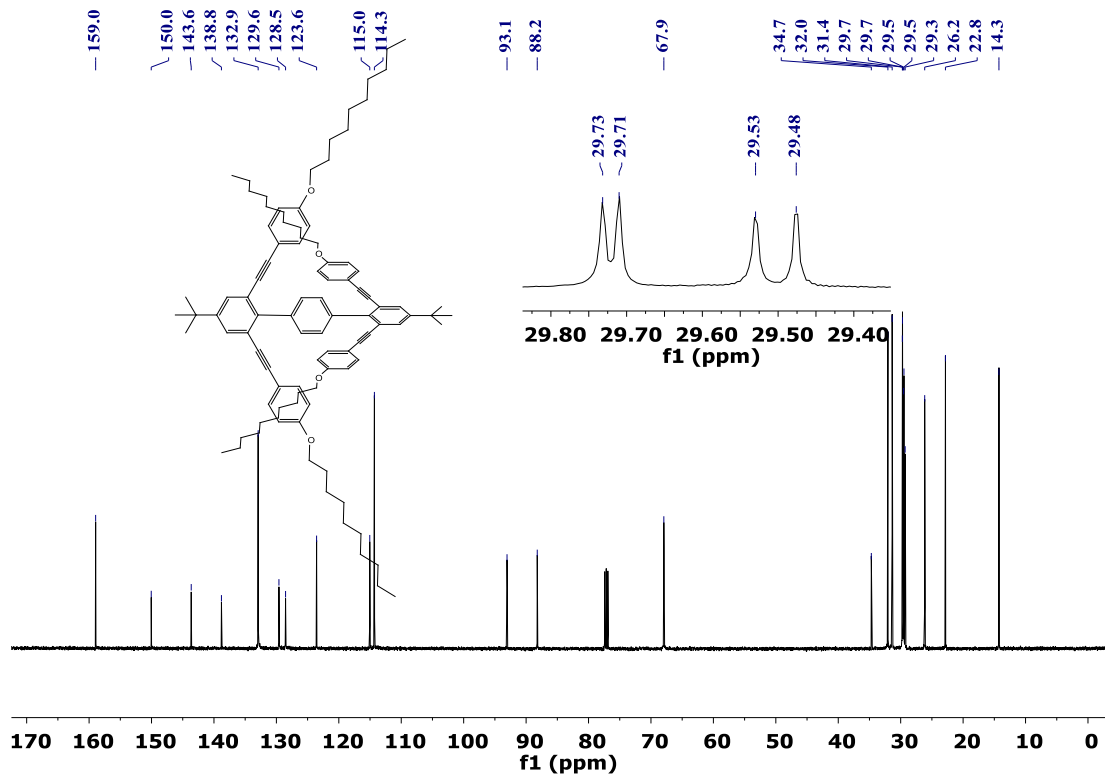


**Figure S27.** ^{13}C NMR spectrum for compound **2d** in CDCl$_3$ at 298 K.
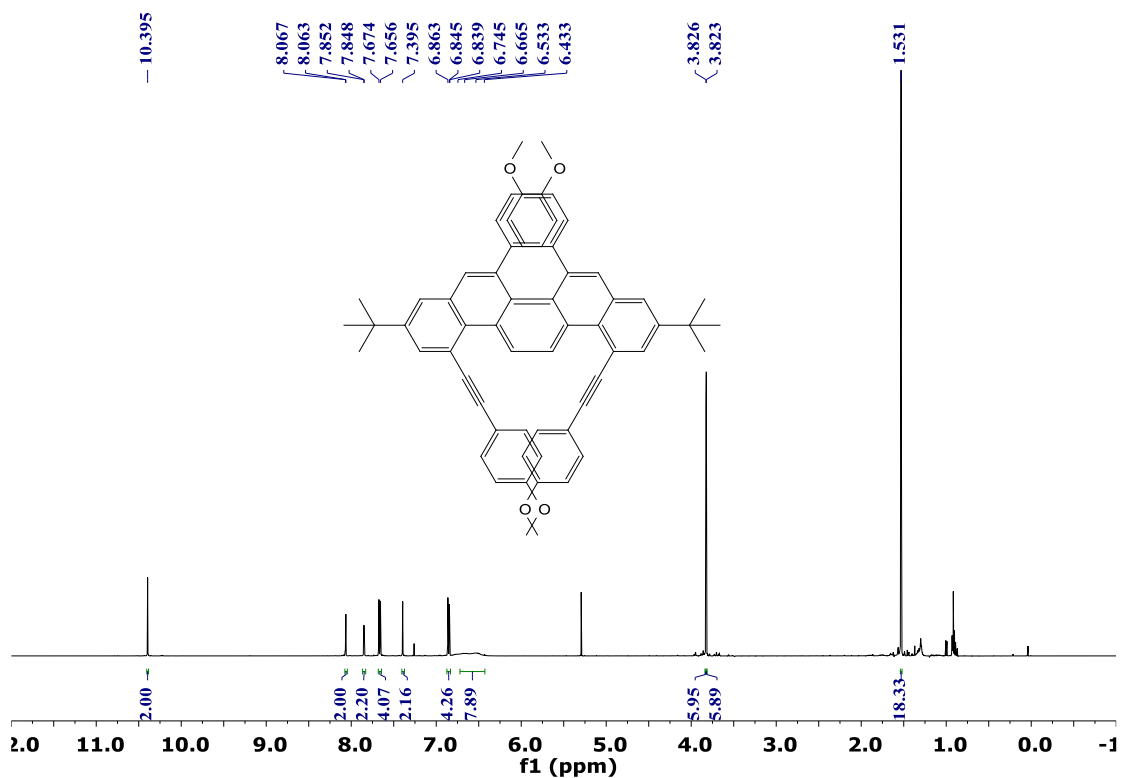
**Figure S28.** ^{1}H NMR spectrum for compound **4a** in CDCl$_3$ at 298 K.
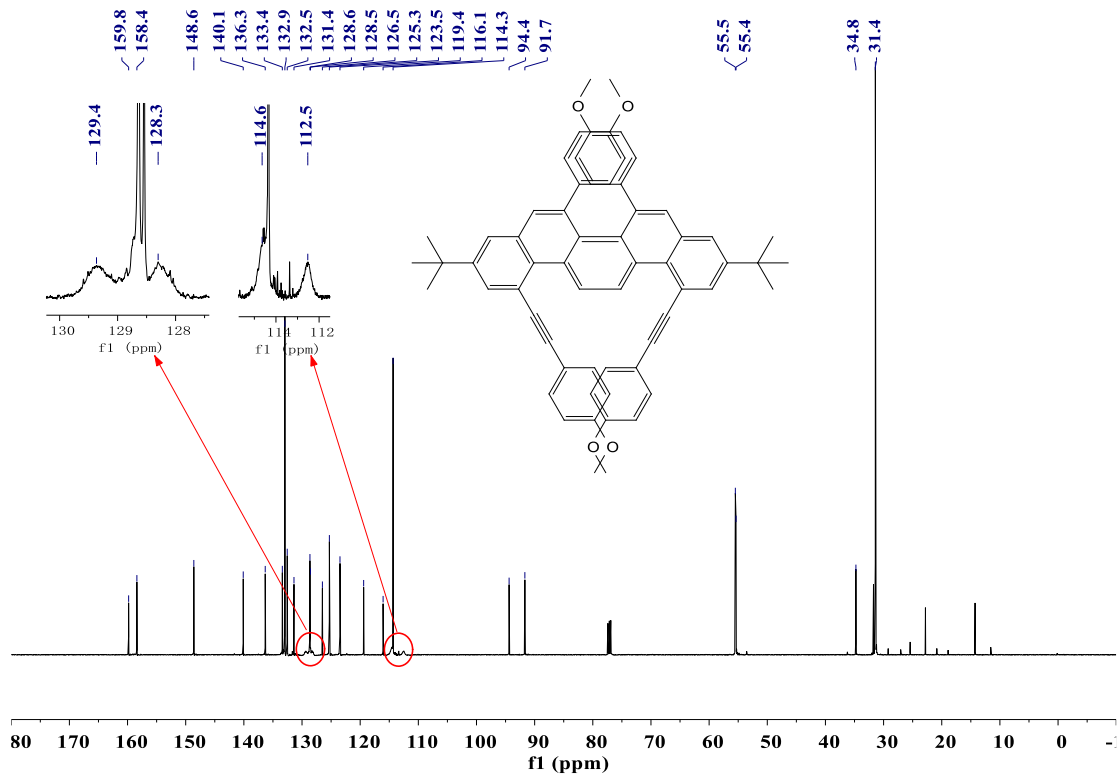


**Figure S29.** ^{13}C NMR spectrum for compound **4a** in CDCl$_3$ at 298 K.
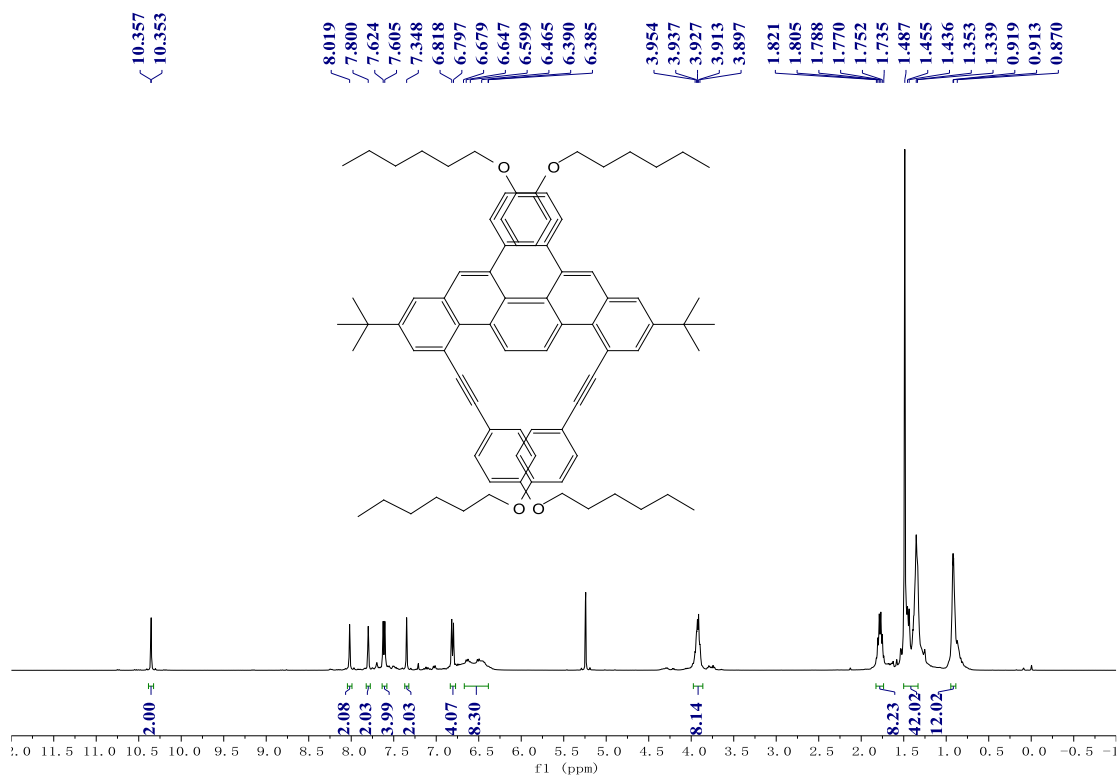
**Figure S30.** $^1$H NMR spectrum for compound **4b** in CDCl$_3$ at 298 K.
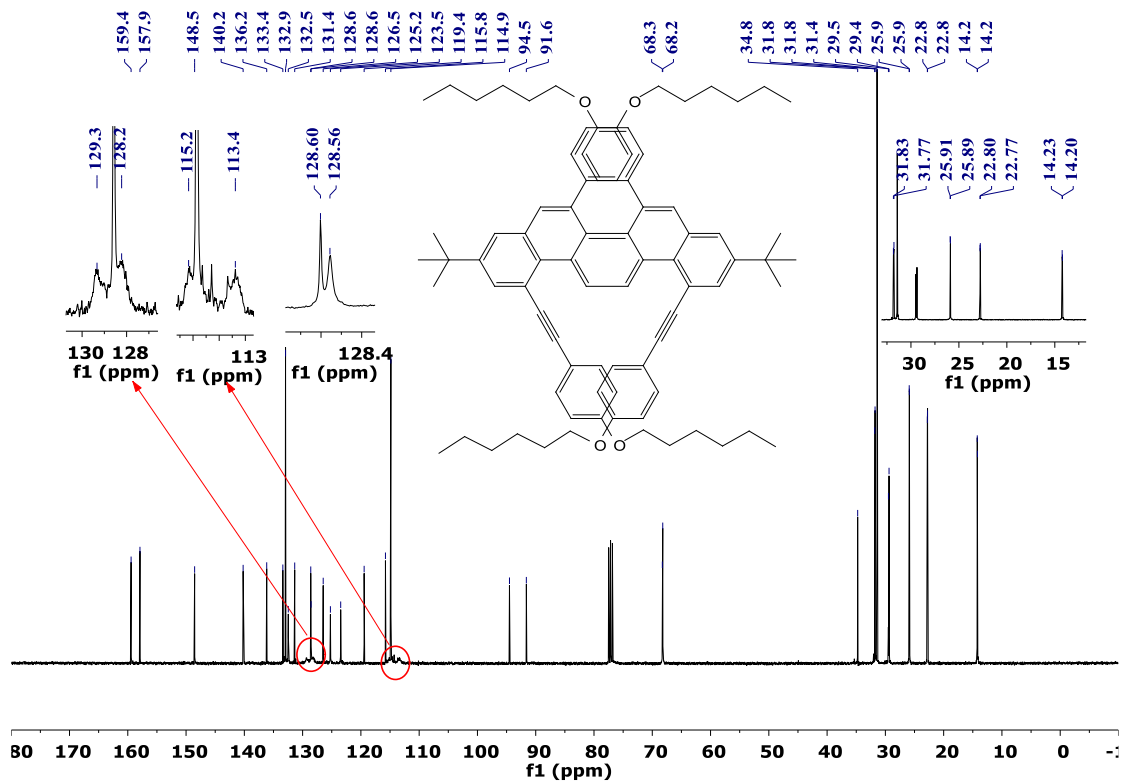


**Figure S31.** $^{13}$C NMR spectrum for compound **4b** in CDCl$_3$ at 298 K.
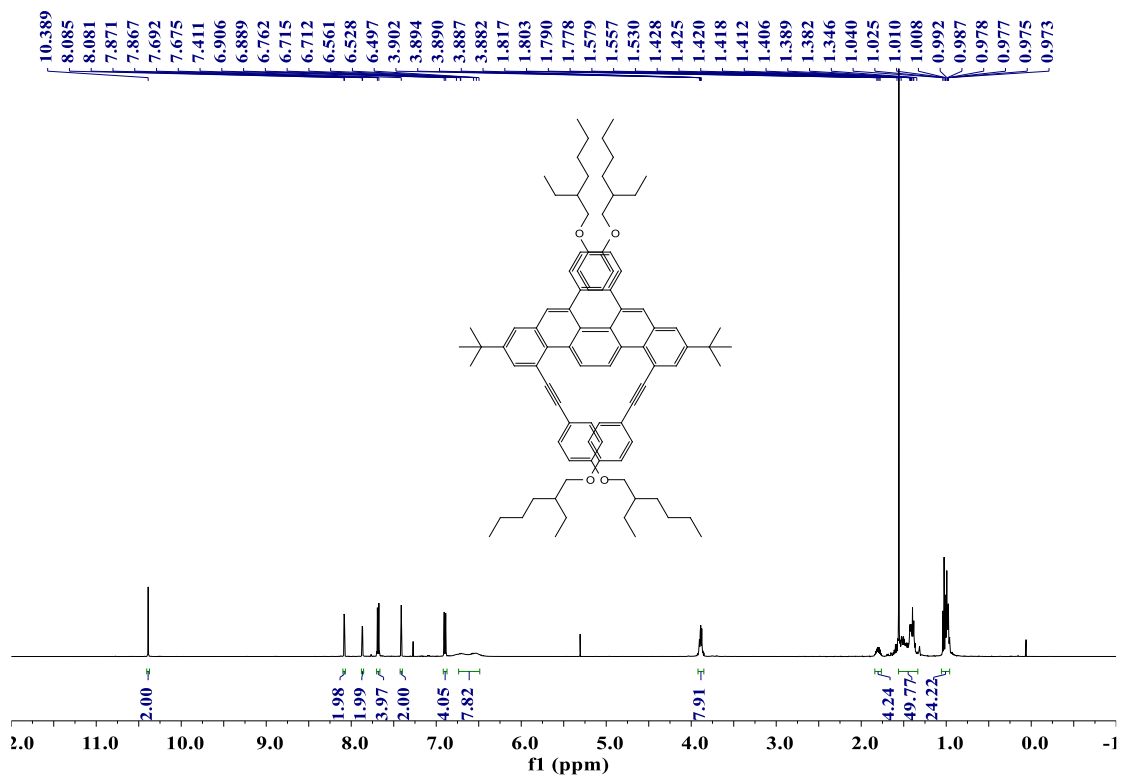
**Figure S32.** $^1$H NMR spectrum for compound **4c** in CDCl$_3$ at 298 K.
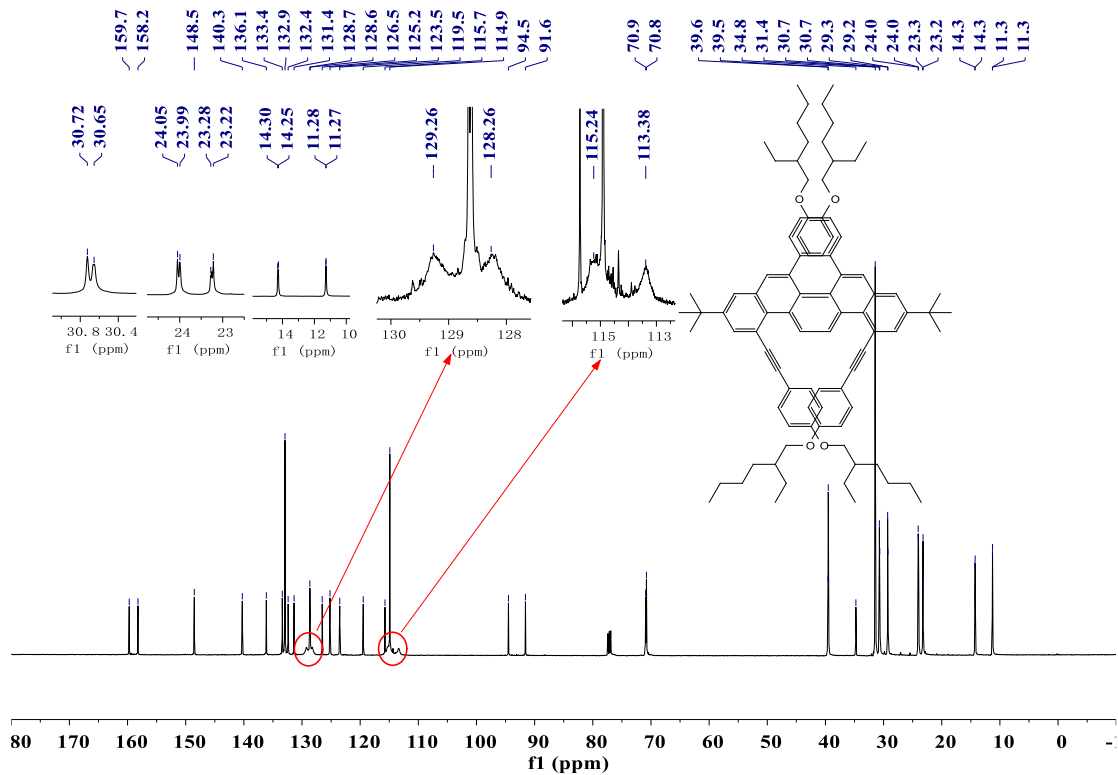


**Figure S33.** $^{13}$C NMR spectrum for compound **4c** in CDCl$_3$ at 298 K.
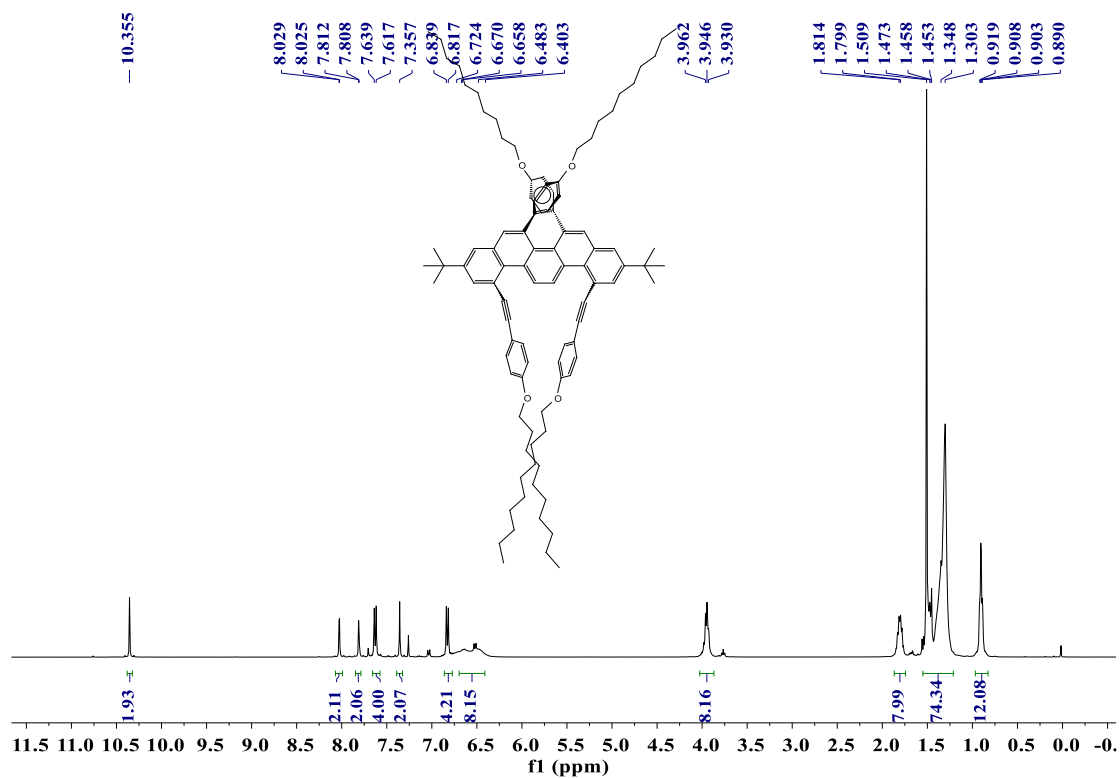
**Figure S34.** $^{1}$H NMR spectrum for compound **4d** in CDCl$_3$ at 298 K.
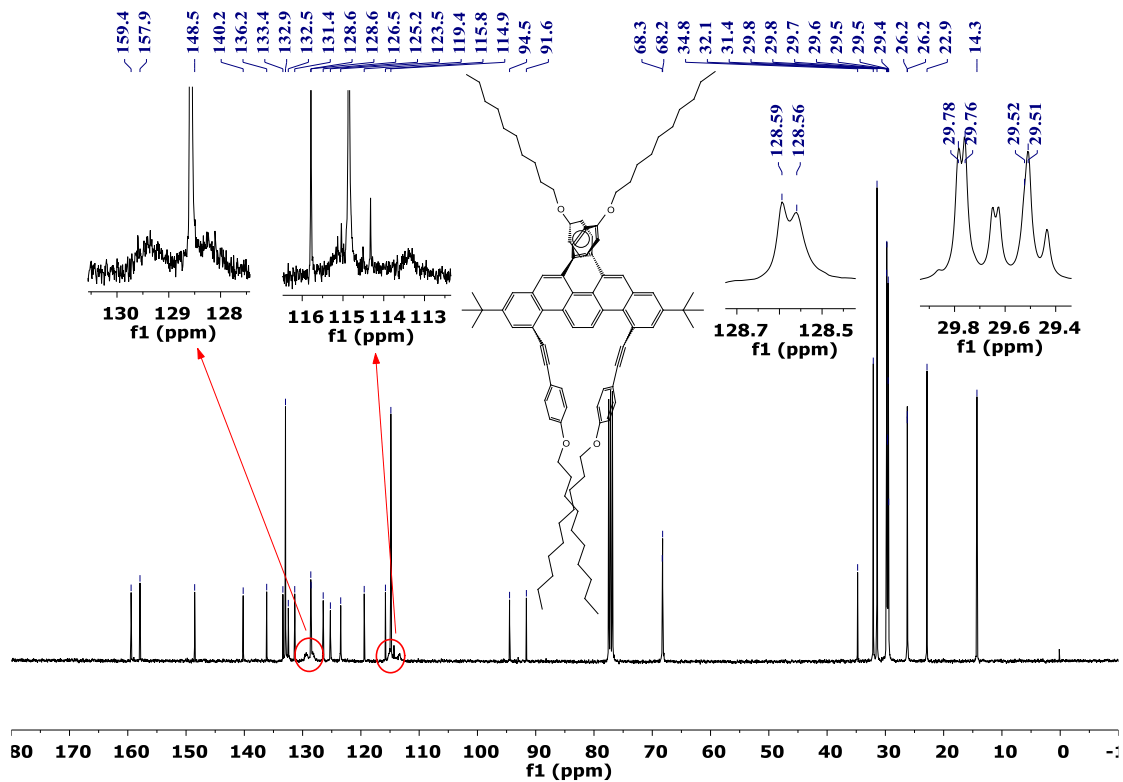


**Figure S35.** $^{13}$C NMR spectrum for compound **4d** in CDCl$_3$ at 298 K.
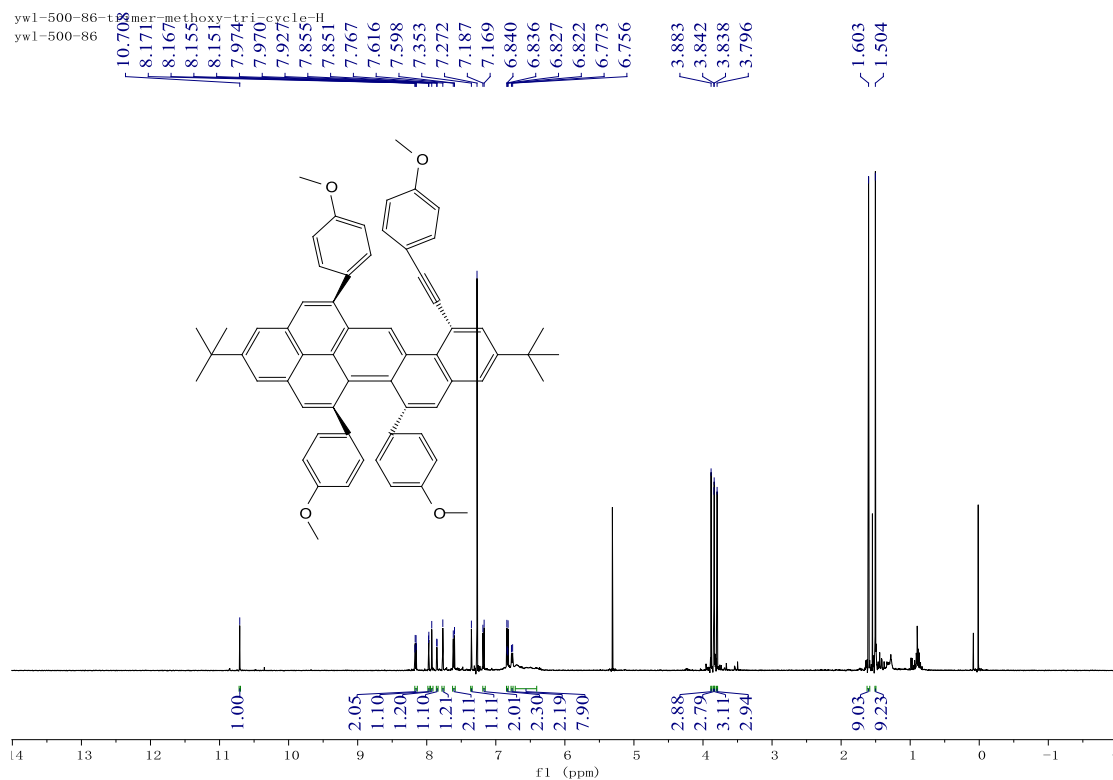
**Figure S36.** $^{1}$H NMR spectrum for compound **7a** in CDCl$_3$ at 298 K.
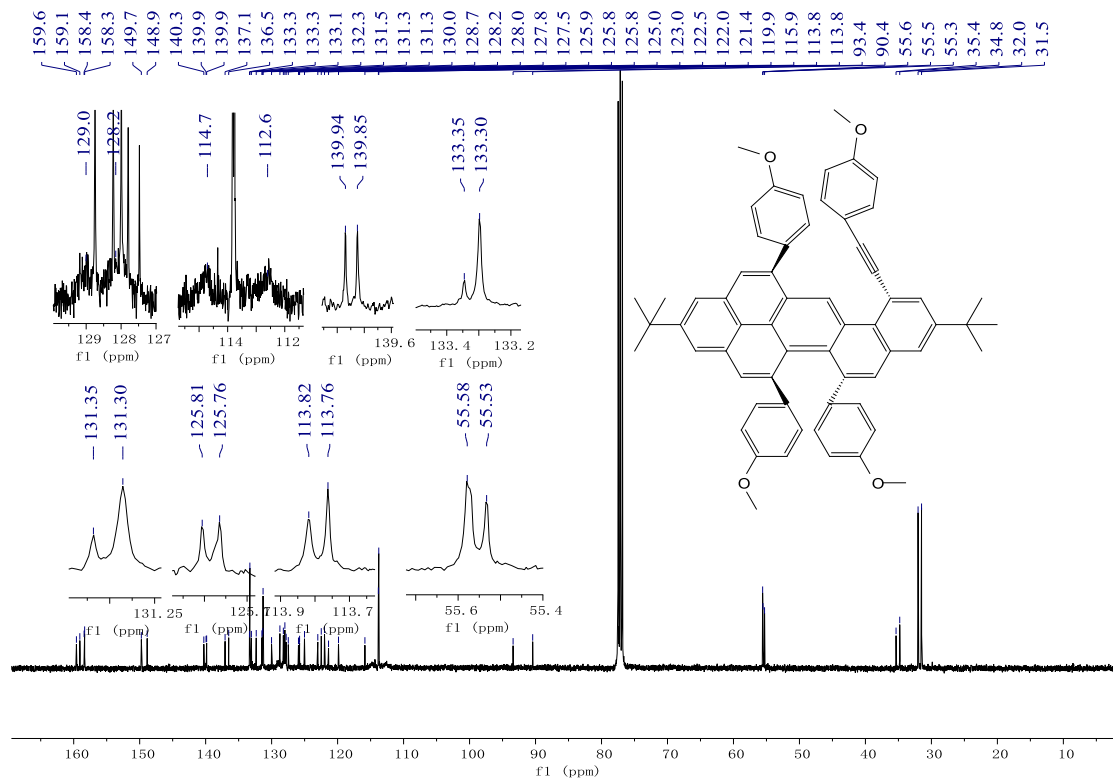


**Figure S37.** $^{13}$C NMR spectrum for compound **7a** in CDCl$_3$ at 298 K.
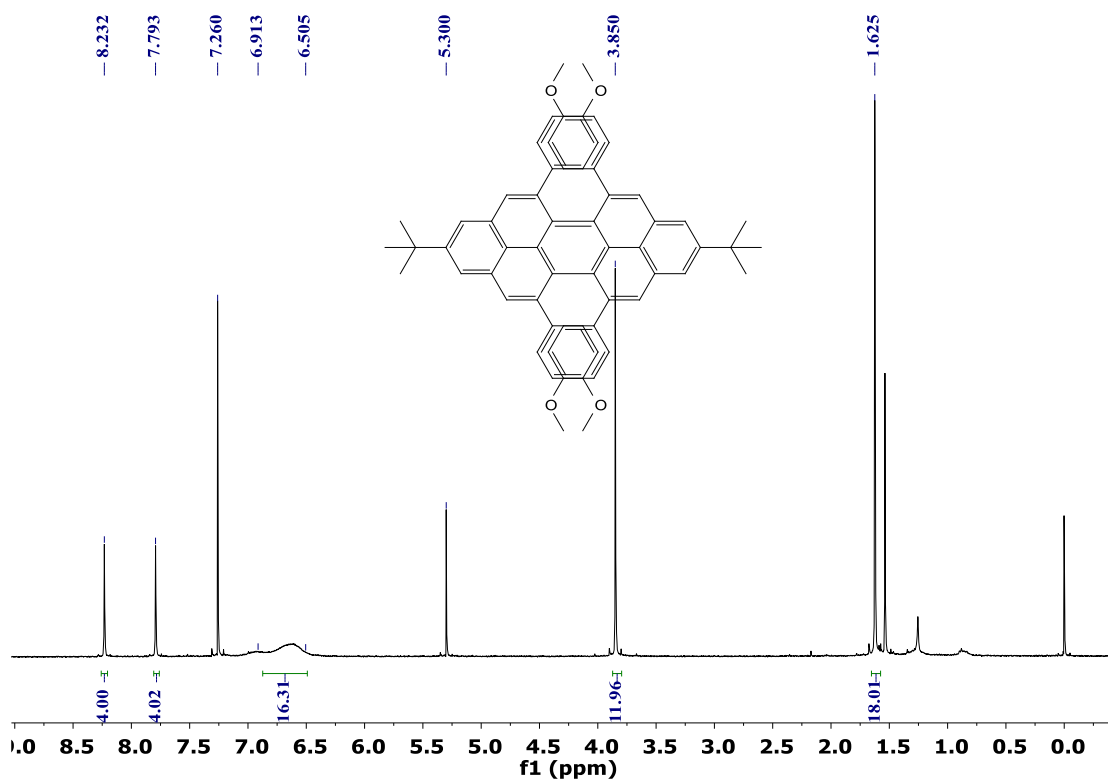
**Figure S38.** $^1$H NMR spectrum for compound **8a** in CDCl$_3$ at 298 K.
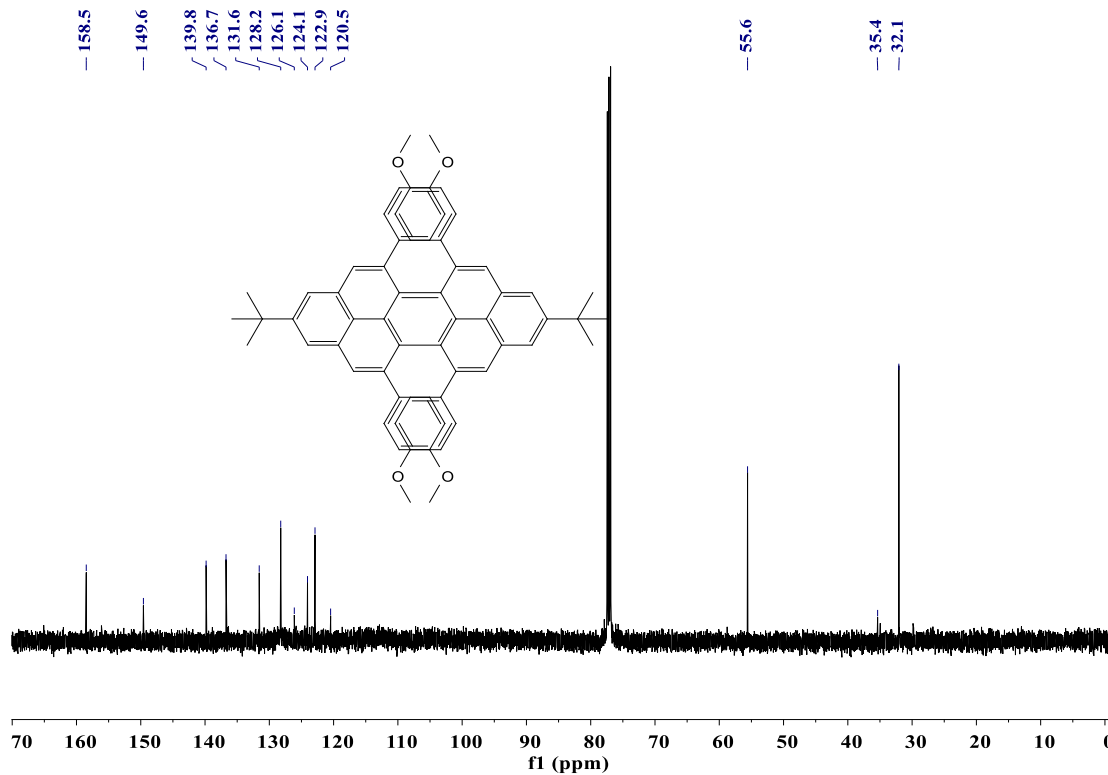


**Figure S39.** $^{13}$C NMR spectrum for compound **8a** in CDCl$_3$ at 298 K.
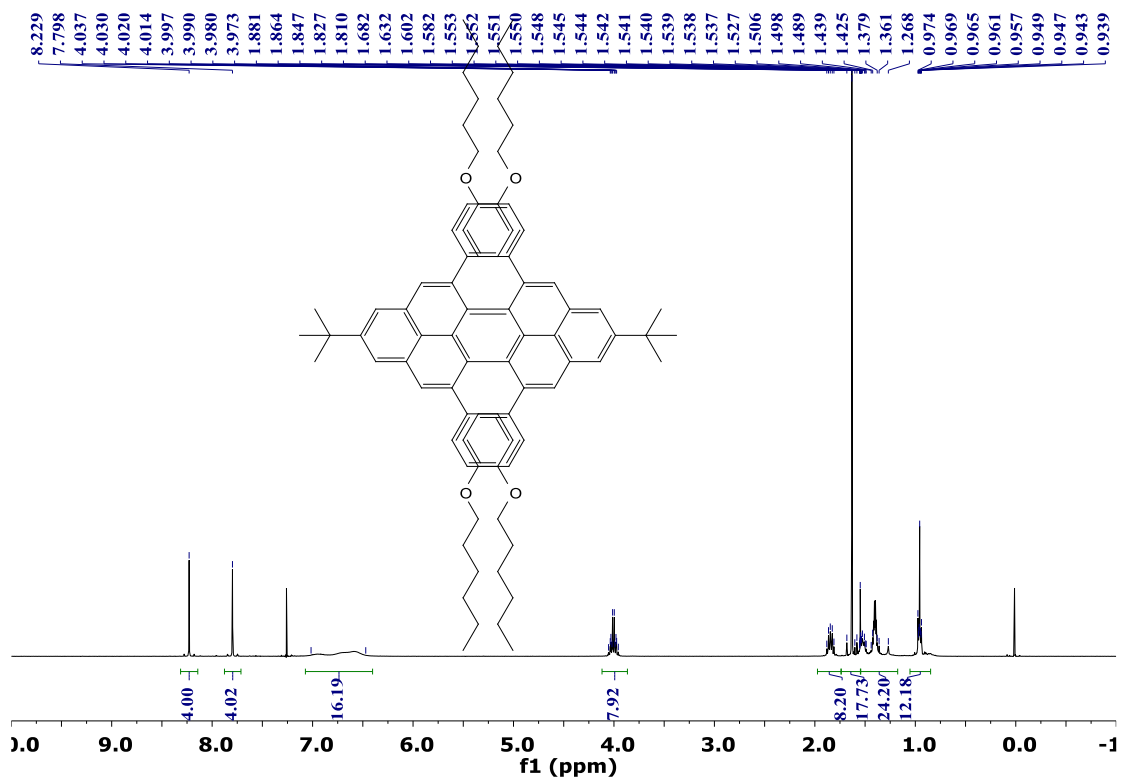
**Figure S40.** $^1$H NMR spectrum for compound **8b** in CDCl$_3$ at 298 K.
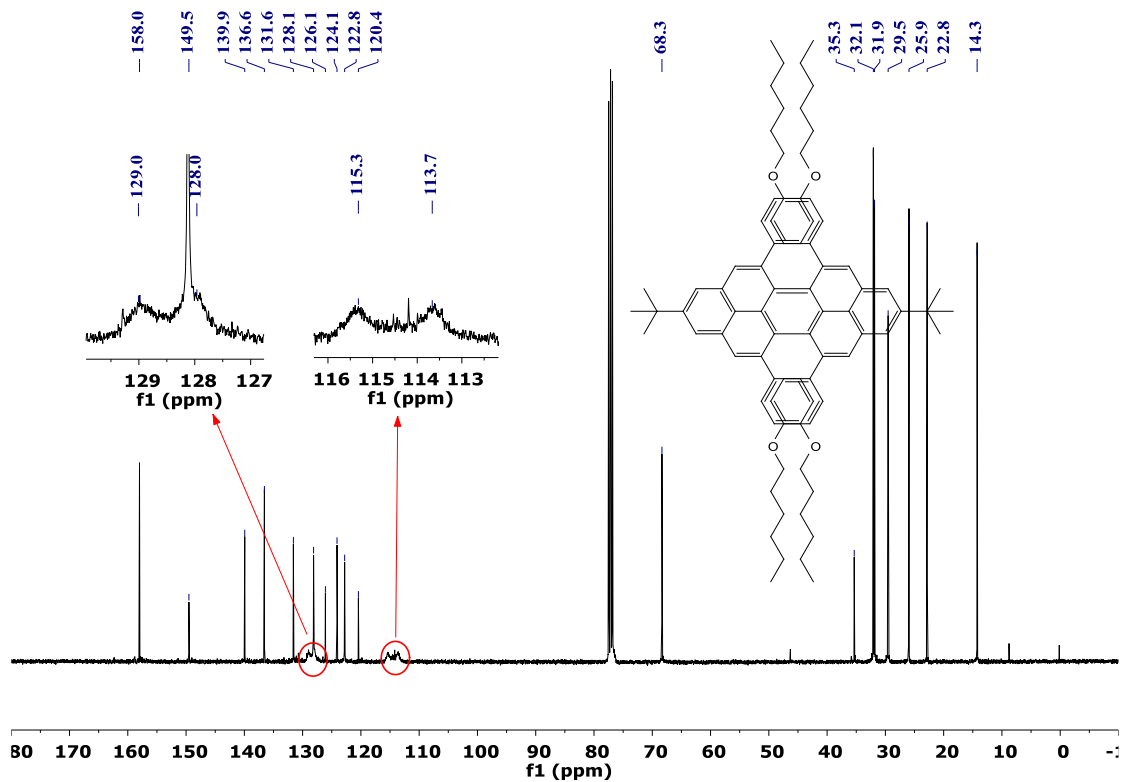


**Figure S41.** $^{13}$C NMR spectrum for compound **8b** in CDCl$_3$ at 298 K.
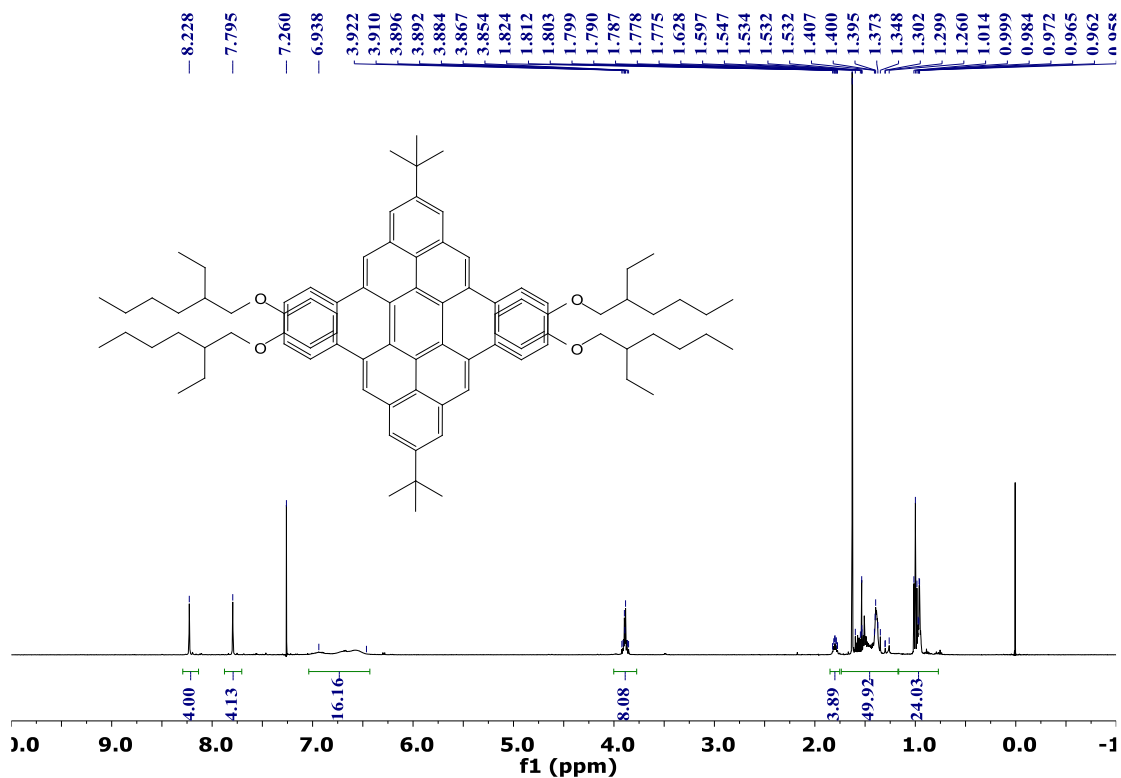
**Figure S42.** $^1$H NMR spectrum for compound **8c** in CDCl$_3$ at 298 K.
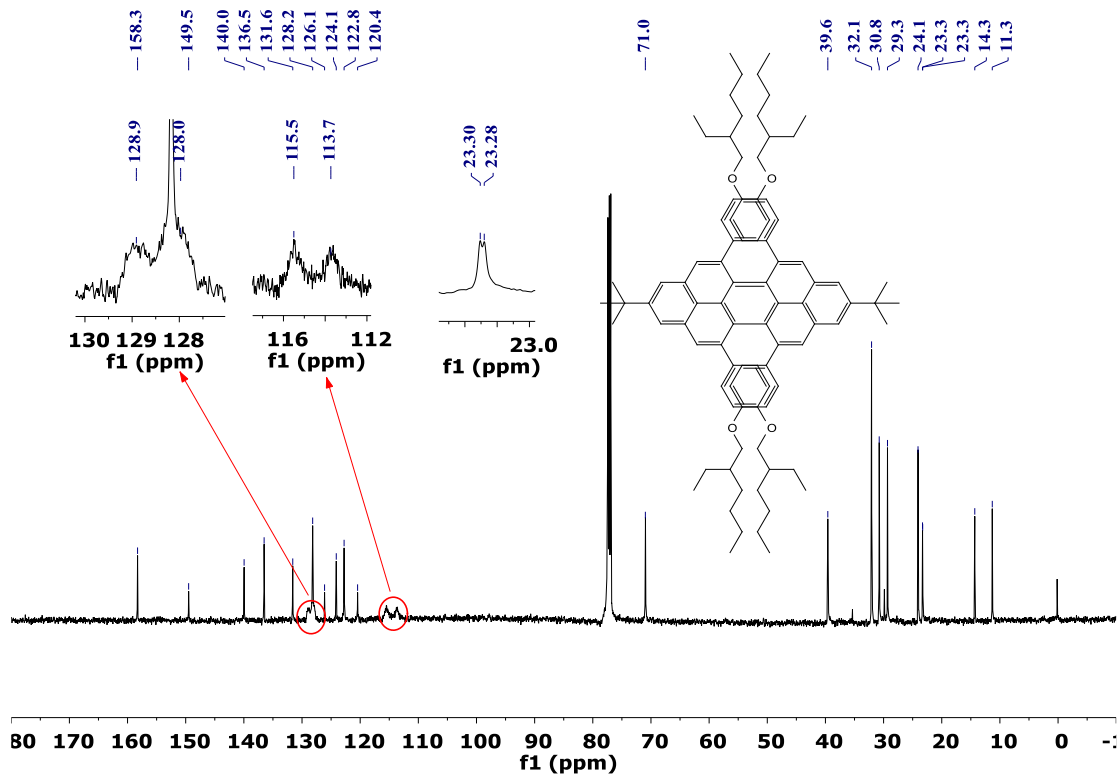


**Figure S43.** $^{13}$C NMR spectrum for compound **8c** in CDCl$_3$ at 298 K.
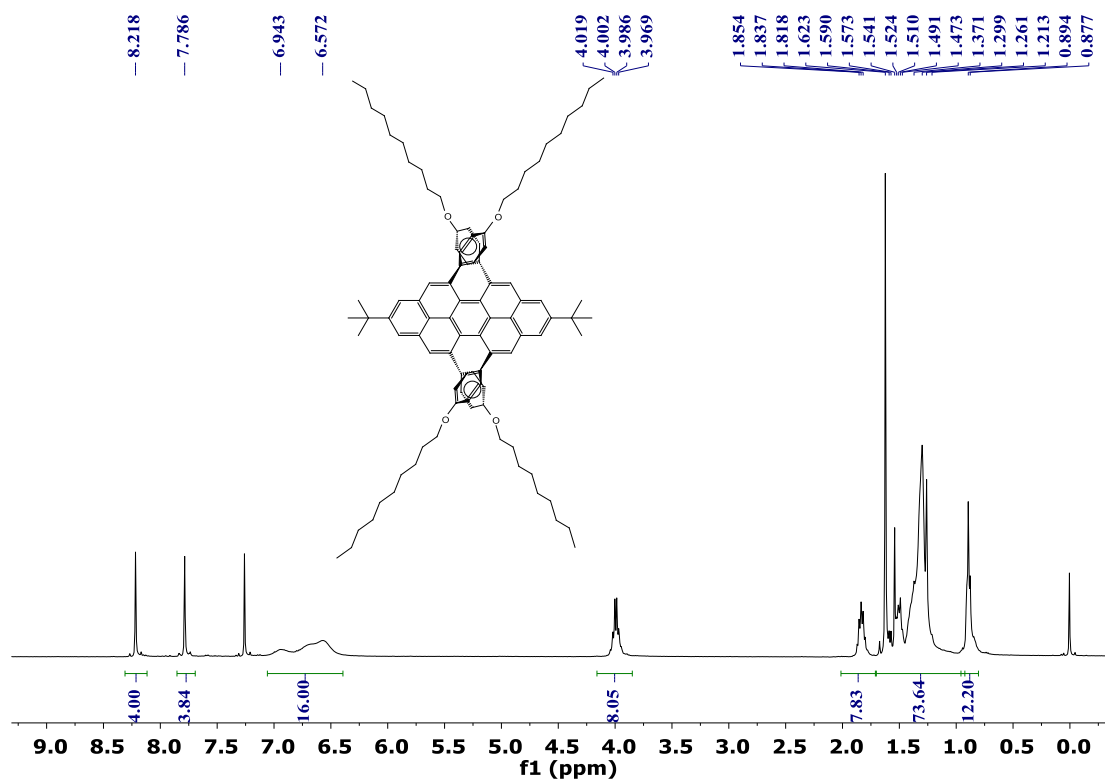
**Figure S44.** $^1$H NMR spectrum for compound **8d** in CDCl$_3$ at 298 K.
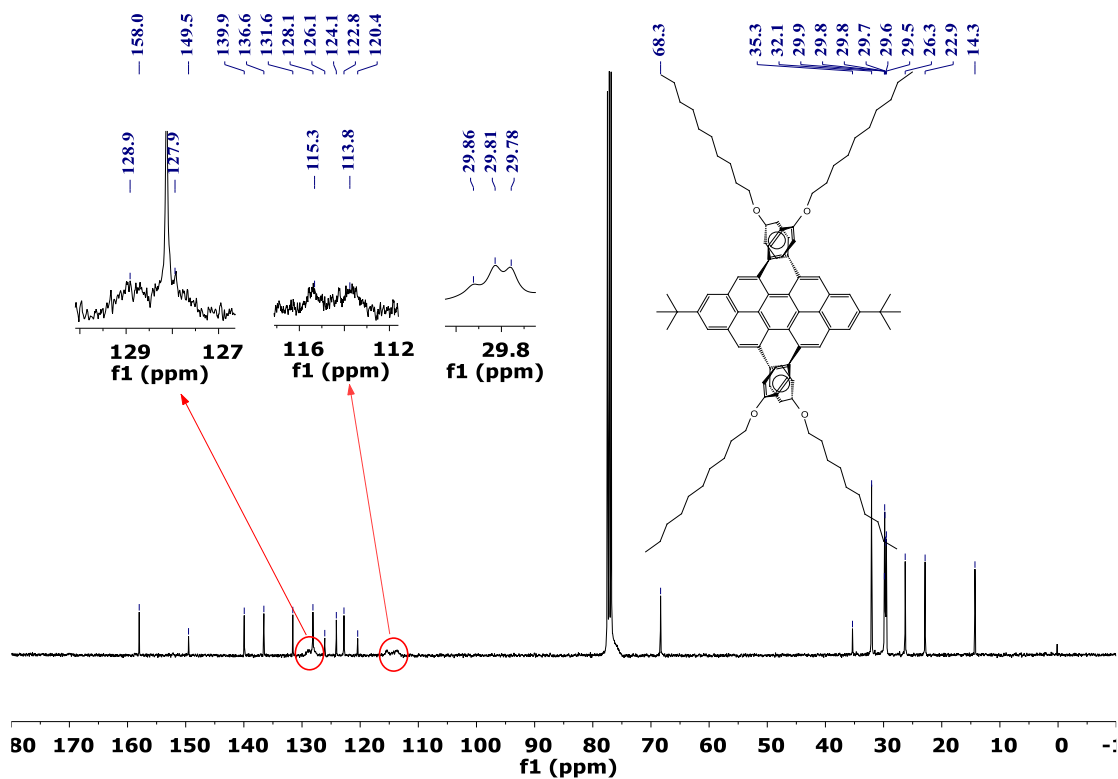


**Figure S45.** $^{13}$C NMR spectrum for compound **8d** in CDCl$_3$ at 298 K.

# 7. References

[1] SMART: v.5.626, Bruker Molecular Analysis Research Tool. **2002**.

[2] SAINTPlus: v.6.36a, Data Reduction and Correction Program, Bruker AXS: Madison, WI, **2001**.

[3] SADABS: v.2.01, an empirical absorption correction program. **2001**.

[4] SHELXTL: v.6.10, Structure Determination Software Suite, Sheldrick, G.M. **2001**.

[5] Gaussian 09, Revision A.02, Frisch, M. J.; Trucks, G. W.; Schlegel, H. B.; Scuseria, G. E.; Robb, M. A.; Cheeseman, J. R.; Scalmani, G.; Barone, V.; Mennucci, B.; Petersson, G. A.; Nakatsuji, H.; Caricato, M.; Li, X.; Hratchian, H. P.; Izmaylov, A. F.; Bloino, J.; Zheng, G.; Sonnenberg, J. L.; Hada, M.; Ehara, M.; Toyota, K.; Fukuda, R.; Hasegawa, J.; Ishida, M.; Nakajima, T.; Honda, Y.; Kitao, O.; Nakai, H.; Vreven, T.; Montgomery, J. A., Jr.; Peralta, J. E.; Ogliaro, F.; Bearpark, M.; Heyd, J.J.; Brothers, E.; Kudin, K. N.; Staroverov, V. N.; Kobayashi, R.; Normand, J.; Raghavachari, K.; Rendell, A.; Burant, J. C.; Iyengar, S. S.; Tomasi, J.; Cossi, M.; Rega, N.; Millam, N. J.; Klene, M.; Knox, J. E.; Cross, J. B.; Bakken, V.; Adamo, C.; Jaramillo, J.; Gomperts, R.; Stratmann, R. E.; Yazyev, O.; Austin, A. J.; Cammi, R.; Pomelli, C.; Ochterski, J. W.; Martin, R. L.; Morokuma, K.; Zakrzewski, V. G.; Voth, G. A.; Salvador, P.; Dannenberg, J. J.; Dapprich, S.; Daniels, A. D.; Farkas, Ö.; Foresman, J. B.; Ortiz, J. V.; Cioslowski, J.; Fox, D. J. Gaussian, Inc., Wallingford CT, **2009**

[6] Gierschner, J.; Mack, H.-G.; Lüer, L.; Oelkrug, D., *J. Chem. Phys.* **2002,** *116*, 8596.

[7] Negri, F.; Zgierski, M. Z., *J. Chem. Phys.* **1994,** *100*, 2571.

[8] Tommasini, M.; Longhi, G.; Abbate, S.; Zerbi, G., *J. Raman Spectrosc.* **2014,** *45*, 89.

[9] Yang, W.; Monteiro, J. H. S. K.; de Bettencourt-Dias, A.; Catalano, V. J.; Chalifoux, W. A., *Angew. Chem. Int. Ed.* **2016,** *55*, 10427.

[10] Schmidt, M. W.; Baldridge, K. K.; Boatz, J. A.; Elbert, S. T.; Gordon, M. S.; Jensen, J. H.; Koseki, S.; Matsunaga, N.; Nguyen, K. A.; Su, S.; Windus, T. L.; Dupuis, M.; Montgomery, J. A., *J. Comput. Chem.* **1993,** *14*, 1347.

[11] Gordon, M. S.; Schmidt, M. W. in Theory Appl. Comput. Chem. (Eds.: Dykstra C.E., Frenking G., Kim K.S., Scuseria G.E.), Elsevier, Amsterdam, **2005**, pp. 1167–1189.

[12] Weigend, F.; Ahlrichs, R., *Phys. Chem. Chem. Phys.* **2005,** *7*, 3297.

[13] Becke, A. D., *J. Chem. Phys.* **1993,** *98*, 5648.

[14] Lee, C.; Yang, W.; Parr, R. G., *Phys. Rev. B* **1988,** *37*, 785

[15] Su, P.; Li, H., *J. Chem. Phys.* **2009,** *131*, 014102.

[16] Grimme, S.; Antony, J.; Ehrlich, S.; Krieg, H., *J. Chem. Phys.* **2010,** *132*, 154104.